NTNU – Trondheim
Norwegian University of
Science and Technology

The Effects of Near-fault Earthquakes On a High-rise Structure In The Oslo Area

Karin Harnæs Hoel
Bjørn Thomas Svendsen

Civil and Environmental Engineering
Submission date: June 2012
Supervisor: Anders Rönnquist, KT
Co-supervisor: Ragnar Sigbjörnsson, KT

Norwegian University of Science and Technology
Department of Structural Engineering

Department of Structural Engineering
Faculty of Engineering Science and Technology
NTNU - The Norwegian University of Science and Technology

ACCESSIBILITY

OPEN

MASTER THESIS 2012

SUBJECT AREA:	DATE:	NO. OF PAGES: 174
Structural Dynamics	11.06.2012	(14 + 122 + 38)

TITLE:

The Effects of Near-fault Earthquakes On a High-rise Structure In The Oslo Area

Effekten av near-fault jordskjelv på høyhusbygning i Oslo området

BY:

Karin Harnæs Hoel
Bjørn Thomas Svendsen

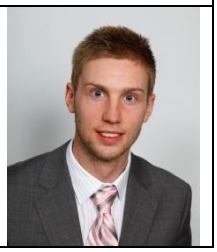

SUMMARY:

The objective of the presented research is to evaluate the seismic response of a high-rise structure located in a seismic environment. For this purpose, the Oslo Plaza building located in Oslo, Norway, was chosen. A numerical element model of the building was created in the structural analysis program SAP2000 with emphasis on the soil-structure interaction representation. A structural monitoring process with the intention of calibrating the model was performed. The focus was to estimate and evaluate the dynamic behavior and response of the high-rise structure to strong ground motion, with emphasis on near-fault ground motion. For this purpose, simulations and modifications of ground motion data was performed. The seismic response of the structure with emphasis on important damage parameters of special concern for tall structures such as displacement, interstory drift and base shear were investigated.

It was found that near-fault earthquakes results in larger seismic response than far-fault earthquakes for the high-rise structure considered. The near-fault ground motion rendered larger interstory drift which was found to be decisive at critical floors, as expected. Analyses of the existing point bearing foundation resulted in less seismic response than an alternative foundation representation modeled in SAP2000. Oslo Plaza was found to perform well considering the response parameters taken into consideration for the different seismic scenarios. A seismic design according to Eurocode 8 and the National Annex of Norway is sufficient for high-rise structures like Oslo Plaza. An exception was found investigating the P-Δ effects. The study does not incorporate design checks of the structure.

Keywords: Near-fault Ground Motion; High-rise Structure; Interstory Drift; Soil-structure Interaction; Oslo; Structural Monitoring.

RESPONSIBLE TEACHER: Associate Professor Anders Rönnquist.
SUPERVISORS: Associate Professor Anders Rönnquist and Adjunct Professor Ragnar Sigbjörnsson.
CARRIED OUT AT: Department of Structural Engineering, NTNU.

Department of Structural Engineering
Faculty of Engineering Science and Technology
NTNU - The Norwegian University of Science and Technology

MASTER THESIS SPRING 2012

For

Karin Harnæs Hoel and Bjørn Thomas Svendsen

Earthquake design practice of traditional Norwegian buildings according to Eurocode 8

Jordskjelvsdesign etter Eurocode 8 for typiske norske bygninger

Seismic design was fully introduced for Norwegian land based structures with the new standard EN 3491-12. This standard was introduced as a transitional phase to the current standard Eurocode 8. With the exception of a few types of structures, all new buildings as well as extension of buildings shall be controlled by the new earthquake standard.

Today, it is common practice to use elastic reaction design with an initial control if the structure possibly satisfies the given criteria in order to exclude further control of seismic actions. Furthermore, if the seismic design cannot be excluded, the structural elements and connections are controlled for elastic forces and reactions. It is a great need to further develop design methods for Norwegian hazard levels which better utilize the capabilities of the standard in addition to take into account the Norwegian building traditions.

The master thesis shall identify how the new Eurocode 8 affects Norwegian buildings and how the new recommendations can be formulated for the design of various types of buildings. With this, it is of particular interest to identify and concretize problems associated with high-rise steel and concrete buildings. The evaluation of methods of analyses to use depending on the type of structure is of concern. A consideration of how to improve properties of structures that possibly may come out porly by the new regulations is of interest.

Literature study, State-of-the-art:

- Near-fault earthquake hazard in the Oslo area.
- Numerical finite element modeling of a high-rise concrete structure, Oslo Plaza.
- Soil-structure interaction – theory and implementation for the chosen structure.
- Analyses of the structure according to different methods stated in the literature including the Eurocode 8 standard.
- Structural monitoring and different methods for processing of data.

Case study:

- Numerical FE-model of existing structure in SAP2000.
- Establish dynamic properties like natural vibration frequencies and mode shapes of the structure.
- Evaluate and control results by hand calculations.
- System identification by full scale measurements, i.e. structural monitoring.
- Implement methods of analysis stated in the literature and the Eurocode 8 provision and evaluate seismic response parameters.
- Frequency domain solutions and time domain solutions (linear).
- Comparison and evaluation of results due to seismic response according to Eurocode 8 and recommendations found in the literature.

It is up to the candidates to select and place emphasis on the different subjects chosen to be investigated in the thesis. The thesis must be written according to current requirements according to The Department of Structural Engineering, NTNU.

Supervisors: Associate Professor Anders Rönnquist and Adjunct Professor Ragnar Sigbjörnsson, NTNU.

The thesis must be submitted to The Department of Structural Engineering at NTNU by June 11, 2012.

PREFACE

This thesis was completed the spring semester 2012 at The Department of Structural Engineering, part of The Faculty of Engineering Science and Technology at The Norwegian University of Science and Technology, NTNU, in Trondheim.

The thesis is a continuation of the project work carried out in the fall semester of 2011 within the field of structural dynamics and earthquake engineering – *earthquake design practice of traditional Norwegian buildings according to Eurocode 8*.

Working within this field of engineering has been very interesting. The complexity of working with a high-rise structure and performing analyses on a comprehensive model has been challenging but very rewarding.

First we would like to give a special thanks to our supervisors, Associate Professor Anders Rönnquist and Adjunct Professor Ragnar Sigbjörnsson. We would like to express our gratitude to Prof. Rönnquist for providing theoretical basis, discussions and for being able to perform structural monitoring. Prof. Sigbjörnsson has been very helpful with theoretical advices, discussions and useful Matlab scripts for performing simulations of ground motion records and interpretation and processing of data. We would also like to thank Adjunct Professor Amir Kaynia for his help and advices regarding the implementation of soil-structure interaction in our model, and Senior Engineer Paal Brokka Rike for helping with the structural monitoring process.

At last, we would like to thank Chief Engineer at Oslo Plaza, Svein Fredrik Willadsen and Erik Bjørhovde, Regional Manager of OKK Entreprenører AS Department of Oslo. Willadsen and the hotel management provided us with construction and architectural drawings and let us perform the structural monitoring. Bjørhovde provided us with help regarding information about the foundation work of Oslo Plaza. We would also like to thank Arnkjell Løkke for proofreading this thesis.

Trondheim, June 11, 2012

Karin Harnæs Hoel

Bjørn Thomas Svendsen

ABSTRACT

The objective of the presented research is to evaluate the seismic response of a high-rise structure located in a seismic environment. For this purpose, the Oslo Plaza building located in Oslo, Norway, was chosen. A numerical element model of the building was created in the structural analysis program SAP2000 with emphasis on the soil-structure interaction representation. A structural monitoring process with the intention of calibrating the model was performed. The focus was to estimate and evaluate the dynamic behavior and response of the high-rise structure to strong ground motion, with emphasis on near-fault ground motion. For this purpose, simulations and modifications of ground motion data was performed. The seismic response of the structure with emphasis on important damage parameters of special concern for tall structures such as displacement, interstory drift and base shear were investigated.

It was found that near-fault earthquakes results in larger seismic response than far-fault earthquakes for the high-rise structure considered. The near-fault ground motion rendered larger interstory drift which was found to be decisive at critical floors, as expected. Analyses of the existing point bearing foundation resulted in less seismic response than an alternative foundation representation modeled in SAP2000. Oslo Plaza was found to perform well considering the response parameters taken into consideration for the different seismic scenarios. A seismic design according to Eurocode 8 and the National Annex of Norway is sufficient for high-rise structures like Oslo Plaza. An exception was found investigating the P-Δ effects. The study does not incorporate design checks of the structure.

Keywords: Near-fault Ground Motion; High-rise Structure; Interstory Drift; Soil-structure Interaction; Oslo; Structural Monitoring.

SAMMENDRAG

I denne rapporten er den seismiske responsen til en høy bygning evaluert. Til dette formålet ble Oslo Plaza valgt, lokalisert i Oslo, Norge. Ved hjelp av elementanalyseprogrammet SAP2000 ble det laget en numerisk elementmodell av bygningen med vekt på å representere interaksjonen mellom jord og konstruksjon på en god måte. Det ble foretatt målinger på den virkelige bygningen i den hensikt å kalibrere modellen. Fokuset i arbeidet har vært å estimere og evaluere den dynamiske responsen fra jordskjelv på den gitte bygningen med hovedfokus på near-fault jordskjelv. Det har i dette øyemed blitt foretatt simuleringer og modifikasjoner av tidsserier fra tidligere jordskjelv. Forskyvning både totalt og relativt mellom etasjene samt skjærkraft i bunn av bygningen er viktige parametere for høye bygninger og er blitt tillagt spesiell vekt ved evalueringen av den seismiske responsen.

Resultatet av analysene viste at near-fault jordskjelv ga større seismisk respons enn far-fault jordskjelv. Near-fault jordskjelv ga høyere relativ forskyvning mellom etasjene som viste seg å være avgjørende i kritiske etasjer. Analyser av det eksisterende fundamentet ga mindre seismisk respons enn alternativ utførelse utført på modellen i SAP2000. Ved å se på de ulike responsparametere ble det funnet at Oslo Plaza ikke vil få store skader av jordskjelvene som ble analysert. Seismisk dimensjonering etter Eurokode 8 og det norske nasjonale tillegget er tilstrekkelig for høye bygninger som Oslo Plaza med unntak av undersøkelser av P-Δ effekten. Oppgaven inneholder ikke en dimensjoneringskontroll av konstruksjonen.

Nøkkelord: Near-fault jordskjelv; Høy bygning; Relativ etasjeforskyvning; Interaksjon mellom jord og konstruksjon; Oslo; Kontrollmålinger på konstruksjon.

CONTENT

NOMENCLATURE

Latin letters

A	Area
$A_{0,ta}$, A_{ta}	Trace amplitude
a_g	Design peak ground acceleration for ground type A
a_{gR}	Reference peak ground acceleration for ground type A
a_{g40Hz}	Reference peak ground acceleration at 40 Hz
a_k	Constant, Fourier coefficient
a_v	Design vertical ground acceleration
a_0	Dimensionless parameter
a	Acceleration
$a(t)$	Acceleration vector
B	Foundation breadth
b	Width
b_k	Constant, Fourier coefficient
$C(\omega)$	Dynamic damping
C^*	Modal damping
$\mathbb{C}$	Damping matrix
$\mathbb{C}_f$	Foundation damping matrix
$\mathbb{C}^*$	Modal damping matrix
c_0, c_k	Constant, coefficient, Fourier amplitude
c_u	Shear strength
D	Foundation depth
D_{fault}	Average displacement of fault
d	Foundation thickness
d_c	Distance to area center
d_P	Pile diameter
d_r	EC8 design interstory drift
E	Modulus of elasticity / Young's modulus
E_p	Modulus of elasticity / Young's modulus of pile material
E_x	EC8 load in x-direction
E_y	EC8 load in y-direction
E_z	EC8 load in z-direction
$e(t)$	White noise vector
F	Horizontal force
$\mathbb{F}$	Force matrix
f	Frequency
f_c	Corner frequency
f_{max}	Cutoff frequency
f_y	Required yield strength
f_0	Required elastic strength
G	Shear modulus

G_s	Shear modulus of soil
g	Gravity, 9.81 m/s^2
h	Story height
h_{dl}	Dimensionless story height
h_i	Section dimension
h_{tot}	Total height of building
I	Second moment of inertia
I_x	Second moment of inertia about the y-axis (in the x-direction)
I_y	Second moment of inertia about the x-axis (in the y-direction)
I_a	Arias intensity
i	Mode number (index variable)
j	Floor number
K_{static}	Static stiffness
$K(\omega)$	Dynamic stiffness
K_p	Pile stiffness
K_w	Wall stiffness
K^*	Modal stiffness
$\mathbb{K}$	Stiffness matrix
$\mathbb{K}_f$	Foundation stiffness matrix
$\mathbb{K}^*$	Modal stiffness matrix
k	Index variable
k^*	Generalized stiffness
$k(\omega)$	Dynamic stiffness factor
L	Foundation length
L^*	Modal load
$\mathbb{L}^*$	Modal load vector
l	Average pile length
M_L	Local Magnitude
M_w	Moment Magnitude
M_0	Seismic moment
M^*	Modal mass
$\mathbb{M}$	Mass matrix
$\mathbb{M}_f$	Foundation mass matrix
$\mathbb{M}^*$	Modal mass matrix
m	Mass
$m(x)$	Mass per unit length
m_s	Mass of slab
m_w	Mass of wall
m^*	Generalized mass
N	Total number of floors in the structure
n	Number of degrees-of-freedom
n_f	Number of floors
n_w	Number of walls
P_{tot}	Total gravity load

$\mathbb{P}(t)$	Time varying load matrix
$p(t)$	External dynamic load
$\mathbb{Q}_f$	Load vector for soil-structure interaction
$\mathbb{Q}_i$	Load vector determined from free-field displacements
q	Behavior factor
R	Modal response quantities
R_y	Reduction factor
r	Equivalent foundation radius
r_s	Gravity/Shear-ratio (sensitivity ratio)
r_t	Normally distributed time-series
S	Soil factor
Sa	Pseudo spectral acceleration
Sd	Pseudo spectral displacement
Sv	Pseudo spectral velocity
S_x	Spectral density
T	Time
T_n	Natural vibration period
T_B, T_C, T_D	Natural vibration period parameters
$\mathbb{T}$	Influence matrix
t	Time
t_s	Slab thickness
t_w	Wall thickness
$\mathbb{u}, \dot{\mathbb{u}}, \ddot{\mathbb{u}}$	Displacement, velocity, acceleration matrices
$\mathbb{u}_f, \dot{\mathbb{u}}_f, \ddot{\mathbb{u}}_f$	Free-field displacement, velocity and acceleration matrices
$\mathbb{u}_i, \dot{\mathbb{u}}_i, \ddot{\mathbb{u}}_i$	Interaction displacement, velocity and acceleration matrices
u	Displacement
$u_g, \dot{u}_g, \ddot{u}_g$	Displacement, velocity and acceleration of tri-axial ground acceleration record
$u_{g0}, \dot{u}_{g0}, \ddot{u}_{g0}$	Displacement, velocity and acceleration of the ground
V	Shear force
V_b	Base shear
V_s	Soil shear wave velocity
V_{tot}	Total seismic story shear
$\mathbb{v}, \dot{\mathbb{v}}, \ddot{\mathbb{v}}$	Displacement, velocity, acceleration vectors
x	Length parameter
$x(t)$	Periodic function
$Y, \dot{Y}, \ddot{Y}$	Modal amplitude displacement, velocity and acceleration
$\mathbb{Y}$	Modal amplitude displacement matrix
$\dot{\mathbb{Y}}$	Modal amplitude velocity matrix
$\ddot{\mathbb{Y}}$	Modal amplitude acceleration matrix
y	Width parameter
$y(t)$	Total system response
z	Height of story mass

Greek letters

β	Soil hysteretic damping
β_{ij}	Frequency ratio
γ_l	Seismic factor
Δ	Epicentral distance (Chapter 2) / interstory drift (Chapter 7)
δ_j	Interstory drift
ζ	Damping ratio
θ	Rotation angle
θ_{EC8}	Sensitivity factor
μ	Ductility factor
μ_r	Shear strength of fractured rock
ν	Poisson's ratio
ν_{EC8}	Reduction factor
ρ	Soil density
ρ_{ij}	Correlation factor
σ, σ^2	Standard deviation, variance
τ	Time integration parameter
$\boldsymbol{\Phi}$	Modal matrix
φ_k	Phase angle
$\psi(x)$	Shape function
ω	Cyclic frequency
ω_n	Natural undamped cyclic frequency
ω_D	Damped cyclic frequency
$\boldsymbol{\omega}$	Cyclic frequency matrix
$\Delta\omega$	Frequency segment

Symbols with both Latin and Greek letters

Δu	Difference in displacement between two floors

Abbreviations

CQC	Complete quadric combination
DOF	Degrees-of-freedom
EC8	Eurocode 8
EOM	Equation of motion
EW	East-west
FEM	Finite element method
IDR	Interstory drift ratio
NS	North-south
NTNU	The Norwegian University of Science and Technology

PGA	Peak ground acceleration
PGV	Peak ground velocity
PSV	Peak spectral velocity
PF	Participation factor
MDOF	Multiple-degree-of-freedom
SDOF	Single-degree-of-freedom
SRSS	Square-root-sum-of-squares
SSI	Soil-structure interaction

1 INTRODUCTION

This thesis is motivated by an ongoing discussion on the performance of high-rise structures in seismic areas where near-fault earthquakes may occur. Near-fault ground motion may cause undesirable response of tall structures which regular building provisions do not account for in the design procedure.

Norway is considered a low-seismicity area. However, looking back at historical earthquakes, the city of Oslo was affected by a magnitude 5.4 earthquake in 1904 that caused widespread minor damage. The earthquake occurred around 100 km south of Oslo within the Permean rift structure that runs in the north-south direction along the Oslo fjord. Deep clay deposits under the city led to soil amplification of the seismic waves resulting in severe damage on structures [1]. It is not unlikely that a similar event may happen again; either at the same location or even closer to the city center. Today all buildings in Norway have to be designed according to the Eurocode 8 provision. Buildings built before the Eurocode 8 provision became operative were not designed for taking seismic hazard into account. A structure exposed to strong ground motions may contract large forces and deformations if the ground motion is near-fault. The Permean rift structure makes Oslo an area where near-fault ground motion is likely to occur. The clay deposits may also lead to soil amplification. For this reason, the effects of near-fault ground motion on structures need special attention for this area.

Westergaard [2] described in 1933 that external loads caused by pulse excitations, typically loads from blasts or near-fault earthquakes, causes a wave of deformations that travels through the building. Such waves gets reflected at the top, returns to the base, gets reflected again and this goes on until the energy from the wave is absorbed in the building and dies out. High-rise structures are in particular vulnerable to such pulse excitations. Due to the reflection of the deformation waves displacements at the top of the buildings gets amplified. Deformations at intermediate stories of high-rise structures may also occur depending on the duration of the pulse relative to the fundamental period of vibration of the building. Near-fault ground motion may cause pulse-like excitations leading to the concern that underlies the objective of this thesis.

The objective of the presented research is to create and calibrate a numerical finite element (FE) model of a high-rise structure located in the seismic environment of Oslo. Furthermore the objective is to estimate and evaluate the dynamic behavior and response of the high-rise structure to strong ground motion, with emphasis on near-fault ground motion. Analyzing the soil-structure interaction to get the best possible representation of the foundation is emphasized.

In the work of this thesis the second tallest building in Norway, Oslo Plaza, is studied. The building is modeled in the structural analysis program SAP2000. The seismic response of the structure with emphasis on important damage parameters of special concern for tall structures is subject for investigation. To represent the strong ground

motion adequately, simulations and modifications of ground motion data will be carried out.

This thesis is divided into 9 chapters and 10 appendices. In the following a short presentation of each chapter is introduced.

Chapter 2 gives an introduction of the theoretical background. Earthquakes with emphasis on near-fault earthquakes are introduced first, before the fundamental procedure for analyzing earthquake response is presented. The theory behind soil-structure interaction and important ground motion parameters used in the work of the thesis are presented last.

Chapter 3 provides a presentation of the numerical FE-model including the soil-structure interaction representation. Results of the modal analysis are presented along with an estimation of the first two natural vibration periods of the structure.

Chapter 4 describes the simulation and the performance of the structural monitoring process along with results from the measurements.

Chapter 5 presents the different methods of analyses performed in this study along with the description of the strong ground motion data that forms the basis for the analyses. The procedures for modification of data are presented. The chapter ends with a discussion of different methods of scaling of ground motion.

Chapter 6 provides the presentation and interpretation of the results of the analyses performed.

Chapter 7 contains evaluation of the results obtained in Chapter 6 for the structure considered with focus on interstory drift and P-Δ effects, the importance of foundation type and the difference between near-fault and far-fault earthquakes regarding structural response.

Chapter 8 summarizes the observations made throughout the work of the thesis.

Chapter 9 provides suggestions for further work.

2 THEORETICAL BACKGROUND

This chapter gives a brief introduction to the theory applied in this thesis. The theory behind near-fault earthquake motions and its influence on high-rise structures includes several important fields of engineering. Extensive literature is to be found within this area. The subjects do not cover all the theory in detail, but presents the fundamental principles and theory. The first section covers a brief introduction of earthquakes. This is followed by an explanation of near-fault ground motions versus far-fault ground motions and an investigation of how to represent near-fault ground motion. Further, the theory of earthquake response by modal analysis is covered before an extensive description of soil-structure interaction (SSI) is presented. Last, ground motion parameters including the presentation of white noise are explained.

It is assumed that the reader has knowledge about structural dynamics, structural monitoring of buildings and processing of data obtained from this procedure including various theoretical methods applied. However, basic terms and procedures will be explained during the presentation of this work.

2.1 EARTHQUAKES

The essential background and understanding of why earthquakes occur comes from the knowledge of the physical structure of the earth. A large earthquake will produce enough energy to cause measurable shaking in a number of points around the world. The different types of seismic waves will reflect and refract at the boundaries between the different layers, reaching the surface by different paths. The earth consists of six continental-sized plates and about 14 subcontinental plates [3]. There are three distinct types of plate boundaries; divergent, convergent and transform plate boundary.

Tectonic earthquakes occur where it is sufficient stored elastic strain energy to cause fracture propagating along a fault plane. As relative movement of the plate occurs, elastic strain energy is stored in the materials near the boundary as shear stresses increase on the fault planes that separate the plates. When the shear stress reaches the shear strength of the rock, the rock fails and the energy is released. This release of energy is experienced as an earthquake [3]. Earthquakes may also occur within the plates but the magnitude of such earthquakes is often moderate.

An earthquake produces different types of seismic waves: body waves and surface waves. Body waves can be classified as P-waves and S-waves. P-waves involve successive compression and rarefaction of the medium. P-waves can travel through both fluids and solids. S-waves cause shearing deformations as they travel through a material. Since fluids have no shear stiffness they cannot sustain S-waves. The stiffness of the material will affect the speed the body waves travel in. Since geotechnical materials are stiffest in compression P-waves travel faster than the other seismic waves

and are the first to arrive at a particular site [4]. Figure 2-1 and figure 2-2 illustrates body waves.

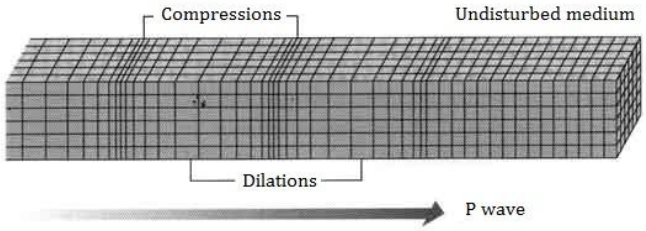

Figure 2-1: Illustration of a P-wave [5].

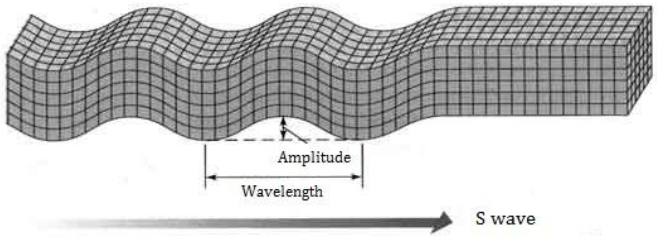

Figure 2-2: Illustration of an S-wave [5].

Surface waves results from interaction between body waves and the surface. They travel along the surface of the earth with amplitudes that decrease almost exponentially with depth. The surface waves are more prominent at distances farther away from the source of the earthquake. At a distance greater than about twice the thickness of the crust of the earth the surface waves will produce the peak ground motion [3].

To describe the location of an earthquake, it is necessary to use accepted terminology as shown in figure 2-3. The point in the fault where the rupture that leads to an earthquake begins and the point from where the first seismic waves originate is called the focus or hypocenter. The focus is located a focal depth beneath the surface and the point on the surface directly above the focus is called the epicenter. The distance between a site and the epicenter is called epicentral distance and the distance between the site and the focus is known as hypocentral distance [3].

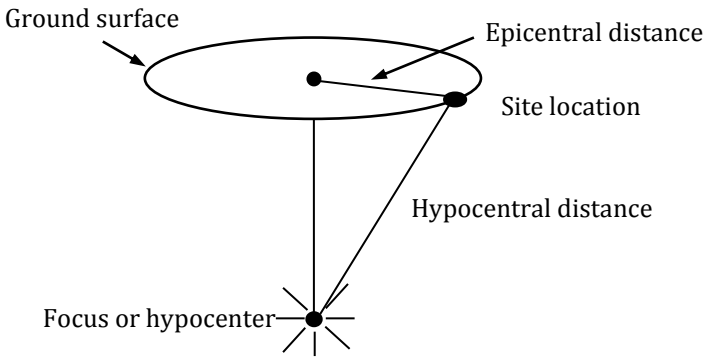

Figure 2-3: Notation for the description of earthquake location.

An earthquake releases large amounts of energy. To avoid large numbers in the description of the size of the earthquake, magnitude scales are used. The magnitude scale is logarithmic due to the large spread in earthquake size. Different types of magnitude scales exist, and the two most common are described here.

The Local Magnitude scale, M_L, was developed by Charles Richter. This magnitude scale is not suited to measure earthquakes with magnitude 7.5 or larger, or which is located more than 1000 km away from the point of measure [4], [3]. This magnitude scale is defined as

$$M_L = \log_{10} A_{ta}(\Delta) - \log_{10} A_{0,ta}(\Delta) \tag{2.1}$$

where A_{ta} is the maximum trace amplitude at a distance Δ, Δ is the epicentral distance and $A_{0,ta}$ is the standard trace amplitude at 100 km from the epicenter.

The Moment Magnitude scale, M_w, is the most correct measure of earthquake magnitude. This is a scale based on the seismic moment which is a direct measure of the factors that produce rupture along the fault [3]. This magnitude scale is defined as

$$M_w = \frac{2}{3}\log_{10} M_0 - 10.7 \tag{2.2}$$

$$M_0 = \mu_r A D_{fault} \tag{2.3}$$

M_0 is defined as the seismic moment, μ_r is the shear strength of fractured rock, A is the area of the fault and D_{fault} is the average displacement of the fault. The Moment Magnitude scale is often used today as it represents the magnitude in the best way for comparison between earthquake magnitudes.

2.2 NEAR-FAULT EARTHQUAKES

The energy released in an earthquake is stored strain energy in the volume around a fault surface. When fault rupture occurs in close vicinity to the place in question we call it near-fault. The epicentral distance that defines a near-fault earthquake is often in the range of 10 – 30 km.

Near-fault earthquakes can lead to severe damage as was seen in the 1994 Northridge, California earthquake, the 1995 Kobe earthquake and 1999 Chi-Chi earthquake. Near-fault earthquakes have unique characteristics which are found to impose greater strength demand than far-fault records. This has led to more attention around near-fault earthquakes in recent years. In this section the important characteristics of near-fault earthquakes and far-fault earthquakes and the difference between these two types of ground motions are presented.

2.2.1 *IMPORTANT CHARACTERISTICS OF NEAR-FAULT EARTHQUAKES*

Ground motions recorded within the near-fault region of an earthquake at stations located towards the direction of the fault rupture are qualitatively quite different from far-fault earthquake ground motions [6]. The main difference between near-fault and far-fault earthquakes is that near-fault earthquakes are dominated by one or few strong pulses. In a near-fault earthquake the seismic energy is concentrated in one or a few cycles that causes high lateral displacement demands on engineering structures. The large deformation demands this cause on fixed-base and base-isolated buildings have been of special concern [6].

Strong ground motions in the vicinity of a fault contain a strong long-period velocity pulse with high energy input. Far-fault ground motions are normally broad-frequency-banded, containing a wider variety of frequencies than near-fault ground motions. An earthquake is started by a shear dislocation in a point on a fault and then spreads with a velocity close to the shear wave velocity [7]. This propagation of fault rupture causes most of the seismic energy to be represented in a single large pulse shown early in the ground motion records. Ground motion pulses from near-fault earthquakes are stronger in the direction the fault propagates [8]. The radiation pattern of shear dislocations causes the large pulse motion to be oriented perpendicular to the fault plane [7]. As a result the fault-normal component normally imposes a larger deformation and strength demand over a wide range of vibration periods than the fault parallel component. This difference is not found for far-fault earthquakes [6]. The difference in deformation and strength demand between the fault-normal and fault-parallel component for near-fault earthquakes are primarily caused by the difference in peak ground acceleration, velocity and deformation. Figure 2-4 illustrates the difference in the ground motion acceleration for the 1976 Friuli earthquake. Here, the north-south (NS) component and the east-west (EW) component representing the fault-parallel and fault-normal component of the earthquake are plotted.

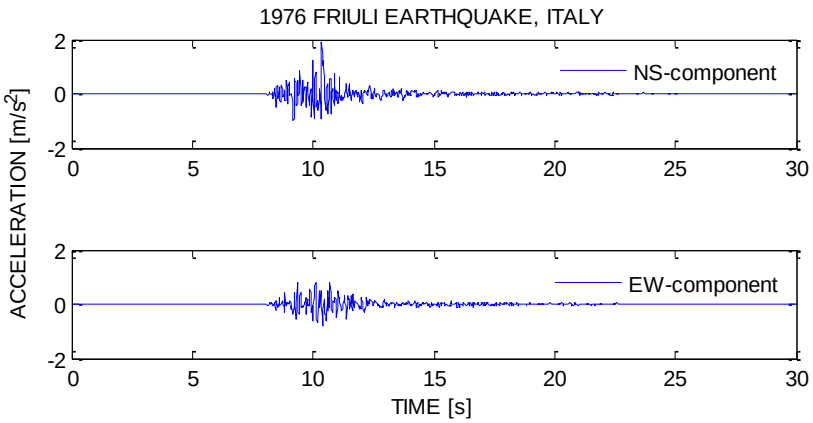

Figure 2-4: Ground motion acceleration plots for the two components of the 1976 Friuli earthquake.

This difference is important to take into account when analyzing the response of a structure to a near-fault record. Switching the direction of the record with respect to the

main axis of the structure may be of importance for the seismic response of the structure considered. The worst case situation should be investigated.

The fault-parallel component often has a larger amplification factor when the response spectra are normalized with respect to peak ground acceleration, velocity and deformation. The amplification factor increases with the number of cycles. Since the fault-normal component of a near-fault earthquake is dominated by one cycle of large ground velocity whereas the fault-parallel component often contains several, the former gets a smaller amplification factor. This difference is not found for far-fault earthquakes [6].

When using observed data from both near-fault and far-fault earthquakes to construct response spectra it is found that the velocity sensitive region for near-fault ground motion is much narrower and the acceleration-sensitive and displacement-sensitive region much wider compared to far-fault ground motion. The narrow velocity-sensitive region is also shifted to longer periods for near-fault ground motions. This is illustrated in figure 2-5 by tri-partite plots [6].

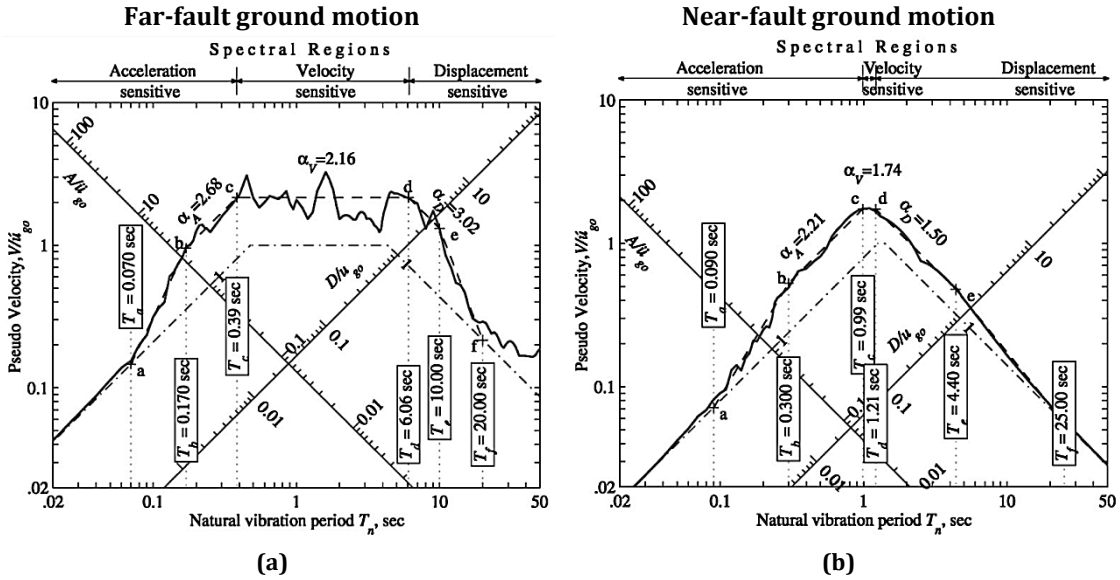

Figure 2-5: Response spectra for fault normal components in tri-partite plots [6]. (a) Far-fault ground motion, the 1952 Kern County earthquake. (b) Near-fault ground motion, the 1994 Northridge earthquake.

Observations show that for near-fault ground motions $\dot{u}_{g0}/\ddot{u}_{g0}$ are typically much larger and $u_{g0}/\dot{u}_{g0}$ much smaller compared to far-fault motions [6]. Here, u_{g0}, $\dot{u}_{g0}$ and $\ddot{u}_{g0}$ are the displacement, velocity and acceleration of the ground respectively.

During an earthquake a structure is allowed to undergo plastic deformations and the yield strength required, f_y, is therefore less than the minimum strength required for the structure to remain elastic, f_0. This leads to the definition of a reduction factor

$$R_y = \frac{f_0}{f_y} \tag{2.4}$$

This reduction factor depends on the ductility factor μ which represents the maximum ductility a structure can sustain without resulting in unacceptable consequences or fracture [9]. μ is a property of the structure alone while the reduction factor also depends on the earthquake record. R_y approaches 1 at very short natural vibration periods and R_y approaches the ductility factor at very long natural vibration periods for both near-fault and far-fault earthquakes [6].

Earthquake records show that in the acceleration-sensitive region the strength reduction factor for near-fault ground motions is systematically and significantly smaller compared to far-fault ground motions. For a given ductility factor a near-fault ground motion will therefore impose a larger strength demand than a far-fault ground motion, with both demands expressed as a fraction of their respective elastic demands. This lead to the concern that strength reduction factors based on far-fault motion used today may be non-conservative for short period structures, and worst case scenario is that this can lead to structural damage and human injury. When the natural vibration period of the structure, T_n, is normalized with the period where the motion shifts from acceleration-sensitive to velocity-sensitive, T_c, the difference almost disappears. The difference in T_c can therefore explain much of the difference in the reduction factor for short-period structures. Investigation also shows that the ratio between peak deformation of an inelastic system and the corresponding elastic system for near-fault motion is systematically and significantly larger than for far-fault motions. As a result the peak deformation of inelastic systems may be underestimated. This difference is also primary caused by the difference in T_c for the two types of excitation. Recognizing this connection it is possible to derive design equations for R_y that explicitly use the spectral regions. In this way the same set of equations can be used for different ground motions [6].

A study by Rupakhety et al. [10] was aimed at quantifying ground-motion parameters and response spectra in the near-fault region. A large number of recorded near-fault ground motion data were collected and studied, with special emphasis on forward-directivity effects. Properties of elastic response spectra of forward-directivity affected near-fault ground motion were investigated and a model to estimate mean spectral shapes to such ground motions was proposed. The model is a continuous function of the undamped natural period of single-degree-of-freedom (SDOF) oscillators, and its parameters are magnitude dependent. Several of the parameters in the model were shown to be dependent on earthquake size, and the number of free variables could be reduced. The available data for the study were not sufficient to constrain an empirical model to estimate peak ground velocity (PGV) as a function of earthquake magnitude and source-to-site distance, but a weak dependence of PGV on moment magnitude was observed.

2.2.2 *REPRESENTATION OF NEAR-FAULT GROUND MOTION*

It has been observed that dominant pulses in the velocity records of near-fault ground motions resemble simple waveforms which can be represented by analytical expressions. Commonly used waveforms are simple triangular pulses, square waves, sine waves and wavelets of different types [10]. By evaluation of both the elastic and inelastic response of a SDOF system caused by rectangular, triangular and ramp-like pulses, it has been found that the two most important parameters controlling the peak elastic response are the pulse amplitude and pulse duration relative to the period of vibration of the SDOF system [8]. The amplitude of the pulse is representative of the PGV and the pulse period is linearly related to the seismic moment. Studies have shown that the pulse period is also closely related to the SDOF period where the peak spectral velocity (PSV) attains its maximum value. If the pulse were simple and harmonic with infinite duration, the PSV would occur exactly at the pulse period. The near-fault velocity pulses however have finite duration, defined by the pulse period and number of half-cycles. The period where the PSV reaches its maximum will therefore be a fraction of the pulse period. The fraction depends on the number of half-cycles of the pulse [10].

The simple pulse models mentioned are capable of accurately predicting the peak response of a SDOF system at long periods. It is found that a simple pulse model can capture the peak response of a SDOF system if its undamped natural period of vibration is greater than about 0.7 times the period of the pulse [8]. If the SDOF system has a period shorter than 0.7 times the pulse period, the peak response of a SDOF system will typically be larger than that to an equivalent pulse fitted to it. It is in general accepted that simple pulses can be used to estimate peak response of long period SDOF systems to near-fault ground motion. It has further been assumed that simple pulses can represent the response of a multiple-degree-of-freedom (MDOF) system if the pulse adequately describes the first mode response of the system. This assumption may not always be correct. Tall buildings respond in multiple modes of vibration in contrast to shorter structures where the first mode of vibration is the predominant one. The simple pulse model may be adequately accurate for short structures as it does not contain higher frequencies that can capture the higher modes of vibration. This may not be the situation for how tall structures respond [8].

To represent near-fault earthquakes correctly when analyzing structural response of tall structures it is important to study both how well simple pulses capture the peak response and whether or not high modes of vibration are important in the total response. This has been done by Rupakhety and Sigbjörnsson [8]. They used structural models of a single-bay generic steel moment resisting frames (SMRF) of 9, 12, 15 and 18 stories and ground motion records from a near-fault ground motion database. Only records with a clear and dominant pulse in their velocity time-series were considered. The study used the interstory drift ratio (IDR) as the response parameter of interest. IDR serves as an important indicator of damage for tall structures subjected to strong

ground motions. It is also a parameter related to the story shears and describes local damage at the story level. IDR is defined as follows

$$IDR(j,t) = \delta_j = \frac{\Delta u}{h} \cdot 100\ \% \tag{2.5}$$

where h is the height between floor j and $j-1$. t is the time when the interstory drift value occurs in the time-series. Δu is defined as the difference in displacement between the two floors considered

$$\Delta u = u_j - u_{j-1} \tag{2.6}$$

The maximum interstory drift at story j is given by

$$IDR_{max}(j) = max|IDR(j,t)| \tag{2.7}$$

Equivalent pulses were fitted to the ground motion records. An investigation of the IDR for a specific earthquake and the IDR at the roof for several earthquakes was performed. The height-wise distribution of interstory drift was also investigated. Figure 2-6 shows the results found for an 18 story single-bay generic SMRF. The IDR is plotted against height normalized by total frame height. The black, gray and white bars represent the contribution of the first, second, and third modes respectively. Maximum IDR for all modes of vibration is shown as a solid line for the actual record and a dashed line for the equivalent pulse [8].

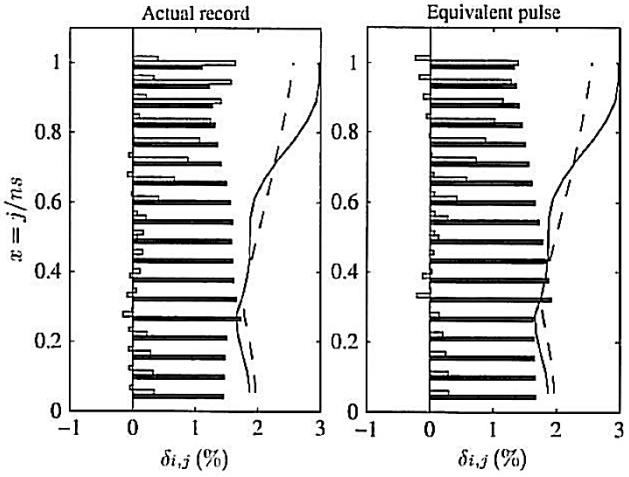

Figure 2-6: 18 story single-bay generic steel moment resisting frame [8].

As can be seen from figure 2-6 the higher mode contributes significantly to maximum interstory drift of tall frames subjected to near-fault ground motions. The importance of the higher modes is significant in the upper portion of the frame as the frame gets taller. The maximum IDR strongly depends on the ratio between the fundamental period of vibration and the pulse period. It is shown that the largest interstory drift demand occurs when the fundamental period of the frame is close to the pulse period. The

simple equivalent pulses used were not able to adequately simulate the higher modes of vibration for all structures. The study showed that on average the elastic IDR for the equivalent simple pulses were 1.4 times smaller than when an actual near-fault ground motion record was used.

If a simple pulse is going to adequately simulate the interstory drift demand of a tall frame, the fundamental period of the frame has to be at least 1.5 times the pulse period. Structures that will be most affected by the earthquake will be those whose fundamental period is close to the equivalent pulse period. For this reason, the simple pulse models might not be a good way to model pulse-like ground motion. These results only hold for elastic structures and cannot be extended to inelastic structures. In inelastic structures the relative importance of the different modes will be different from those in the elastic structure. This difference comes from both the development of ductility in the structural members and the lengthening of vibration period due to inelasticity. The initial elastic period of the building relative to the pulse period and the maximum ductility allowed in the structure will play an important role [8].

For near-fault earthquakes the response spectrum based on far-fault records may lead to underestimation of forces and displacement in the structure. A better approximation to render results is obtained by using the simple pulse model. However, neither of these methods renders an adequate representation of the strong ground motion for high-rise structures. However, the importance of considering these methods performed in research is inevitable. A reasonable approach is to use existing records of near-fault ground motion and scale the records appropriately. The question whether or not existing records obtained from other locations truly can represent a near-fault earthquake at the given site is important. If a thorough analysis of the fault parameters at the given site is performed, this may be done. An average of several near-fault ground motion records may be used to render results as well. In addition, by simulation to generate new near-fault ground motion records, the representation to analyze tall structures for possible new near-fault earthquakes may be adequate. This will be subject of investigation in the preceding chapters.

2.2.3 ASSESSMENT OF EARTHQUAKE RISK IN THE OSLO REGION

Oslo, the capital of Norway, is located in a low-seismicity area within an aborted Permean rift structure that runs in the north-south direction of the Oslo fjord, see figure 2-7(a). During the last glaciation large parts of the Oslo area were submerged and the sea-level change and land uplift that followed left areas with deep clay deposits. The sediment thicknesses vary dramatically over short distances due to the high relief of the basement rocks. The clay deposits are characterized as soft soils [1]. The Oslo rift zone consists of granites and magmatic rocks. The south-eastern part of the rift zone is tilted approximately 3 km vertically and is filled with lithified sediments. Deformed gneisses largely constitute the area outside the rift zone. The rift boundary fault follows a north-

south trend, and the main eastern rift boundary can be traced as the eastern boundary fault of the city of Oslo.

It has not been recorded any considerably damaging earthquakes in Oslo to date, but historical records do show some concentration of seismic activity along the rift. Earthquakes of moderate size with magnitude between 3 and 4 are felt in the region every 3-4 years, see figure 2-7 (b). Studies by Molina and Lindholm [1] have shown that rift structures are sites for infrequent large earthquakes that are not easily predicted based on background seismicity. According to these studies the rift zone considered is capable of generating an earthquake with magnitude larger than 6. An earthquake with magnitude of 4.7 is reported to have occurred in 1647. The last major earthquake was in 1904 as mentioned above. The occurrence of the 1904 earthquake led to the installation of the first seismometer in Norway. The focal depth has more recently been estimated to 28 km [1].

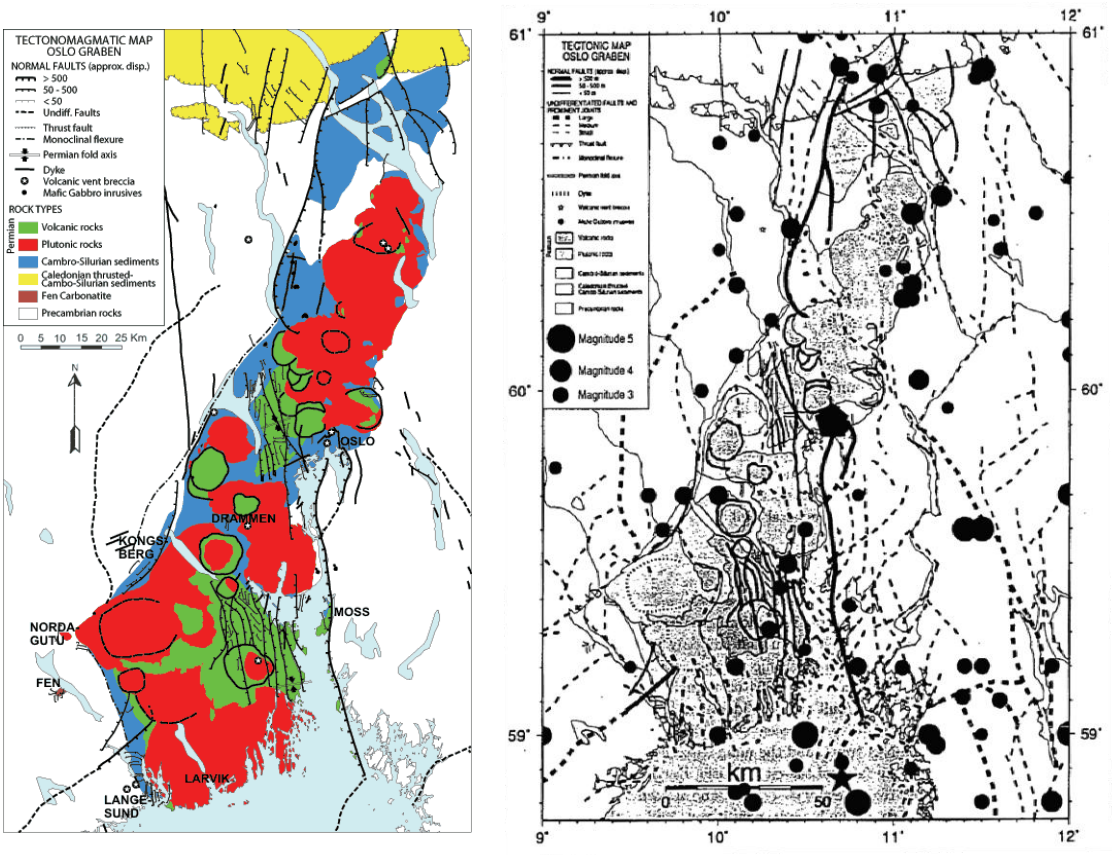

(a) **(b)**

Figure 2-7: Overview of the Oslo Rift zone. (a) Tectonomagmatic map of the Oslo region. (b) Earthquakes and geology of the Oslo Rift zone [1].

NORSAR and NGI [11] carried out a regional study in 1998 to estimate the seismic hazard for the Oslo region. The peak ground acceleration at a 0.002 annual exceedance frequency, i.e. a 500 year return period, was found to be 0.4 - 0.5 m/s^2. A normalized elastic response spectrum at 5% damping was computed probabilistically for the given

return period and is used in the national appendix of Norway in the Eurocode 8, hereafter referred to as EC8.

Molina and Lindholm [1] conducted a seismic risk scenario for Oslo including soil amplification and building classifications with two earthquake sources; one very close to the city and one near the 1904 epicenter. Both scenarios exhibit strong dependencies on the soft clay underlying large part of Oslo. The risk scenario indicates that as much as 45% of the buildings would be damaged if a magnitude 6 earthquake would occur on the eastern rift boundary fault near Oslo. Not all buildings could be categorized and these are probably many of the poorest structures so that the 45% estimate is non–conservative. This does not include secondary damages such as fires and liquefaction as a result of the earthquake. The study strongly indicates the importance of conducting analyses of certain types of buildings that might be exposed to earthquakes of magnitude 6 or larger such as near-fault earthquakes might cause.

2.3 Analyzing Earthquake Response

The modal analysis implemented in a finite element approach is the fundamental procedure used in structural analysis programs to perform seismic analyses of structures. This forms the fundamental procedure for analyzing earthquake response. The modal response to earthquake loading and the forming of response spectra is presented here.

2.3.1 Modal response to earthquake loading

Modal analysis is a procedure commonly used to determine the dynamic response of a structural system. It is a method restricted to linear systems with classical damping properties [12]. In the following the theory of modal response to earthquake loading is presented, and the essential theory is taken from Chapter 13 by Chopra [12] and lecture notes from structural dynamic courses [13].

For a multi-degree-of-freedom (MDOF) system subjected to a time varying load the equation of motion may be formulated as follows:

$$\mathbb{M}\ddot{\mathbb{v}} + \mathbb{C}\dot{\mathbb{v}} + \mathbb{K}\mathbb{v} = \mathbb{P}(t) \tag{2.8}$$

Here $\mathbb{M}$ represent the mass matrix, $\mathbb{C}$ the damping matrix and $\mathbb{K}$ the stiffness matrix of the system. $\mathbb{v}$, $\dot{\mathbb{v}}$ and $\ddot{\mathbb{v}}$ describes displacement, velocity and acceleration of the structure and $\mathbb{P}(t)$ is the time varying loading. The displacement describes the total displacement of the structure measured to some fixed origin. The movement relative to the ground is not applicable in earthquake engineering since the ground itself is moving. The total displacement is therefore represented as a combination of the ground displacement and the displacement of the structure relative to the ground:

$$\mathbb{v} = \mathbb{u} + \mathbb{T}u_g(t) \tag{2.9}$$

$\mathbb{T}$ is an influence matrix also termed strain matrix, derived from the shape functions used in the finite element formulation. u_g is ground motion displacement.

Only the relative motions $\mathbb{u}$ between the masses and the base due to structural deformations produce elastic forces and damping forces. Furthermore, if the system is affected by an earthquake and if it is assumed that earthquake action is induced by a tri-axial acceleration record acting simultaneously at all foundation degrees-of-freedom, combining eq. (2.8) and eq. (2.9) the equation of motion becomes:

$$\mathbb{M}\ddot{\mathbb{u}} + \mathbb{C}\dot{\mathbb{u}} + \mathbb{K}\mathbb{u} = \mathbb{P}(t) - \mathbb{M}\mathbb{T}\ddot{u}_g(t) \tag{2.10}$$

$-\mathbb{M}\mathbb{T}\ddot{u}_g$ can be treated as the effective earthquake load. Here, $\ddot{u}_g$ is the tri-axial ground acceleration record the system is exposed to given as a 3×1 column vector, $\mathbb{T}$ is the $n \times 3$ influence matrix (n being the number of degrees-of-freedom). $\mathbb{M}$ is the $n \times n$ mass matrix of the discretized system. The ground motion may be obtained from specific ground motion acceleration data or through the concept of response spectra.

Taking the equation of undamped free vibration and assuming simple harmonic motion

$$\mathbb{u} = \boldsymbol{\Phi}_i Y_i \sin \omega_i t \tag{2.11}$$

the equilibrium equation becomes:

$$-{\omega_i}^2 \mathbb{M}\boldsymbol{\Phi}_i + \mathbb{K}\boldsymbol{\Phi}_i = 0 \tag{2.12}$$

where $\boldsymbol{\Phi}_i$ and ω_i are the ith mode and frequency of free vibration respectively. The n vectors in $\boldsymbol{\Phi}_i$ form a basis set of vectors in that any vector in the n dimensional space may be obtained as a combination of the mode shapes:

$$\mathbb{u} = \boldsymbol{\Phi}\mathbb{Y} \tag{2.13}$$

$\mathbb{Y}$ is the modal amplitude and $\boldsymbol{\Phi}$ is the modal matrix. Each column in the modal matrix represents a mode shape.

Combining eq. (2.10) and eq. (2.13) and premultiplying with $\boldsymbol{\Phi}^T$ results in:

$$\boldsymbol{\Phi}^T\mathbb{M}\boldsymbol{\Phi}\ddot{\mathbb{Y}} + \boldsymbol{\Phi}^T\mathbb{C}\boldsymbol{\Phi}\dot{\mathbb{Y}} + \boldsymbol{\Phi}^T\mathbb{K}\boldsymbol{\Phi}\mathbb{Y} = -\boldsymbol{\Phi}^T\mathbb{M}\mathbb{T}\ddot{u}_g(t) \tag{2.14}$$

where

$$\boldsymbol{\Phi}^T\mathbb{M}\boldsymbol{\Phi} = \mathbb{M}^* \tag{2.15}$$

$$\boldsymbol{\Phi}^T\mathbb{C}\boldsymbol{\Phi} = \mathbb{C}^* \tag{2.16}$$

$$\boldsymbol{\Phi}^T \mathbb{K} \boldsymbol{\Phi} = \mathbb{K}^* \tag{2.17}$$

$$\boldsymbol{\Phi}^T \mathbb{M} \mathbb{T} = \mathbb{L}^* \tag{2.18}$$

By doing this the uncoupled set of equations are obtained:

$$\mathbb{M}^* \ddot{\mathbb{Y}} + \mathbb{C}^* \dot{\mathbb{Y}} + \mathbb{K}^* \mathbb{Y} = -\mathbb{L}^* \ddot{u}_g(t) \tag{2.19}$$

The system can be represented as n uncoupled SDOF systems:

$$M_i^* \ddot{Y}_i + C_i^* \dot{Y}_i + K_i^* Y_i = -L_i^* \ddot{u}_g(t) \quad i = 1,2, \ldots . n \tag{2.20}$$

The second order ordinary differential equation is obtained by dividing through by M_i^*. Thus, for each mode i:

$$\ddot{Y}_i + 2\zeta_i \omega_i \dot{Y}_i + \omega_i^2 Y_i = \frac{-L_i^*}{M_i^*} \ddot{u}_g(t) \tag{2.21}$$

ζ_i is the damping ratio of the ith mode, and is defined as

$$\zeta_i = \frac{C_i^*}{2 M_i^* \omega_i} \tag{2.22}$$

The participation factor for the ith mode is defined as:

$$PF = \frac{L_i^*}{M_i^*} = \frac{\boldsymbol{\Phi}_i^T \mathbb{M} \mathbb{T}}{\boldsymbol{\Phi}_i^T \mathbb{M} \boldsymbol{\Phi}_i} \tag{2.23}$$

The magnitude and unit of the participation factor will depend on the type of normalization used for the mode shapes. However, the effect of this does not have any consequence for the actual response of the system found in the end. The participation factor defines how much each mode contributes to the response of the system.

The second order equation, eq. (2.20), for each mode can be solved using the Duhamel Integral

$$Y_i(t) = \frac{-L_i^*}{M_i^*} \frac{1}{\omega_i} \int_0^t \ddot{u}_g(\tau) e^{-\zeta_i {\omega_i}^2 (t-\tau)} \sin \omega_D (t-\tau) \, d\tau \tag{2.24}$$

$$i = 1,2, \ldots , n$$

or by step-by-step integration schemes such as the Newmark method. When the modal amplitudes are found the total displacement of the structure is found using eq. (2.13).

A convenient way to determine the dynamic forces in the structure is to use modal analysis. By performing a static analysis of the structure subjected to external forces, and a dynamic analysis of the nth-mode SDOF system excited by a dynamic force, combining the modal responses will render the dynamic response of the structure.

The forces acting on the structure, $\mathbb{F}$, more precisely the nodal forces, are obtained from the displacement

$$\mathbb{F} = \mathbb{K}\mathbb{u} = \mathbb{K}\boldsymbol{\Phi}\mathbb{Y} \tag{2.25}$$

In the equation of undamped free vibration $\mathbb{K}\boldsymbol{\Phi}_i = {\omega_i}^2\mathbb{M}\boldsymbol{\Phi}_i$ it is possible to rewrite the last equations to obtain another expression of the force

$$\mathbb{F} = \mathbb{M}\boldsymbol{\Phi\omega^2}\mathbb{Y} \tag{2.26}$$

A static analysis of the structure can be used to obtain the member forces and member stresses once the nodal forces are found. Modern computer analysis can abstract the member displacements once $\mathbb{u}$ is known and thereby compute the member forces and stresses directly.

2.3.2 RESPONSE SPECTRA

A convenient way to obtain the maximum response such as displacement, velocity and acceleration, is to use generalized response spectra. Generalized response spectra are found in provisions such as EC8. A response spectrum is a plot of the maximum acceleration, velocity or displacement as a function of period for a SDOF system when subjected to an earthquake ground motion [14]. In the following, the definition of terms for response spectra evaluation is presented. The theory behind this is taken from Chopra [12], Clough and Penzien [5] and lecture notes from structural dynamic courses [13].

The pseudo spectral velocity, Sv, the pseudo spectral displacement, Sd, and the pseudo spectral acceleration, Sa, is defined by

$$Sv_i = \left[\int_0^t \ddot{u}_g(\tau) e^{-\zeta_i {\omega_i}^2 (t-\tau)} \sin \omega_{Di}(t-\tau)\, d\tau\right] max \tag{2.27}$$

$$Sd_i = \frac{1}{\omega_i} Sv_i \tag{2.28}$$

$$Sa_i = \omega_i Sv_i \tag{2.29}$$

These relationships use the equation of the undamped free vibration. The prefix pseudo stems from the fact that for the spectral velocity, the velocity term is used from the

definition of strain energy and not the peak relative velocity, $\dot{u}_0$. This has negligible effect and the prefix pseudo is only introduced as a formality. However, Sa differs, in most cases, from the actual maximum acceleration by only a few percent.

The maximum modal response $Y_{i,max}$ for the ith mode is defined as

$$Y_{i,max} = \frac{L_i^*}{M_i^*}\frac{1}{\omega_i}Sv_i = \frac{L_i^*}{M_i^*}Sd_i = \frac{L_i^*}{M_i^*}\frac{1}{\omega_i^2}Sa_i \tag{2.30}$$

The displacement and nodal forces is given by

$$\mathbb{u}_{i,max} = \boldsymbol{\Phi}_i Y_{i,max} = \boldsymbol{\Phi}_i \frac{L_i^*}{M_i^*}\frac{1}{\omega_i}Sv_i = \boldsymbol{\Phi}_i \frac{L_i^*}{M_i^*}Sd_i = \boldsymbol{\Phi}_i \frac{L_i^*}{M_i^*}\frac{1}{\omega_i^2}Sa_i \tag{2.31}$$

$$\mathbb{F}_{i,max} = \mathbb{K}\mathbb{u}_{i,max} = \mathbb{K}\boldsymbol{\Phi}_i Y_{i,max} = \mathbb{K}\boldsymbol{\Phi}_i \frac{L_i^*}{M_i^*}\frac{1}{\omega_i}Sv_i \tag{2.32}$$

$$\mathbb{F}_{i,max} = \mathbb{M}\boldsymbol{\Phi}_i \frac{L_i^*}{M_i^*}\omega_i Sv_i = \mathbb{M}\boldsymbol{\Phi}_i \frac{L_i^*}{M_i^*}Sa_i \tag{2.33}$$

Only the components in the direction of excitation will contribute to the base shear, $V_{i,max}$, in the same direction. It can be shown by using virtual work that these are selected by the influence vector, $\mathbb{T}$:

$$V_{i,max} = \mathbb{T}^T\mathbb{F}_{i,max} = \mathbb{T}^T\mathbb{M}\boldsymbol{\Phi}_i \frac{L_i^*}{M_i^*}Sa_i = \frac{(L_i^*)^2}{M_i^*}Sa_i \tag{2.34}$$

$\frac{(L_i^*)^2}{M_i^*}$ is the effective modal mass and has the units of mass [kg]. The effective modal mass express how much mass participates in each mode. It and can be used to define the effective weight

$$V_{i,max} = \frac{(L_i^*)^2}{M_i^*}g\left(\frac{Sa}{g}\right)_i = Effective\ Weight_i\left(\frac{Sa}{g}\right)_i \tag{2.35}$$

The sum of all the effective weights for a given influence vector $\mathbb{T}$ should equal the total weight of the structure.

Response spectra may be derived from a specific ground motion, or it may be derived from statistical analysis resulting in so-called uniform hazard spectra [12]. A response spectrum derived from a specific ground motion is often jagged, and is not suitable for design purposes. The uniform hazard spectra derived from statistical analyses are presented as smooth curves and straight lines, and is thus preferred for design purposes. The latter is what is most often used in building codes.

A response spectrum may be elastic or inelastic. The elastic spectrum is rarely used in design of buildings since it does not account for inelasticity in the structure. Buildings, with some exceptions, are not normally designed to resist earthquake forces in their elastic range, but may experience inelastic, permanent damage. The inelastic spectrum is scaled from the elastic spectrum by the use of a structural behavior factor, q. The behavior factor allows for ductility and energy dissipation of the structure. The energy dissipation capacity of the structure is equal to unity in the elastic response spectrum, and by assigning a value of $q > 1$ lower seismic forces to design for through an inelastic response spectrum is obtained. The scaled spectrum reduces the inelastic problem to an equivalent elastic one.

2.3.3 COMBINATION OF MODAL MAXIMA

The different modes will not obtain their maximum responses at the same instance. The response spectra only provide the maximum amplitude of the response, not the sign or time of the maximum. When mode i reaches its maximum response the response in the other modes are not known. In general

$$\mathbb{u}_{max} \leq \boldsymbol{\Phi}\mathbb{Y}_{\boldsymbol{max}} \tag{2.36}$$

To be able to use response spectra techniques for MDOF systems the modal quantities, R_i (base shear, nodal displacement, nodal forces, member stresses etc.) must be combined. The combinations are achieved using statistical methods. EC8 does not require R_i to be computed for all modes. However, EC8 [15], 4.3.3.3.1(3) states the following:

- The effective mass of the structure for the modes considered much reach 90% of the total mass of the structure.
- The analysis must include all modes with effective modal mass greater than 5% of the total mass.

Several methods for summing the response of the individual modes exist. The simplest way is to superpose all the different modes

$$R_{tot} = \sum_{i=1}^{n} R_i \tag{2.37}$$

This will render a conservative result since the different modes will not reach their maximum value at the same time.

A better approximation is the *square-root-sum-of-squares* (SRSS) rule for modal combination which may be used if all modal responses can be regarded as independent of each other

$$R_{tot} = \sqrt{\sum_{i=1}^{N} {R_i}^2} \tag{2.38}$$

The SRSS method implies that there is no correlation between the responses of the different modes. The maximum of each mode is then independent of the maximum in other modes. This is the case for two-dimensional structure analyses, but in three-dimensional structures different modes in different directions may have natural frequency of vibrations that are fairly close. When one of these modes is excited by an earthquake the other mode with a similar frequency is likely to be strongly excited as well. The SRSS rule is in this case shown to give non-conservative results for the estimation of the maximum response.

For three-dimensional analysis alternative modal combination methods have been proposed. The *complete quadratic combination* (CQC) rule for modal combination may be expressed on the form

$$R_{tot} = \sqrt{\sum_{i=1}^{N}\sum_{j=1}^{N} \rho_{ij} R_i R_j} \tag{2.39}$$

ρ_{ij} is the correlation coefficient between the two modes *i* and *j,* and R_i and R_j is the peak response of the two modes.

The CQC rule for modal combination is set to default in the structural analysis program SAP2000. Here, the correlation factor is defined as

$$\rho_{ij} = \frac{8\sqrt{\zeta_i \zeta_j}(\beta_{ij}\zeta_i + \zeta_j){\beta_{ij}}^{3/2}}{(1-{\beta_{ij}}^2)^2 + 4\zeta_i\zeta_j\beta_{ij}(1+{\beta_{ij}}^2)^2 + 4(\zeta_i^2 + \zeta_j^2){\beta_{ij}}^2} \tag{2.40}$$

where

$$\beta_{ij} = \frac{\omega_i}{\omega_j} \tag{2.41}$$

is the frequency ratio between mode *i* and *j*. The correlation coefficient depends on the damping and for a structure with no damping ρ_{ij} will become zero and the CQC rule becomes the SRSS rule for modal combination.

When the modal results are combined it is important that the combination is used for the required response only, for instance axial force or bending moment. To exemplify; the bending moment should not be found by computing the maximum story shears for then again to render bending moments. The correct way is by combining the maximum bending moments in each mode. This is important to emphasize.

2.4 SOIL-STRUCTURE INTERACTION (SSI)

The importance of local soil properties on the earthquake response of structures have been illustrated by numerous earthquakes through the years. Geotechnical factors can have a strong influence on the performance of structures during earthquakes, and this is a field of engineering of great importance. To be able to determine the free-field earthquake motions for a given structure, a site-dependent dynamic response analysis for the given foundation is necessary. This can, in many cases, be the most important step in the earthquake resistant design of any structure.

There are two primary ways geotechnical materials influence the damage on structures caused by earthquakes [16]

- Amplification or attenuation of seismic waves caused by the geotechnical materials.
- Permanent deformations of mass of soil through ground failure (settlement or landslide).

Geotechnical material represents all types of soil. The geotechnical materials can be represented as classified in EC8 for design purposes, and are stated in table 2-1 [15].

Table 2-1: Geotechnical materials as classified in EC 8 [15].

GROUND TYPE	DESCRIPTION OF STRATIGRAPHIC PROFILE	SHEAR WAVE VELOCITY [m/s] $v_{s,30}$	SHEAR STRENGTH [kPa] c_u
A	Rock or rock-like geological formation, including at most 5 m of weaker material at the surface.	> 800	-
B	Deposits of very dense sand, gravel or very stiff clay, at least several tens of metres in thickness, characterised by a gradual increase of mechanical properties with depth.	360 - 800	> 250
C	Deep deposits of dense or medium dense sand, gravel or stiff clay with thickness from several tens to many hundreds of metres.	180 - 360	70 - 250
D	Deposits of loose-to-medium cohesionless soil (with or without some soft cohesive layers), or of predominantly soft-to-firm cohesive soil.	< 180	< 70
E	A soil profile consisting of a surface alluvium layer with v_s values of type C or D and thickness varying between about 5 m and 20 m, underlain by stiffer material with v_s > 800 m/s.		
S_1	Deposits consisting, or containing a layer at least 10 m thick, of soft clays / silts with a high plasticity index (PI > 40) and high water content.	< 100 (indicative)	10 - 20
S_2	Deposits of liquiefiable soils, of sensitive clays, or any other soil profile not included in types A - E or S_1.		

The two primary ways mentioned above may cause significant damage on structures, and it must be considered in a seismic hazard evaluation.

Soil-Structure Interaction (SSI) evaluates the total response of the linked systems of the structure, the foundation and the geologic media in contact with the foundation for a specified free-field ground motion [16]. It can be defined as the process in which the response of the soil influences the motion of the structure and the motion of the structure influences the response of the soil [17].

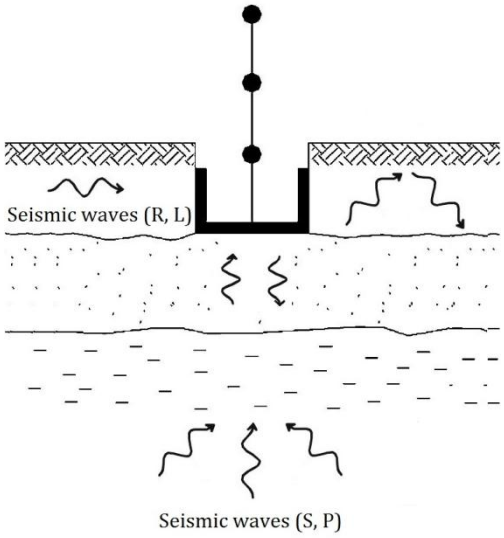

Figure 2-8: Illustration of SSI on the structure response [18].

An illustration of SSI on the structure response is shown in figure 2-8. The soil layers away from the structure are subjected to seismic excitation consisting of numerous incident waves; shear waves, dilatational waves and surface waves. The nature of these waves is determined both by the seismological conditions and the geometry, stiffness and damping of the soil deposits. This motion is called the free-field motion at the site of the foundation. Around the structure and its foundation the seismically deforming soil will force the embedded foundation to move, and subsequently the supported structure. The foundation has different rigidity from the soil which would lead the motion of the foundation to be different from the free-field motion even without the structure. The motion induced at the foundation level generates oscillations in the superstructure which develop inertia forces and overturning moments at its base. Thus, the foundation and the surrounding soil will experience additional dynamic forces and displacements [19].

Structures founded on bedrock can be analyzed assuming that their base is fixed, but this assumption can be non-conservative when the restraint of the structure is less than rigid. Soil flexibility will increase the structural period which in turn will reduce the response when using acceleration design spectra that decrease monotonically with increasing structural period. The cyclic movement of the soil in contact with the foundation of the structure causes energy to be radiated away from the structure, tending to reduce its motion. This is known as radiation damping. These effects lead to the conclusion that SSI is beneficial for seismic response in many cases [9].

EC8 part 5 [20], 6.1 states that it is not necessary to take dynamic soil-structure interaction into account apart from a few combinations of structure geometry and soil conditions. The effect of SSI should be taken into account for:

- Structures where P-Δ (2nd order) effects play a significant role.
- Structures with massive or deep-seated foundations.
- Tall and slender structures such as towers and chimneys.
- Structures supported on very soft soil.
- The effect of the interaction between piles and the surrounding soils during earthquake needs to be considered when the piles pass through interfaces between very soft soils and much stiffer soils.

Soil-structure interaction can be approached in different ways with different methods for analysis of structures. The theory behind the two most common ways of including SSI in design of structures, direct analysis and substructure analysis, is presented below.

2.4.1 DIRECT ANALYSIS

A direct analysis takes SSI into account in a dynamic analysis by the use of the finite element method. In this type of analysis the entire system represented by the soil, the foundation and the structure, is modeled together as shown in figure 2-9 and analyzed in a single step.

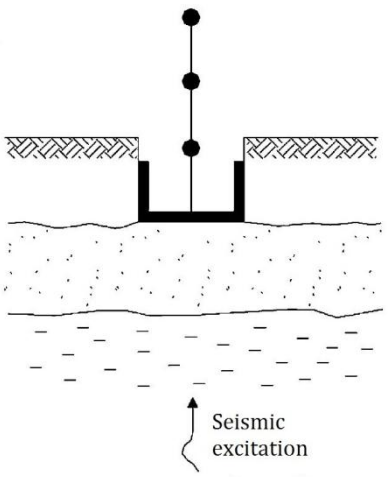

Figure 2-9: Representation of the entire system [18].

The complexity of the problem to solve is beyond the capability of closed form solutions. Numerical solutions are required in a finite element approach. In a direct analysis, the structure is often discretized with finite beam elements and the soil with solid finite elements [16]. Following a method described by Pecker [19] and referring to figure 2-10, the principle of a direct analysis for soil-structure interaction can be described.

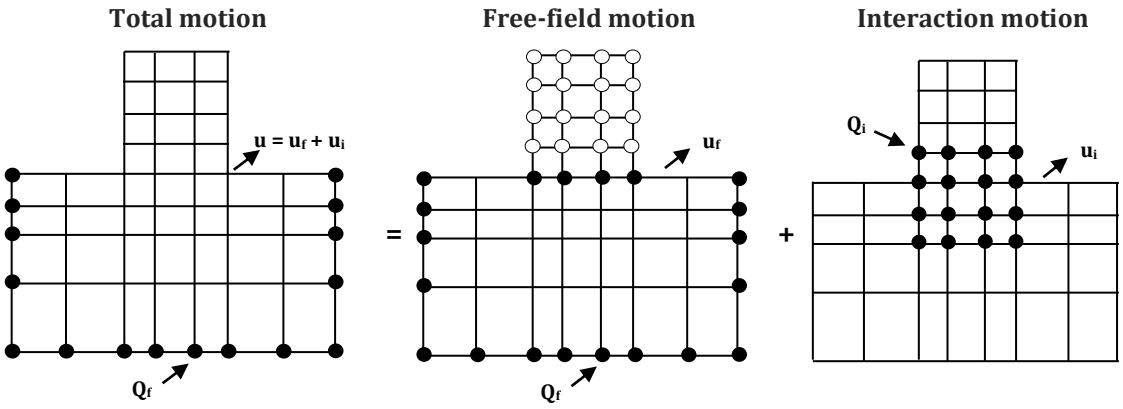

Figure 2-10: Schematic representation of the SSI problem [19].

Starting with the equation of motion (EOM) representing the total motion of the system

$$\mathbb{M}\ddot{\mathbb{u}} + \mathbb{C}\dot{\mathbb{u}} + \mathbb{K}\mathbb{u} = \mathbb{Q}_f \tag{2.42}$$

where $\mathbb{M}$ denotes the mass matrix, $\mathbb{C}$ denotes the damping matrix and $\mathbb{K}$ denotes the stiffness matrix of the total system. $\mathbb{Q}_f$ denotes the load vector. Since the source of the motion represented through the earthquake focus is not included in the finite element (FE) model, the load vector $\mathbb{Q}_f$ is assigned a nonzero value on the boundary of the model. In order for the motion not to be influenced by the presence of the structure, the boundary of the model is sufficiently remote from the structure. To ensure that seismic waves are not reflected at the boundary condition but instead emanate in order to avoid noise to be caused in the model, a model representing a big part of the ground underneath the structure is desirable. For the free field motion the equation of motion becomes

$$\mathbb{M}_f\ddot{\mathbb{u}}_f + \mathbb{C}_f\dot{\mathbb{u}}_f + \mathbb{K}_f\mathbb{u}_f = \mathbb{Q}_f \tag{2.43}$$

This is the model of the system without the structure. Furthermore, by letting the total displacement of the system consist of the free field displacement and the interaction displacement

$$\mathbb{u} = \mathbb{u}_i + \mathbb{u}_f \tag{2.44}$$

the equation of motion representing the interaction can be described as

$$\mathbb{M}\ddot{\mathbb{u}}_i + \mathbb{C}\dot{\mathbb{u}}_i + \mathbb{K}\mathbb{u}_i = -\mathbb{Q}_i \tag{2.45}$$

$\mathbb{Q}_i$ is the load vector determined from the free field displacements. It is important to emphasize that $\mathbb{Q}_i$ only has nonzero components at the nodes of the elements representing the interaction between the structure and the soil. For the interaction motion, $\mathbb{Q}_i$ can be expressed as

$$\left[\mathbb{M} - \mathbb{M}_f\right]\ddot{\mathbb{u}}_f + \left[\mathbb{C} - \mathbb{C}_f\right]\dot{\mathbb{u}}_f + \left[\mathbb{K} - \mathbb{K}_f\right]\mathbb{u}_f = \mathbb{Q}_i \tag{2.46}$$

This equation is important. If it is difference in the mass between the soil and the structure, then there is interaction. This is obvious, because if there is no difference then there is no building with mass in the system. If it is difference in the stiffness between the soil and the structure, then there is interaction. In other words; letting $\mathbb{M}$ be the total mass of the system and $\mathbb{M}_f$ the mass of the soil (free-field), the difference between these masses must represent the mass of the structure. As a conclusion, the difference obtained from that stated in eq. (2.46) must represent the contribution from the structure in the area of interaction.

By excluding the damping term from eq. (2.46), the phenomena of inertial interaction and kinematic interaction can be explained. If the foundation is infinitively stiff, the stiffness term will be equal to zero and the equation reduces to

$$\left[\mathbb{M} - \mathbb{M}_f\right]\ddot{\mathbb{u}}_f = \mathbb{Q}_i \tag{2.47}$$

Interaction is only generated by inertial forces in the structure equivalent to the forces $\mathbb{Q}_i$ at the base of the structure that give rise to a support motion. This is called *inertial interaction*. In this case, there is no difference between the total stiffness of the system and the soil stiffness. This is equivalent as modeling on bedrock or a rock like geological formation.

If the entire model consists of an embedded structure under the assumption of that the structure has zero mass above the ground and that the structure is equally distributed to the soil mass for the embedded part, the equation reduces to

$$\left[\mathbb{K} - \mathbb{K}_f\right]\mathbb{u}_f = \mathbb{Q}_i \tag{2.48}$$

This is called *kinematic interaction*. The forces, $\mathbb{Q}_i$, in the system is generated by the difference in stiffness from the total system and the foundation, which can be interpreted as the stiffness of the structure. In other words; the forces are generated by interaction between the structure and the soil. It is a result of the fact that the foundation is prevented from following displacements imposed by the soil.

In the representation of the theory behind direct analysis as a method of performing SSI, it has been emphasized to avoid writing the mass matrix, the damping matrix and the stiffness matrix for the structure itself, but rather look at the elements and nodes representing the area of interaction. A direct analysis requires a lot of effort in finding a model that represents the entire system correctly. This leads to introducing a method applicable to linear problems that may include SSI in an easier way by decomposing the SSI problem and solve the global problem in successive steps. The method explained above is undoubtedly suitable for nonlinear systems.

2.4.2 SUBSTRUCTURE ANALYSIS

A substructure analysis, or multi-step (superposition) method, breaks down the SSI-problem into three parts. These three parts are then combined by superposition to formulate the complete solution under the assumption of linear soil and structure behavior.

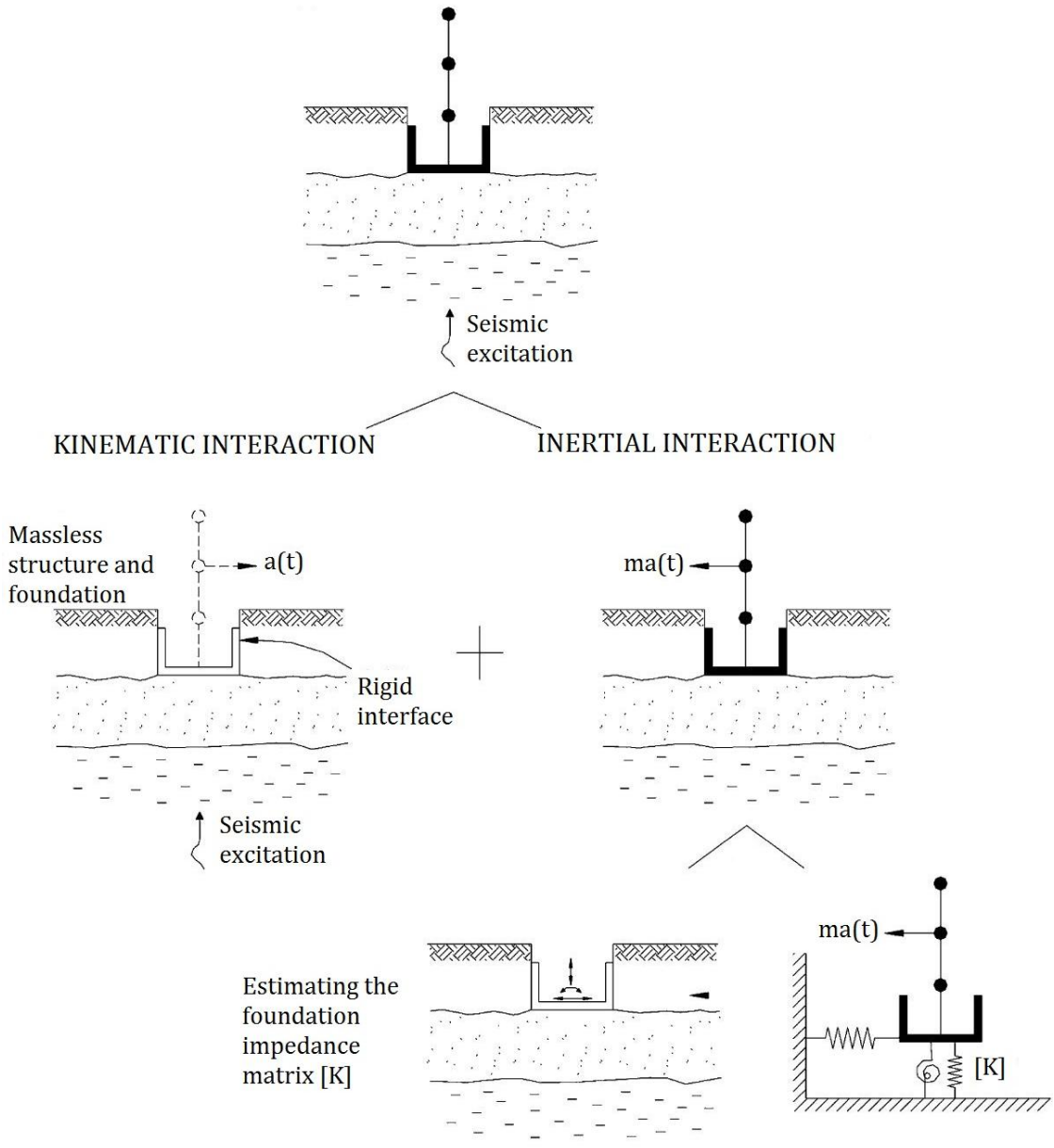

Figure 2-11: Geometry of the SSI problem for the complete substructure analysis [18].

Referring to figure 2-11 the three steps in a substructure analysis are as follows [16], [18], [21]:

- *Kinematic interaction*. Determination of the consistent base motion, which is the acceleration input motion at the base of the structure. This is also known as foundation input motion (FIM). In this calculation the foundation and structure is assumed mass-less. A central task in this step is the calculation of the free-field seabed motion for a given bedrock-outcrop motion. This analysis is known as site response or soil amplification.

- *Foundation impedance*. Determination of the frequency-dependent foundation impedance, often referred to as soil spring and damping, at the base of the structure. It describes the stiffness and damping characteristics of the foundation-soil interaction and accounts for the stratigraphy of the soil and the geometry and stiffness of the foundation. The foundation impedance consists of a static part and a dynamic part in which both usually have to be taken into consideration. 6 degrees-of-freedom (3 translational and 3 rotational) are used to represent the complete foundation.

- *Inertial interaction*. Computation of the earthquake response of the structure supported on the soil springs and subjected to the consistent base motion. It refers to the response of the complete system to the forces associated with the acceleration of the structure due to the kinematic interaction.

This decomposition gives rise to solution techniques based on the principle of superposition. It allows SSI-problems to be solved based on these three steps to obtain the total solution.

Foundation impedance consists of static foundation impedance and dynamic foundation impedance as mentioned above. There are three important factors affecting the impedance of a foundation [18]:

1. The shape of the foundation (arbitrary, circular, rectangular, strip).
2. The foundation embedment (surface foundation, embedded foundation, pile foundation).
3. The type of soil profile (deep uniform, multi-layer, shallow stratum on rock).

The foundation impedance can in most cases be estimated from appropriate expressions and charts. For most buildings the expressions for rectangular foundation shapes can be implemented and this is what is being emphasized here.

The static stiffness is altered by dynamic loading effects. Normal design practice is to assume that the stiffness and damping values of the springs are independent of the frequency of excitation. However, the consequence of a SDOF spring damper model is that the model parameters in fact are frequency dependent.

To include dynamic stiffness and damping of the foundation due to dynamic response the following procedure can be implemented [18], [22]:

$$K(\omega) = K_{static} k(\omega) \tag{2.49}$$

$$C(\omega)_{tot} = C(\omega) + \frac{2\beta K(\omega)}{\omega} \tag{2.50}$$

where β is the soil hysteretic damping. Material damping associated with soil springs is strain dependent and 5% is often chosen. A model dashpot represents the dissipation of energy arising from the soil itself (material damping) and from the radiation of the seismic waves away from the foundation. Radiation damping can be significant, but the presence of harder layers reflecting radiated energy may significantly reduce the damping. Material damping can be neglected with respect to radiation damping if the soil deposits are homogenous and the strain amplitudes are moderate [19]. In the response spectrum analysis, the damping levels due to material and radiation damping should only be taken into account for the modes of vibration involving foundation movement. The higher modes of vibrations are unlikely to involve the foundation soils. Thus, the damping level should depend on the structure alone [9].

The dynamic damping is not included in models as often as dynamic stiffness. The static and dynamic values for the stiffness parameter are obtained from the expressions given in table 2-2 for surface foundations and table 2-3 for embedded foundations [18].

Table 2-2: Dynamic stiffness coefficients for rectangular surface foundations [18].

RECTANGULAR FOUNDATIONS ON HOMOGENOUS HALFSPACE SURFACE			
RESPONSE MODE	STATIC STIFFNESS K		DYNAMIC STIFFNESS k(ω)
	RECTANGLE (L / B = 2)	RECTANGLE (L / B = 4)	GENERAL SHAPES INCLUDING RECTANGULAR SHAPES
Vertical, z	$K_z = \frac{3.3GL}{1-\upsilon}$	$K_z = \frac{2.55GL}{1-\upsilon}$	$k_z = k_z\left(\frac{L}{B}, \upsilon, a_0\right)$ Plotted in graph (a), fig. 2-12
Horizontal, y (lateral direction)	$K_y = \frac{6.8GL}{2-\upsilon}$	$K_y = \frac{5.54GL}{2-\upsilon}$	$k_y = k_y\left(\frac{L}{B}, a_0\right)$ Plotted in graph (b), fig 2-12
Horizontal, x (longitudinal direction)	$K_x = \frac{4.9(1-1.4\upsilon)}{(2-\upsilon)(0.75-\upsilon)}GL$	$K_x = \frac{3.9(1-1.4\upsilon)}{(2-\upsilon)(0.75-\upsilon)}GL$	$k_x \simeq 1$
Rocking, r_x	$K_{r_x} = \frac{0.82GL^3}{1-\upsilon}$	$K_{r_x} = \frac{0.2GL^3}{1-\upsilon}$	$k_{rx} = 1 - 0.20a_0$
Rocking, r_y	$K_{r_y} = \frac{2.46GL^3}{1-\upsilon}$	$K_{r_y} = \frac{1.62GL^3}{1-\upsilon}$	$\upsilon < 0.45$: $k_{ry} \simeq 1 - 0.30a_0$ $\upsilon \simeq 0.5$: $k_{ry} \simeq 1 - 0.25a_0\left(\frac{L}{B}\right)^{0.3}$
Torsional	$K_t = 3.5GL^3$	$K_t = 2.1GL^3$	$k_t \simeq 1 - 0.14a_0$

Table 2-3: Dynamic stiffness coefficients for rectangular embedded foundations [18].

RECTANGULAR FOUNDATIONS EMBEDDED IN HOMOGENOUS HALFSPACE			
RESPONSE MODE	STATIC STIFFNESS K		DYNAMIC STIFFNESS k(ω)
	RECTANGLE (L / B = 2)	RECTANGLE (L / B = 4)	GENERAL SHAPES INCLUDING RECTANGULAR SHAPES
Vertical, z	$K_{z,emb} = K_z \cdot \chi_z$ $\chi_z = \left(1 + 0.16\frac{D}{L}\right) \cdot \left(1 + 0.42\left(\frac{d}{L}\right)^{2/3}\right)^*$	$K_{z,emb} = K_z \cdot \chi_z$ $\chi_z = \left(1 + 0.25\frac{D}{L}\right) \cdot \left(1 + 0.6\left(\frac{d}{L}\right)^{2/3}\right)$	$\upsilon \leq 0.4$ $k_{z,emb} = k\left(1 - 0.09\left(\frac{D}{B}\right)^{3/4} {a_0}^2\right)$
Horizontal, x and y (lateral and longitudinal direction)	$K_{y,emb} = K_y \cdot \chi_y$ $\chi_y = \left(1 + 0.2\sqrt{\frac{D}{L}}\right) \cdot \left(1 + \left(\frac{d}{L}\right)^{0.8}\right)$	$K_{y,emb} = K_y \cdot \chi_y$ $\chi_y = \left(1 + 0.3\sqrt{\frac{D}{L}}\right) \cdot \left(1 + 1.3\left(\frac{d}{L}\right)^{0.8}\right)$	$\upsilon = 0.5 \; and \; L/B \simeq 1 - 2$ $k_{z,emb} = k_{hor,emb} \simeq 1 - 0.09\left(\frac{D}{B}\right)^{3/4} {a_0}^2$ $\upsilon = 0.5 \; and L/B > 3$ $k_{z,emb} = \; k_{hor,emb} \simeq 1 - 0.35\left(\frac{D}{B}\right)^{1/2} {a_0}^{0.35}$
Rocking, r_x	$K_{rx,emb} = K_{rx} \cdot \chi_{rx}$ $\chi_{rx} = 1 + 2.5\frac{d}{L} \cdot \left(1 + 1.4\frac{d}{L}\left(\frac{d}{D}\right)^{-0.2}\right)$	$K_{rx,emb} = K_{rx} \cdot \chi_{rx}$ $\chi_{rx} = 1 + 5\frac{d}{L} \cdot \left(1 + 2\frac{d}{L}\left(\frac{d}{D}\right)^{-0.2}\right)$	$k_{rx,emb} \simeq k_{rx}$
Rocking, r_y	$K_{ry,emb} = K_{ry} \cdot \chi_{ry}$ $\chi_{ry} = 1 + 2.1\left(\frac{d}{L}\right)^{0.6} \cdot \left(1 + \left(\frac{d}{D}\right)^{1.9}\right)$	$K_{ry,emb} = K_{ry} \cdot \chi_{ry}$ $\chi_{ry} = 1 + 3.2\left(\frac{d}{L}\right)^{0.6} \cdot \left(1 + 1.5\left(\frac{d}{D}\right)^{1.9}\right)$	$k_{ry,emb} \simeq k_{ry}$
Torsional	$K_{t,emb} = K_t \cdot \chi_t$ $\chi_t = 1 + 3.7\left(\frac{d}{L}\right)^{0.9}$	$K_{t,emb} = K_t \cdot \chi_t$ $\chi_t = 1 + 6.1\left(\frac{d}{L}\right)^{0.9}$	$k_{t,emb} \simeq k_t$

**d is foundation thickness*

The consideration of dynamic effects starts by considering a rigid rectangular foundation on a deep elastic layer. To quantify frequency effects on dynamically loaded foundations the following dimensionless parameter is defined [18]:

$$a_0 = \frac{\omega B}{V_s} \tag{2.51}$$

where ω is the excitation frequency in radians per second, B is the foundation breadth and V_s is the shear wave velocity of the soil.

In table 2-2 and table 2-3, the shear modulus of the soil is defined as

$$G = \rho V_s^2 \tag{2.52}$$

where ρ is the density of the soil, which can be set to an averaged value of $\rho = 1700\frac{kg}{m^3}$. V_s is the shear wave velocity of the soil.

The variations of stiffness for the different degrees of freedom are as shown in figure 2-12:

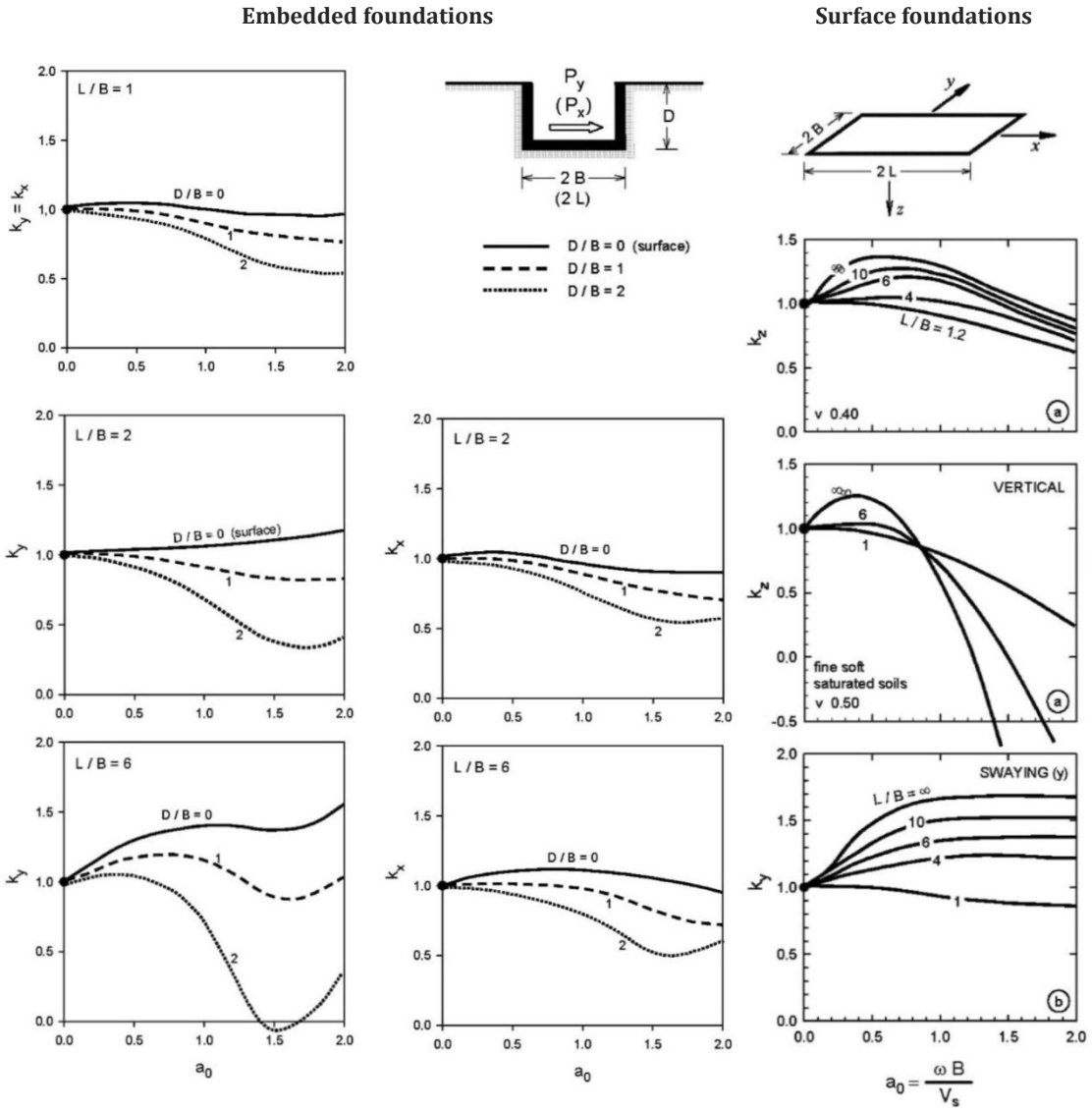

Figure 2-12: Frequency effects of dynamically loaded embedded and surface foundations [18].

The impedance of embedded foundations differs from that of shallow foundations in several important ways. As can be seen from table 2-2 and table 2-3, the static stiffness of embedded foundations is larger than that of surface foundations. Since embedded foundations have greater foundation-soil contact area, this results in larger damping as well [16].

For earthquake loadings a large number of frequencies are present and anything other than a frequency independent approach is not likely to be practical. The inclusion of the frequency effect does not lead to much change in the computed response of structures to earthquake excitation [22].

In the analysis of impedance functions, the above solutions for rectangular surface foundations and embedded foundations can provide reasonable estimates. However, in

some cases it is necessary to account for other potentially significant effects of non-uniform soil profiles, non-rectangular foundation shapes, flexible foundations and the effect of piles under the base slab.

Foundation stiffness can be reasonably estimated using half-space impedance functions. However, solutions for foundations on soil stratum over half-space are a more realistic approach, but it involves deeper knowledge about the soil underlying the foundation. Soils often have a gradual increase of stiffness with depth. The increase of stiffness is caused by the increase in confining pressure with depth and the associated increase in shear modulus, G [18]. As a result of the presence of stiff material, the static stiffness increases and hence the frequency dependence of stiffness and damping is changed [16]. By dividing the soil into homogenous layers with different material properties, this type of soil inhomogeneity can be solved using dynamic finite element formulations. Representing a problem with impedance functions such as springs and dashpots can only be fairly approximate.

The stiffness and damping is less for flexible foundations than for rigid foundations, and it is most significant when there are large deviations between the rigidity of the soil and the slab foundation. The flexibility of the foundation mainly affects the rocking impedance [16].

If the foundation is supported by piles, the impedance functions may be significantly affected. The presence of piles increases the vertical and lateral stiffness and damping of the foundation. Piles can be represented in a model by using distributed Winkler springs attached to beam-column structural elements [16]. EC8, part 5 [20] provides formulas to represent the stiffness of piles.

The substructure analysis method using linear springs and dashpots may be satisfactory in many cases, but it is not a theoretically correct approach. A rigorous treatment of soil-structure interaction using soil springs and dashpots requires that both the spring stiffness and damping are frequency-dependent. This requires the use of frequency domain techniques. A direct analysis is an alternative to the use the substructure method in order to be able to account for several factors such as sloping of the ground, non-uniform soil stratum and foundation embedment. FE-modeling is a more complex method of analysis, but it provides a better and more accurate result.

The importance of dynamic soil-structure interaction for high-rise buildings has been recognized because of two important effects [23]:

1. The response from the structure affects the composition of the frequency spectrum of the soil motion.
2. The soil flexibility affects the dynamic behavior of the structure. The damping of the structure partly stems from vibration energy dissipation through hysteresis and wave radiation.

By implementing soil-structure interaction in the analysis of the structure in one of the abovementioned methods, a more realistic behavior of the structure exposed to earthquake-induced motion is obtained.

2.5 WHITE NOISE

White noise, $e(t)$, can be defined as a sequence of independent and identically distributed random variables of zero mean and variance σ^2. It is a process with a corresponding constant spectral density, S_x, over the whole frequency range [24]. Gaussian white noise is defined as a time-series, r_t, that is normally distributed with zero mean and constant specified standard deviation σ. It implies that the autocorrelation function is given as the *Dirac delta function* and describes an uncorrelated process, i.e. being independent and identically distributed [25].

White noise can in general be implemented in a model as described in figure 2-13 below:

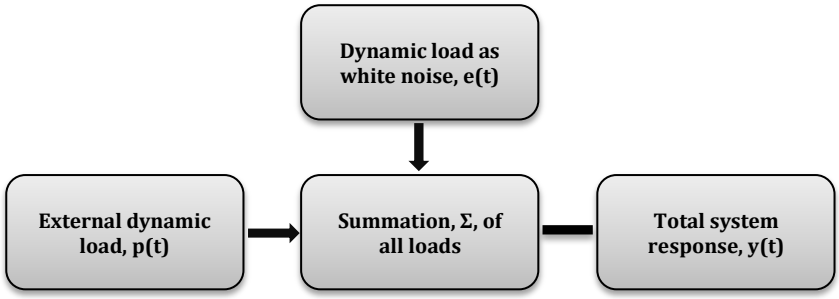

Figure 2-13: White noise implemented in a model [24].

For structural monitoring purposes there are numerous sources of disturbance that may be measured in the structure. The motion and vibration of the structure may be dynamic loads that originate from a variety of sources such as

- Wind loads.
- Seismic loads – earthquakes and aftershocks.
- Human activities – walking and running.
- Working machines – inside the building or in the nearby area.
- Construction work – inside the building or in the nearby area.
- Traffic – cars, buses, metro and other vehicles in the nearby area.

The above mentioned sources of disturbance cannot individually be interpreted as white noise. However, when these disturbances from different sources are combined the resulting dynamic disturbance or interference can be defined as Gaussian white noise.

White noise can be simulated by the use of the function `randn(m,n)` in Matlab. This function returns an m-by-n matrix containing pseudorandom values drawn from the standard normal distribution [26]. The values obtained for a given time-series is in general dimensionless. For the purpose of this study the white noise will be in unit of acceleration [m/s^2], and later be scaled down for implementation in a structural element model. For a detailed description of the code used to generate white noise, it is referred to Appendix A.

Figure 2-14 illustrates how white noise has been generated with peak value of 1 in a random time-series with length corresponding to the approximate length of duration of an earthquake.

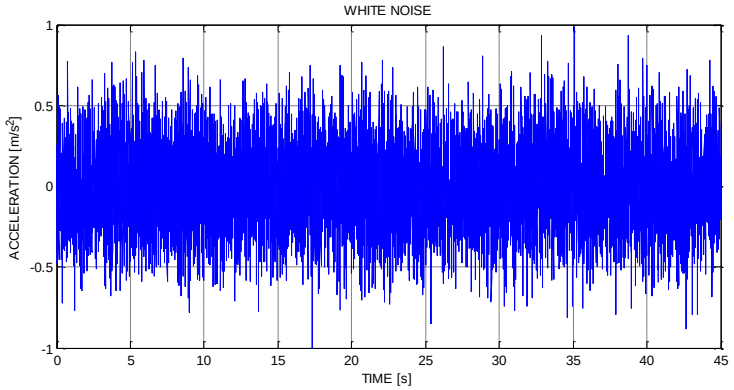

Figure 2-14: White noise generated in Matlab for random x- and y values.

White noise is always present in a structure. Depending on the intensity of the white noise it can be registered as acceleration in a structure. This can be measured by structural monitoring and measurements as will be explained in detail in Chapter 4.

2.6 Ground Motion Parameters

Earthquakes produce complicated loading with various components of motions. These motions span over a wide range of frequencies. Characterization of earthquake motion cannot be complete without taking into consideration its frequency content due to the fact that the frequency content influence the effects of the earthquake motion. Using the applications of Fourier series and Fourier transforms can be very useful for ground motion analyses. In the following, the theory behind this is presented.

2.6.1 Fourier Series

Fourier series play an important role in applications, and it is the basic tool for representing periodic functions. Periodic functions can be expressed using Fourier analysis as the sum of a series of simple harmonic terms of different amplitude,

frequency and phase [27]. Performing a Fourier transformation on a periodic function, $x(t)$, following a description similar as described by Strømmen [28][1] this can be written as

$$x(t) = c_0 + \sum_{k=1}^{\infty} c_k \cos(\omega_k t + \varphi_k) \tag{2.53}$$

where

$$\begin{cases} \omega_k = k \cdot \Delta\omega \\ \Delta\omega = \dfrac{2\pi}{T} \end{cases} \tag{2.54}$$

T is the length of $x(t)$. In eq. (2.53) the amplitude is defined as

$$c_k = \sqrt{a_k^2 + b_k^2} \tag{2.55}$$

The phase angle is defined as

$$\varphi_k = \tan^{-1}\left(\frac{b_k}{a_k}\right) \tag{2.56}$$

where the constants a_k and b_k are given by

$$\begin{bmatrix} a_k \\ b_k \end{bmatrix} = \frac{2}{T}\int_0^T x(t) \begin{bmatrix} \cos\omega_k t \\ \sin\omega_k t \end{bmatrix} \tag{2.57}$$

of the kth harmonic of the Fourier series. A complete description of the ground motion can be provided by Fourier series. This can be stated since the motion can be completely recovered by the inverse Fourier transform. The theory presented above must be evaluated numerically for practical problems involving excitations varying arbitrarily with time, t.

2.6.2 FOURIER SPECTRA

A Fourier amplitude spectrum is a plot of the Fourier amplitude versus frequency. From eq. (2.53), this is c_k versus ω_k. The Fourier amplitude spectrum of a strong ground motion such as an earthquake record expresses the frequency motion very clearly as it shows the distribution of the amplitude of the motion with respect to frequency or period [29].

[1] Chapter 2.5, p. 33.

Fourier amplitude spectra of earthquake motions plotted on logarithmic scales show the characteristic shapes and the valuable information more easily. Fourier acceleration amplitudes tend to be largest over an intermediate range of frequencies. This range is bounded by a corner frequency, f_c, on the low frequency side and a cutoff frequency, f_{max}, on the high frequency side as shown in figure 2-15.

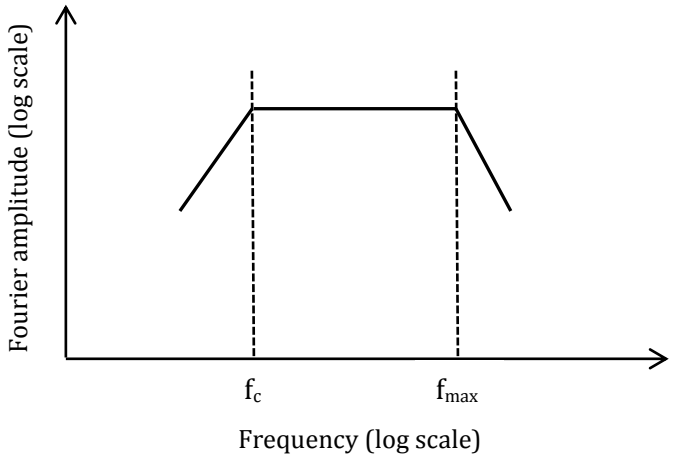

Figure 2-15: Fourier amplitude spectrum with logarithmic scales [3].

Large earthquakes produce greater low-frequency motions, i.e. frequency motions closer to the corner frequency, than smaller earthquakes [3][2].

A Fourier amplitude spectrum may be narrow or broad, or contain several narrow peaks in the same spectrum. A broad spectrum implies that the motion contains several frequencies that produce a jagged, irregular time history. A narrow spectrum implies that the motion has a dominant frequency. A Fourier spectrum indicating several peaks in the same plot will then naturally indicate that the motion contains several dominant frequencies. For a structure these peaks often corresponds to the natural frequency of vibration for the respective modes.

Fourier spectra are valuable to investigate strong ground motion produced by earthquakes and motion caused by sources such as wind or even white noise. Using this kind of spectrum can be useful when it is desired to find the natural frequency of vibration for a structure. The theory presented here has been implemented in the analyses of time-series presented in the work throughout this thesis. To ensure correct use of the theory, other methods such as The Burg Method have been used for comparison. The theory behind the other methods used will not be presented. The underlying theory is based on Fourier series and Fourier analysis.

[2] Chapter 3.3.2.1, p. 72.

2.6.3 ARIAS INTENSITY

To describe the important characteristics of strong ground motion in compact, quantitative form ground motion parameters are essential. Many different parameters exist to characterize amplitude, frequency content and duration of strong ground motions. Earthquake ground motion is complex and one single parameter that accurately describes all important ground motion characteristics is considered as impossible.

Many parameters are primarily related to amplitude, frequency content, or duration of the ground motion, but since all of these characteristics are important, parameters that reflect more than one are useful. Arias intensity is such a parameter.

Arias intensity includes effects of the amplitude, frequency content and duration of a strong motion record and is defined as

$$I_a = \frac{\pi}{2g}\int_0^\infty [a(t)]^2 dt \tag{2.58}$$

Here $a(t)$ is the acceleration vector and g is the gravity. Arias intensity has units of velocity [m/s]. Its value is independent of the method used to define the duration of the strong ground motion since it is obtained by integration over the entire duration rather than over the duration of strong motion [3].

It is common practice to normalize the Arias intensity with to respect to its largest value resulting in a graph starting at zero and building up to unity during the strong ground motion. This will be seen in the plots of Arias intensity presented in the preceding chapters.

3 STRUCTURAL MODELING AND RESPONSE ANALYSIS

3.1 OSLO PLAZA

Oslo Plaza, formally Radisson Blu Plaza Hotel, is the second tallest building in Norway located in the capital of Norway, Oslo. It is a multi-story building with 37 floors and a total height of 117 m. The building consists of the tower rising up from the main building from the 4th floor and up to the top floor. The ground surface of the main building is approximately 3 800 m^2 consisting of a conference part, a tower part and an administration part, whereas the tower part has an approximate ground surface of 975 m^2. Oslo Plaza was designed by White Architects and completed in 1989. It was officially opened on March 14, 1990 [30].

The structural system of the building consists of a concrete wall construction. Four concrete walls are located in the tower providing torsional resistance of the high-rise structure. These walls are supported on concrete columns on the first five floors of the structure. Together with the concrete elevator core, the shear wall system is utilized to support both gravity loads and lateral loads. Cast in situ concrete slabs of varying thickness is located at every floor. Perimeter steel columns support the exterior glass facade distributing the wind load throughout the entire building. The concrete wall construction reaches the 34th floor leaving the top part of the building in a steel frame construction. The top part is constructed and connected to the concrete construction reaching three floors all the way to the very top of the building. The result is a structure with a tower that is stiff laterally and torsionally.

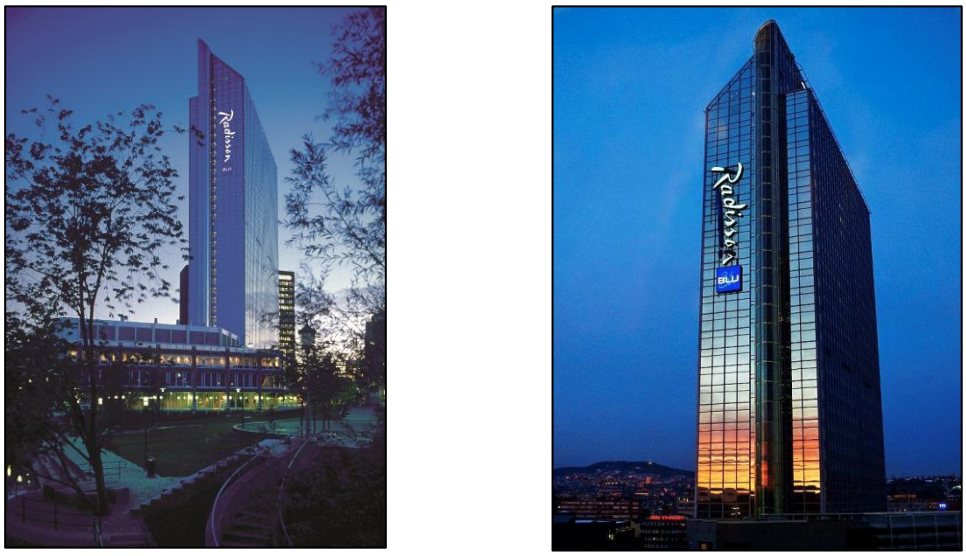

(a) **(b)**

Figure 3-1: Oslo Plaza. (a) The complete building. (b) The tower of Oslo Plaza [30].

3.2 THE FINITE ELEMENT MODEL OF OSLO PLAZA

Oslo Plaza has been modeled using an extensive number of construction and architectural drawings. These have been acquired from the Oslo Municipal Planning & Building Service and from the Oslo Plaza management. In addition to the drawings building inspections, conversations with the contracting firm and the architectural firm and meetings with people holding information about the building has formed the foundation for developing and modeling the structure. Lack of information regarding design and dimensions of the building have been solved by making reasonable assumptions and simplifications supported by the above mentioned people.

3.2.1 NUMERICAL MODELING USING SAP2000

A numerical element model has been created using the finite element structural analysis program SAP2000 (version 15.0.1). The objective of creating a 3D model was to obtain information about the dynamic behavior of the structure and to be able to perform seismic analyses.

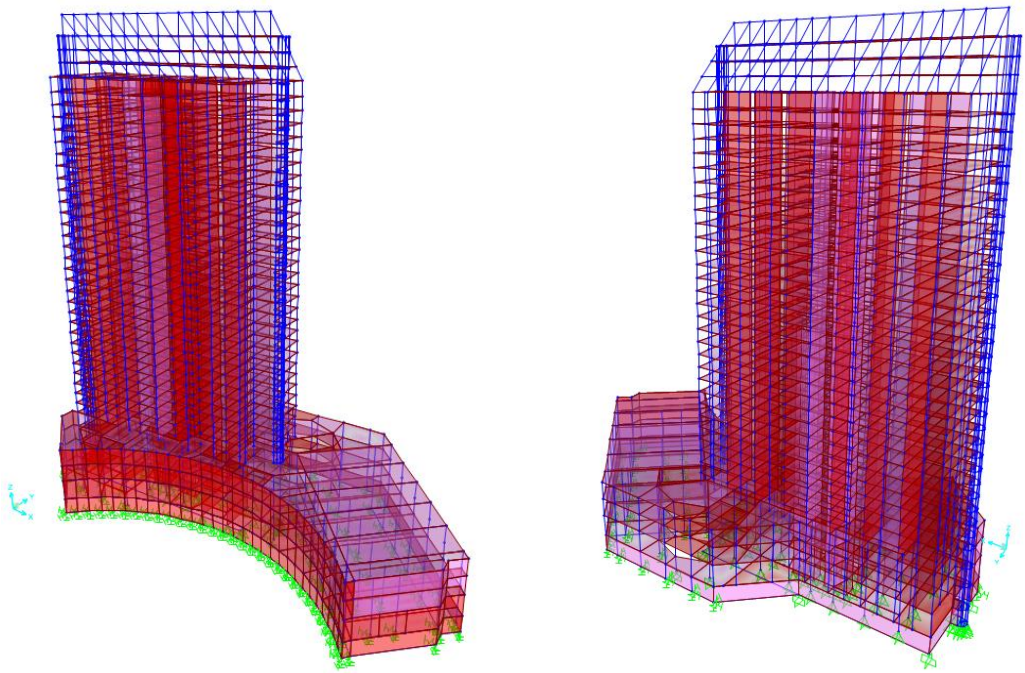

Figure 3-2: The 3D FE-model created in SAP2000.

The development of the numerical FE-model, hereafter referred to as the element model, is not considered a straight forward procedure. Due to the complexity and size of the building considerable time and effort has been spent finding correct materials and structural element properties and to connect elements using constraints.

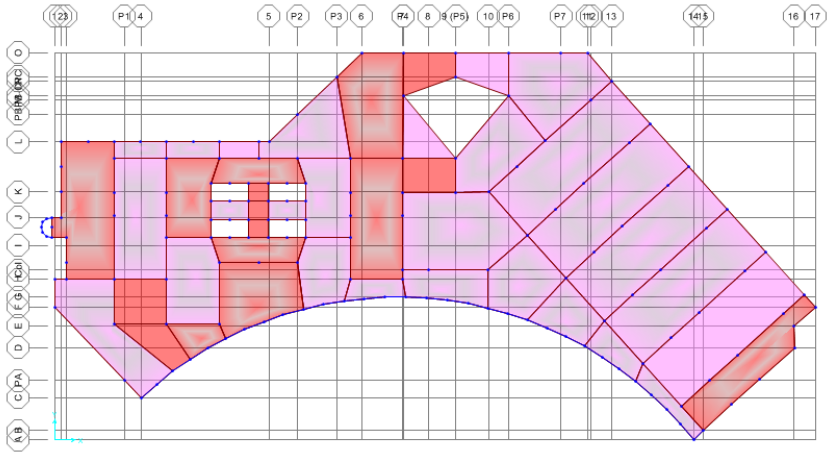

Figure 3-3: The global coordinate system of the element model, plane view.

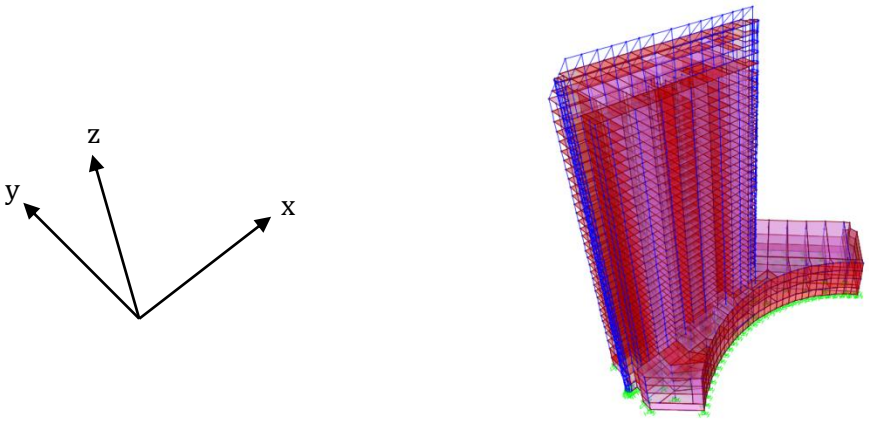

(a) **(b)**

Figure 3-4: Definition of the global coordinate system with the axis-representation in the element model.

The complexity of the foundation work has been a challenge to represent in the element model. In general for the Oslo area the soil conditions are characterized as ground type D, E and even S_1 and S_2 according to table 2-1 in Chapter 2.4. As a consequence of this piles have been used in the foundation work among other foundation methods. A subway leading to Oslo Central Station is located right underneath the structure and this affects the foundation work as well. This is described in further detail in the preceding subchapter.

Table 3-1: Material properties used in the element model.

Material	Weight [kN/m3]	Mass [kg/m3]	Modulus of elasticity, E [MPa]	Poisson ratio, ν
Concrete B35	25	2 548	34 000	0.2
Steel S355	77	7 849	21 000	0.3

The main structural elements and material properties have been determined as described in table 3-1 and table 3-2. The area sections have been assigned as shell elements whereas the other structural elements have been assigned as beam elements.

In general design of buildings with respect to seismic loadings, reduction of the effective moments of inertia of structural components such as beams and columns should be performed. However, taking into consideration the fact that this building most likely was designed to mainly resist wind as lateral load rather than earthquakes, this has not been implemented in the element model. A representation of the dynamic behavior as realistic as possible is desired in the end.

Table 3-2: The main structural elements used in the element model.

Structural element	Material	Dimensions [mm]
Columns	Concrete B35	Circular 600
		Circular 1200
		Rectangular 300 x 400
		Rectangular 400 x 400
		Rectangular 600 x 500
		Rectangular 600 x 600
		Rectangular 800 x 1200
	Steel S355	Tube 200 x 100 x 10
		Tube 250 x 450 x 40
Beams	Steel S355	Flange beam 600 x 1300
Shear walls	Concrete B35	200 mm thickness
		250 mm thickness
		300 mm thickness
		800 mm thickness
Slabs	Concrete B35	140 mm thickness
		220 mm thickness
		250 mm thickness
		270 mm thickness
		290 mm thickness
		340 mm thickness
Foundation walls	Concrete B35	500 mm thickness

The loads used in the element model are mainly self-weight of the structural elements, hereby referred to as dead load, in addition to live loads. It has been chosen to let SAP2000 represent the dead load, and to assign the live loads as presented in table 3-3 according to EC8.

Table 3-3: Loads implemented in the element model.

Floor	Dead load [kN/m^2]	Live load [kN/m^2]	Snow load [kN/m^2]
1 - 4	Calculated in SAP2000	5	2.24 (4th floor)
5 - 33		2	
34		3	2.24
35		3	No snow load on glass facades
36		5	
37		5	

A load combination of

$$Total\ load = 1 \cdot Dead\ Load + 0.3 \cdot Live\ Load + 0.2 \cdot Snow\ Load$$

has been implemented in the element model. It is worth mentioning that the snow load is more or less negligible due to the limited roof area and due to the glass facade.

If performing an optimization of the element model is necessary to obtain a more realistic dynamic behavior, there are numerous ways of doing so. Varying the material properties and obtaining more information about detailing and the use of structural elements are factors worth mentioning. A system identification process is described in Chapter 4 and will be the basis for possibly going through an optimization of the element model.

3.2.2 METHODS OF ANALYZING THE GROUND (SSI)

The response of the structure will, as described earlier, be affected by the soil conditions and the foundation on which it rests known as the soil-structure interaction. For this case in particular the complexity of the foundation work made it necessary to introduce simplifications. Ideally, a full direct analysis of the soil-structure interaction effects using numerical solutions in a finite element approach was desired. This requires a lot of information about the foundation work and soil conditions for and around the specific building. It also requires a lot of effort in geotechnical numerical modeling. Thus, using a substructure analysis by introducing springs as boundary conditions was performed to represent the soil-structure interaction as realistic as possible without doing any numerical modeling.

According to Thorn [31] a detailed description of the foundation work of Oslo Plaza is provided. With the help of Prof. Amir Kaynia using a SSI substructure analysis approach, the foundation could be represented as described in this subchapter.

In the substructure analysis the foundation of the total building is divided in one part for the tower and one part for the rest of the building. The foundation of the tower, hereby referred to as the tower foundation, consists of concrete foundation walls supported by prestressed vertical rock-anchors. The foundation supporting the rest of the structure, hereby referred to as the structure foundation, is mainly supported by piles.

Table 3-4: Properties of the tower foundation [31].

TOWER FOUNDATION (CONCRETE FOUNDATION WALLS)				
Amount of walls	Width [m]	Height [m]	Depth [m]	Concrete quality
47	1.2	2.8	12 - 30	C45

Table 3-5: Properties of the structure foundation [31].

STRUCTURE FOUNDATION (PILES)				
Amount of piles	Cross section [mm^2]	Capacity [kN]	Avg. pile length [m]	Concrete quality
700	275 x 275	2860	17.14	C75

In table 3-4 and table 3-5 the properties of the elements supporting the foundation of the structure is presented. Due to the increased stiffness of a pile-soil system compared to soil-system only, the seismic response of a pile-supported foundation differs from that of a surface foundation. Scattering of seismic waves off the piles may also contribute to such difference [16].

Boundary conditions are represented as springs with both horizontal and vertical stiffness for the concrete foundations walls and for the piles. The equivalent stiffness for the piles is found using EC8 part 5 [20]. The total stiffness of altogether 700 piles was distributed by 76 springs in each horizontal direction and by 76 springs in the vertical direction. The stiffness assigned to each spring is indicated in table 3-6.

Table 3-6: Spring stiffness for horizontal and vertical direction assigned to the element model.

Horizontal stiffness [N/m]	Vertical stiffness [N/m]
1.03E+09	1.56E+09

For the concrete foundation walls the equivalent stiffness in the horizontal and vertical direction was found to be very high. The difference in assigning regular support conditions as boundary conditions versus using springs with the calculated stiffness was negligible. Thus, regular boundary conditions were assigned for the concrete foundation walls in the element model using simply supported and fixed boundary conditions. Detailed calculations are presented in Appendix B.

As described in Chapter 2.4.2, there are several factors that take into account dynamic effects. The reduction for dynamic stiffness is small and thus it is not implemented in the element model. In general, the soil conditions at the site will contribute to the damping of the soil-structure system. However, there is no reason to take damping into consideration in this case due to the fact that the foundation of the structure is modeled with piles and walls on rock. A third factor beside stiffness and damping affecting the dynamic response is mass. The mass properties of the soil can be included by using the formula [21]

$$m_{vertical} = 1.50\rho r^3 \tag{3.1}$$

where ρ is the density of the soil and r is the equivalent foundation radius. Assigning this load on the foundation floor contributes to extra mass and changes the dynamic

behavior of the structure considered. None of these effects mentioned above contributed to significant changes and is thus neglected in the element model.

3.3 THE MODAL ANALYSIS OF THE ELEMENT MODEL

The modal analysis of the final version of the element model in SAP2000 rendered the results as indicated in table 3-7.

Table 3-7: Modal analysis results from SAP2000 of the element model.

Mode	Mode shape	Frequency, f [Hz]	Period of vibration, T [s]	Participating Mass Ratio			Participation Factor [Ns^2]		
				Sum X	Sum Y	Sum Z	X	Y	Z
1	Translation x-direction	0.3408	2.9346	0.44	0.03	0.0002	-4126	-997	81
2	Translation y-direction	0.3668	2.7265	0.47	0.47	0.0015	-1036	4145	-230
3	Rotation about z-axis	0.4307	2.3218	0.47	0.49	0.0015	153	863	-13
4	Deformation in x-direction along z-axis	1.3092	0.7638	0.58	0.49	0.0016	2024	63	58
5	Deformation in y-direction along z-axis	2.2162	0.4512	0.58	0.64	0.0050	-36	2343	-361
6	Translation in z-direction about y-axis	2.2310	0.4482	0.58	0.64	0.0588	-225	521	1446
7	Symmetric deformation in y-direction along z-axis	2.4269	0.4121	0.58	0.66	0.0616	-115	-694	-329
8	2^{nd} deformation in x-direction along z-axis	2.7619	0.3621	0.62	0.66	0.0730	1228	85	666
9	Translation in z-direction, emphasis left side	3.1595	0.3165	0.62	0.66	0.2000	-311	210	2194
10	Local mode	3.2497	0.3077	0.62	0.66	0.2100	0	3	-646

Included in the table is the modal participating mass ratio and the modal participation factor. The modal participating mass ratio is defined as the participating mass per mode divided by the total mass in the given direction. If all modes are included, the ratio for the given direction will be equal to 1.0. The modal participating mass ratio is intended mainly to estimate the accuracy of a solution for base motion. The participation factor is defined as how much the given mode contributes to the response for the given direction. If this value is small the given mode participates little to the total response. Both of these ratios give valuable information to better understand the modal contribution to the response, which is significant for the result of the seismic analyses. In the final model used for the analyses the total of 200 modes was included to obtain the contribution from as many modes as possible and to ensure that the modal participating mass ratio was as close to 1.0 as possible. This rendered more accurate and realistic results in the seismic analyses performed.

The natural vibration periods for the element model seem reasonable for a high-rise structure such as the one analyzed here. The mode shapes for the first 6 modes is shown in figure 3-5.

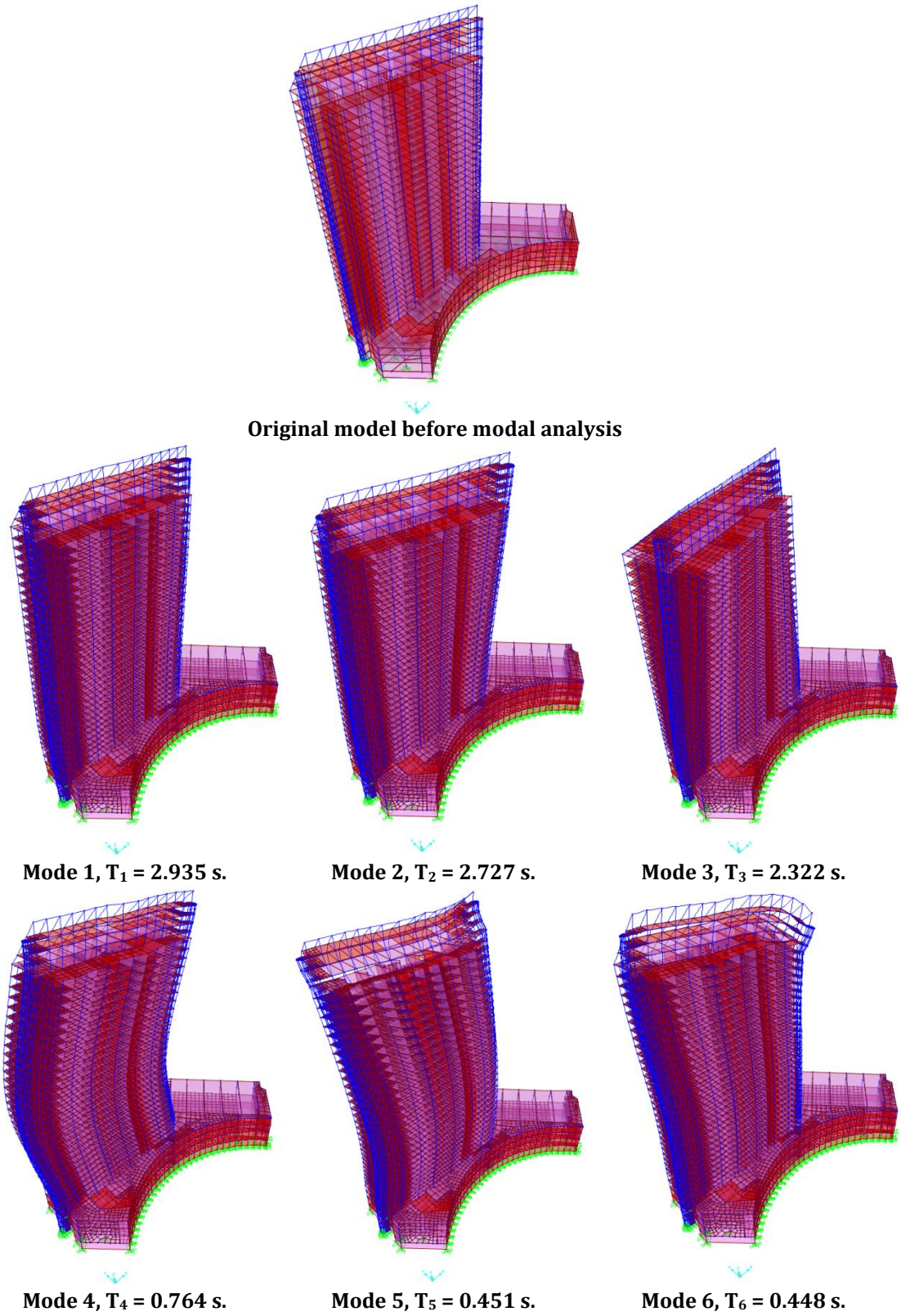

Figure 3-5: The first 6 mode shapes in reference to the original element model as a result of the modal analysis in SAP2000.

The floors play an important role in the overall seismic behavior of the structure. Floors act as horizontal diaphragms that collect and transmit inertia forces to the vertical structural system. It is of great importance that the vertical system acts together in resisting the horizontal seismic action. The final element model was assigned diaphragms on each floor level, meaning that each floor is assigned infinite in-plane stiffness. The advantage of this was obtaining a stiffer element model with reasonable mode shapes contrary to not assigning diaphragms to the model. The difference in the natural vibration period of a model with and without diaphragms is presented in table 3-8. However, even though it may be considered more realistic to have non-rigid floor behavior, using diaphragms resulted in a more stable element model.

Table 3-8: Comparison of natural vibration periods for the element model.

Mode	Natural period of vibration, T [s]		Difference [%]
	Model without diaphragms	Model with diaphragms	
1	3.0811	2.9346	4.8
2	2.9394	2.7265	7.2
3	2.5974	2.3218	10.6
4	0.8142	0.7638	6.2
5	0.5250	0.4512	14.0
6	0.4883	0.4482	8.2
7	0.4616	0.4121	10.7
8	0.4487	0.3621	19.3
9	0.3922	0.3165	19.3
10	0.3564	0.3077	13.7

Table 3-8 indicates a difference in natural vibration period of order 14.5% for the 10 first modes. The difference is greatest for higher modes. Higher modes contribute less than the first modes to the response. For the first 6 modes the difference of natural vibration period is of order 9.2%. This is a significant difference. However, it is as mentioned above considered reasonable to use this element model due to the fact that it resulted in more stable numerical analysis results and more realistic mode shapes. The reason for this is probably mostly due to better constraint assignments for the elements in the model.

3.4 ESTIMATE OF THE NATURAL VIBRATION PERIOD

Estimating the mass and the stiffness of the structure can only render rough estimates of the natural vibration period. Nevertheless, it has been performed as it is considered a necessity to be able to rely on the element model. A rough estimate procedure is to calculate the natural vibration periods for a generalized SDOF system using an assumed shape function. Such a system has the following generalized mass and generalized stiffness

$$m^* = \int_0^{h_{tot}} m(x)\psi^2(x)\,dx \tag{3.2}$$

$$k^* = \int_0^{h_{tot}} EI(x)[\psi''(x)]^2\,dx \tag{3.3}$$

where $m(x)$ and $I(x)$ is mass and second moment of inertia per unit length respectively and $\psi(x)$ is the assumed shape function. The natural frequency then becomes

$$\omega_n = \sqrt{\frac{k^*}{m^*}} \tag{3.4}$$

The analysis will provide *exact* results for rigid structures supported in a way that it can deflect in only one shape, but only *approximate* results for systems with distributed mass and flexibility such as Oslo Plaza.

It is chosen to look at the building as a cantilever beam with constant mass and stiffness. The shape function assumed is

$$\psi(x) = 1 - \cos\frac{\pi x}{2h_{tot}} \tag{3.5}$$

h_{tot} is the total height of the building, 117m. Mass and stiffness is assumed to be continuously distributed over the height. The second moment of inertia is estimated by looking at a general cross-section of the building as a beam section. Calculations of mass and second moment of inertia are given in Appendix C. The result is indicated in table 3-9 below.

Table 3-9: Estimates of generalized mass and 2nd moment of inertia.

Generalized mass, m* [kg/m]	2nd moment of inertia about the y-axis, $I_{TOT,X}$ [m^4]	2nd moment of inertia about the x-axis, $I_{TOT,Y}$ [m^4]
258 406	6 414	960

Using these estimates the two natural vibration periods obtained are T_1 = 2.0898 s and T_2 = 0.8085 s. These values are lower than the two first modes obtained from the modal analysis in SAP2000, as expected. The shape function assumes that the structure is fixed to the ground and does not consider soil flexibility. The cross section is presumed constant. In the real building one of the elevator cores is led to the 18th floor only. In addition, the wall thickness decreases with increasing height of the building. The top of the building is softer than the estimation implies since the shear walls and elevator core stop at the 34th floor. The estimation takes only the tower part of the complete building into consideration. However, another way to estimate the natural vibration period is to

only consider the part of the building between the 4th and 34th floor, but the assumption of a fixed base would be less accurate doing so.

Estimations as carried out above rendered reasonable results of the natural vibration period taking into consideration the estimate of the stiffness and the mass of the building. It was expected to obtain lower values of the periods; nevertheless it was values fairly close to verify the element model in SAP2000.

4 SYSTEM IDENTIFICATION AND STRUCTURAL MONITORING

Full-scale structural monitoring with the use of equipment from NTNU was conducted at Oslo Plaza. The purpose of performing the monitoring was to find the real natural vibration frequencies of the first mode shapes of the structure and compare it with the element model in SAP2000. The experimental data resulting from the test can verify the real structural properties and can be used to fit parameters in the element model to obtain a more realistic model for further structural and seismic analyses.

In the work of seismic analyses of a structure such as Oslo Plaza, there are two primary approaches that describe the work process when modeling:

- *Mathematical modeling*. The dynamic behavior of the structure is described based on mathematical theory in an analytical approach.

- *System identification*. The dynamic behavior of the structure is described based on an experimental approach. Tests are performed on the real structure, and the model is then fitted to the recorded data to obtain a more realistic behavior of the model. Further analyses can then be carried out with an improved model to obtain more realistic results reflecting different seismic scenarios to better represent the behavior of the structure.

In the work presented a combination of both of these approaches is used. The structure is represented as an element model in SAP2000 as described in the previous chapter. This model will be improved by performing a system identification process to find the natural vibration frequencies of the structure. When this has been done, analyses based on mathematical models and mathematical theories are used to find the behavior of the structure exposed to different kinds of seismic actions. The process can be summarized as shown in figure 4-1.

As presented in Chapter 3, the building has been modeled in SAP2000 based on architectural drawings. Even though an element model of the building has been modeled in such a way, the structure itself is more complex than the element model due to unknown parameters occurring in the real life. To include the unknown parameters in the element model system identification methods can be implemented. What is desired in the end is to obtain a realistic model of the structure representing realistic behavior.

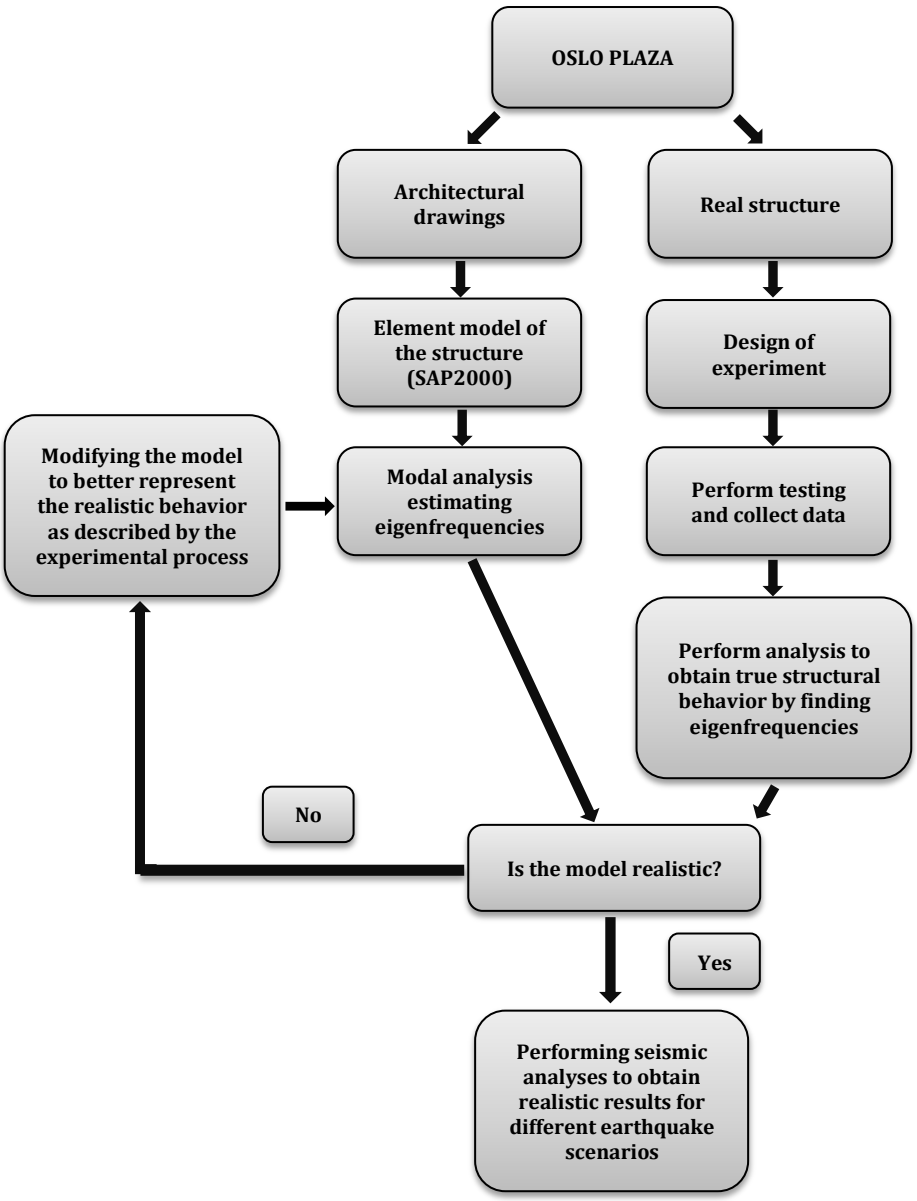

Figure 4-1: Schematic overview of the process of finding a good element model.

This chapter provides information about the simulation of the monitoring procedure, the equipment used and a description of how the monitoring was performed. Results from the monitoring are provided along with a discussion and an interpretation of the data obtained.

4.1 SIMULATION OF THE MONITORING PROCESS

Due to the uncertainty in using monitoring equipment in full scale testing, a simulation of the monitoring process was performed in order to better understand the complete structural monitoring procedure and to be able to select optimal location for the sensors. The simulation also indicated what to expect of the results from the full-scale testing.

As a part of the monitoring process, a simulation of white noise on the structural element model was performed with the objective to obtain an estimate of the first four natural frequencies of vibration of the structure. White noise was simulated in Matlab as described in Chapter 2.5, and implemented in the element model in SAP2000. Figure 4-2 shows the white noise as implemented in SAP2000.

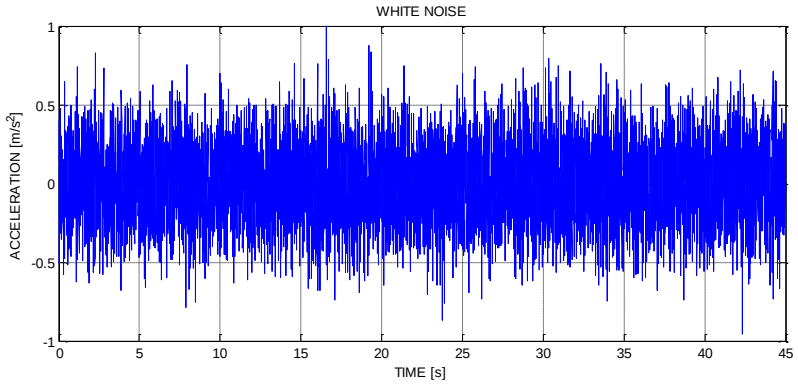

Figure 4-2: White noise with a sampling frequency of 200 Hz implemented in SAP2000.

The procedure consisted of generating a time-series of 45 s with a sampling frequency of 200 Hz with random values assigned as acceleration in m/s^2, in Matlab. This was implemented in the x-direction and the y-direction in SAP2000 on the element model. An analysis was then performed to find the displacement at certain nodal points in the element model corresponding to the placement of the sensors in the building for the structural monitoring process.

The displacement obtained in the element model was then scaled down to represent a displacement of 1 mm in the x-direction on the model and 1 mm in the y-direction on the model, i.e. top displacement. Based on this, time-series of acceleration was then generated and analyzed in Matlab for nodal points corresponding to sensor 1, sensor 2, sensor 3 and sensor 4, see figure 4-3. The scaling was performed as described because 1 mm of displacement in the top of the building is a value that might be expected as structural displacement typically caused by (white) environmental back-ground noise.

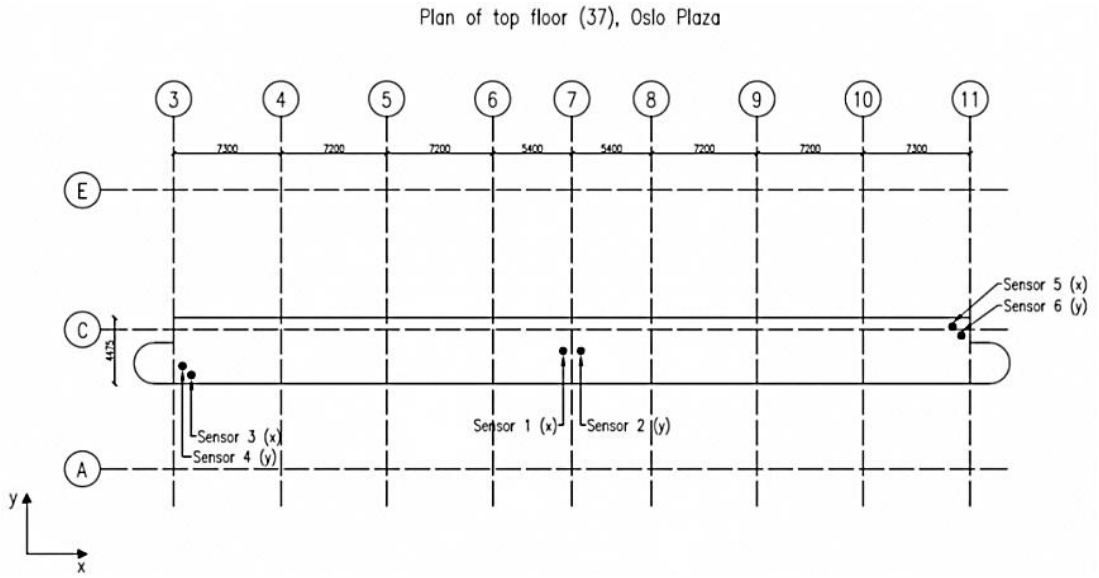

Figure 4-3: Nodal points representing sensor 1, 2, 3 and 4 in the element model.

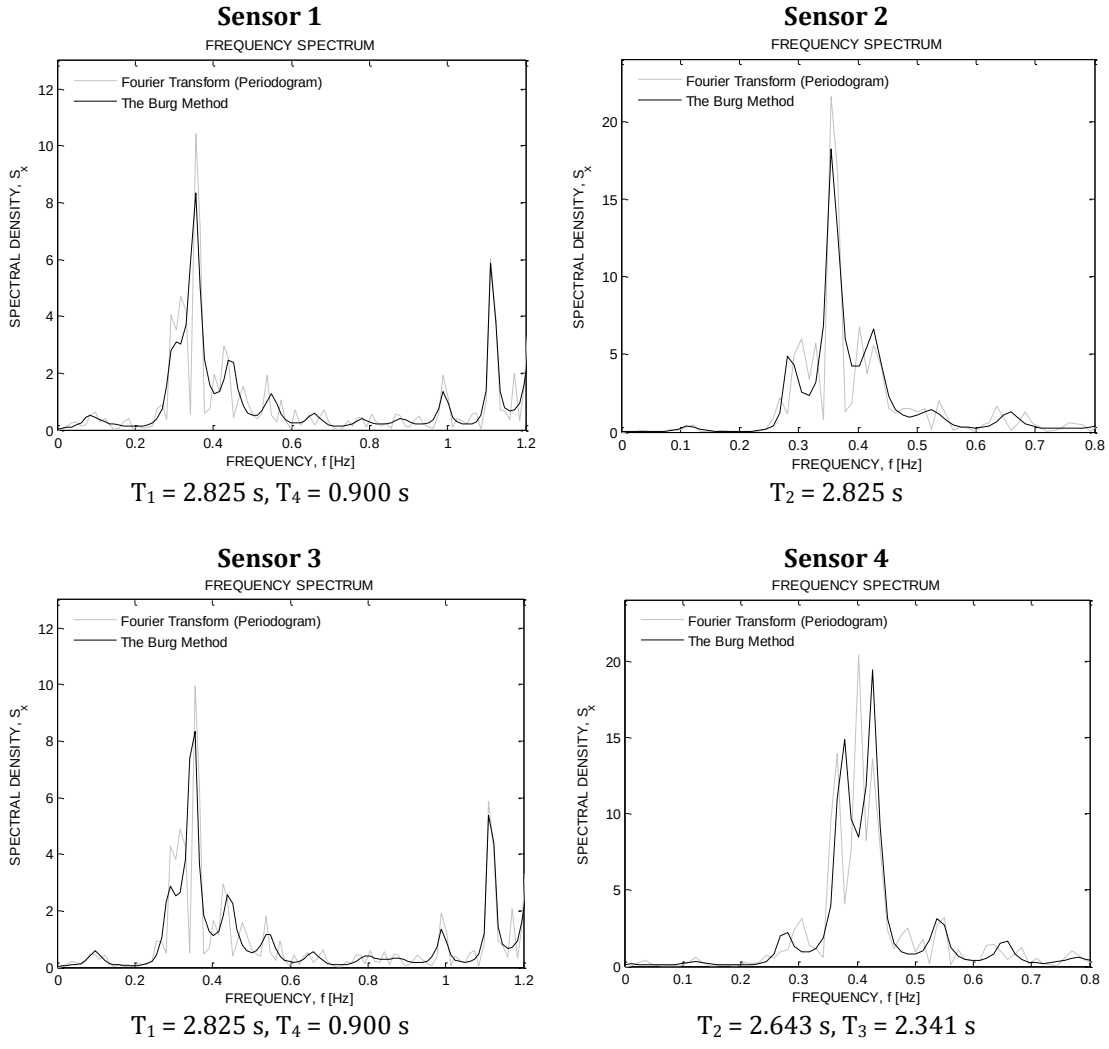

$T_1 = 2.825$ s, $T_4 = 0.900$ s

$T_2 = 2.825$ s

$T_1 = 2.825$ s, $T_4 = 0.900$ s

$T_2 = 2.643$ s, $T_3 = 2.341$ s

Figure 4-4: Results of the analysis obtained from the simulation of white noise.

As figure 4-4 shows, analyzing the data obtained from the simulation in Matlab and SAP2000 renders reasonable estimates of the natural vibration frequencies of the structure based on white noise as source of excitation. A Fourier analysis was used to find the natural vibration frequencies, and an autoregressive (AR) model based on The Burg Method was used for validation of the natural frequencies. The order of the AR model used was 2000 which was found to be the best suited order in the comparison of the methods. This was found by trial and error. The damping ratio in the element model in SAP2000 was set to 5%. As can be seen from table 4-1, there is a difference between the estimates of the natural vibration periods of the element model and from the simulation. This difference may be explained by the frequency resolution of The Burg Method. It is referred to Appendix D for the Matlab-script used to generate the natural frequencies.

Table 4-1: Comparison of results from the element model and the simulation.

Mode	Natural vibration period, T [s]		Detected by sensors			
	Structural element model	Element model simulation	Sensor 1	Sensor 2	Sensor 3	Sensor 4
Mode 1	2.935	2.825	x		x	
Mode 2	2.727	2.825		x		x
Mode 3	2.322	2.341				x
Mode 4	0.764	0.900	x		x	

With this as a basis for performing the structural monitoring the white noise in the structure may render the natural frequencies of vibration. However, this is also dependent on several factors such as the magnitude of the white noise and that the equipment used in the monitoring process will be able to intercept and process the signals.

4.2 EQUIPMENT

Equipment was provided by the structural engineering laboratory at NTNU in order to be able to perform the structural monitoring. Along with various basic equipment needed to perform the testing, the following description of the main equipment is provided here.

Table 4-2: List of equipment used in the monitoring process.

ELECTRONIC EQUIPMENT	NON-ELECTRONIC EQUIPMENT
HBM Spider 8 amplifier	5-wire cables for sensors; 4 x 45 m and 2 x 5 m
6 sensors registering acceleration [m/s^2]	3 undercarriages for sensors
PC	Extension cord, tape line, electronic range finder, tape

A schematic overview of the equipment and how this is connected is presented in figure 4-5.

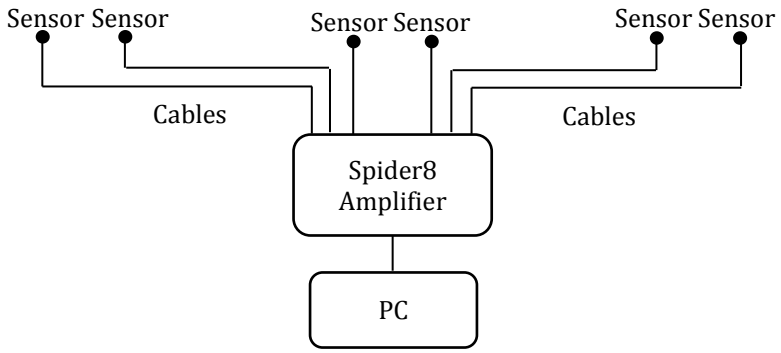

Figure 4-5: Schematic overview of the equipment used in the monitoring process.

The purpose of the amplifier is to receive signals and perform signal conditioning from passive external sensors, i.e. amplification, digitalization, and filtering of data. The amplifier can receive data from maximum 8 channels. Each channel provides excitation from the sensors, and each channel has its own analogue-to-digital converter (A/D converter). All A/D converters operate synchronized to ensure simultaneous measurement on all channels and provides up to 9600 measurements per second from each channel with a resolution of 16 bit [32]. The sensors are connected using 5-wire connection cables. This stabilizes possible sensitivity losses due to the great length of the cables (up to 45 m).

As a part of the metering system a digital anti-aliasing filter was used. The digital low pass filter of the devices is automatically set to a frequency best suited for the sample

rate in use. This means that the software compensate and finds the best filter for the type of measurements performed and for the given sampling frequency.

To conduct the structural monitoring accelerometers were used as sensors. The accelerometer is a device that measures physical acceleration experienced by an object, in this case the structure. It measures the acceleration in one specific direction, a so-called single-axis accelerometer. It detects the magnitude of the proper acceleration in the given direction, measured in the unit of m/s^2.

The sensor measures the acceleration of the free-fall reference frame relative to itself and this is equivalent of the acceleration felt by the object. This is done by measuring weight per unit of mass [33]. Inductive half bridge strain gage accelerometers were used. The minimum acceleration the sensors can measure is 0 m/s^2, and the maximum acceleration is 500 m/s^2. This covers the range of interest well for the purpose of this study.

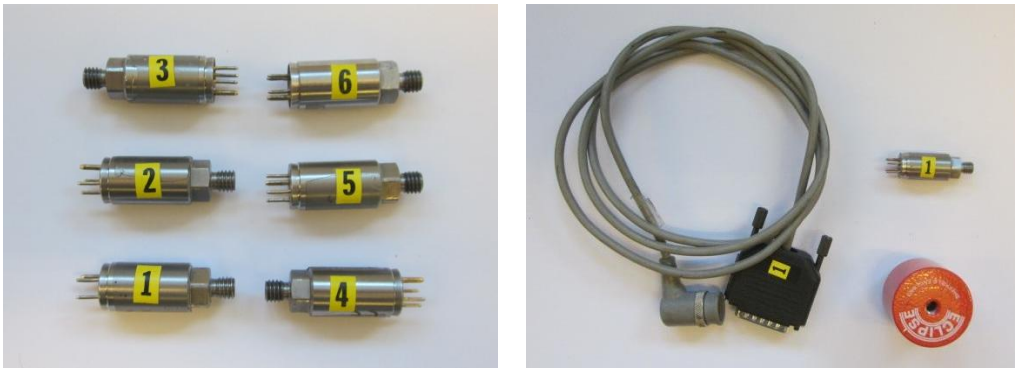

Figure 4-6: The accelerometers, cable connectors and placeholders used in the monitoring process.

The calibration of the sensors is an essential process to perform ahead of the monitoring procedure performed in the field. This was done by calibrating each and one of the sensors with their respective cables. The calibration process consists of two steps:

1. Accelerometer placed vertically, calibrated to 1 g[3].
2. Accelerometer placed horizontally, calibrated to 0 g.

This process was repeated for all of the accelerometers. The sampling frequency used is 50 Hz. The minimum and maximum dynamic range of the accelerometers was set to -1 m/s^2 and 1 m/s^2 respectively.

The dynamic range had to be adjusted individually. Some of the sensors would not accept this dynamic range and to avoid overflow problems of data the values were adjusted ±1 m/s^2.

[3] g is 9.81 m/s^2

4.3 STRUCTURAL MONITORING PROCEDURE

For the structural monitoring process there are two important aspects to consider; the *placing* of the sensors at the given floors and the *time length* for each measurement. It is essential that the building is excited, preferably by strong wind or by earthquake to obtain best possible data from the monitoring process. Due to the limited time to perform the structural monitoring in this study, i.e. within 24 hours, it is unlikely that an earthquake will occur. Hence, wind is an important factor for best possible results.

In the present study 6 sensors measuring structural vibrations in the plane direction, x and y, were located at a given floor. It is important to emphasize that the placing of the sensors provide limited information about the actual mode shapes of the structure. However, an estimate of the natural vibration periods of the first modes is desired to obtain from the monitoring procedure.

4.3.1 PLACING OF SENSORS AND TIME LENGTH

To obtain information about the natural vibration period for the first three mode shapes, the sensors were placed according to figure 4-7 at the top floor of the structure. This floor is located at +108.3 meters above sea level.

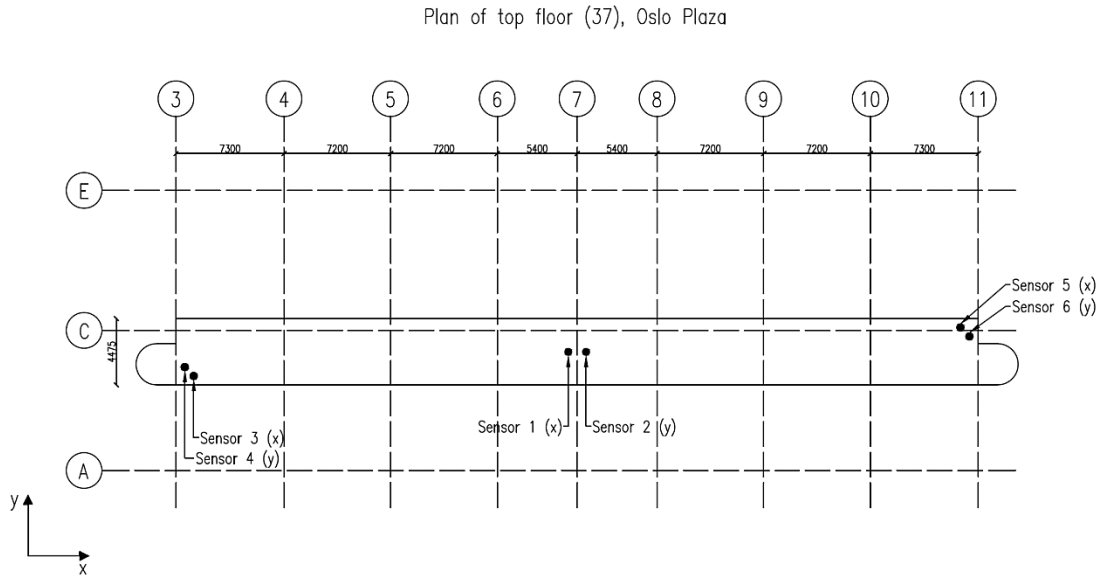

Figure 4-7: Plan of top floor with the placing of sensors.

To obtain information about the natural vibration period for what is assumed is the 4th mode, the sensors were to be placed according to figure 4-8 at the 19th floor after studying floor displacements for the given mode in the element model in SAP2000.

Unfortunately, through the structural monitoring process it was decided to keep the sensors at the top floor due to the lack of vibration in the structure.

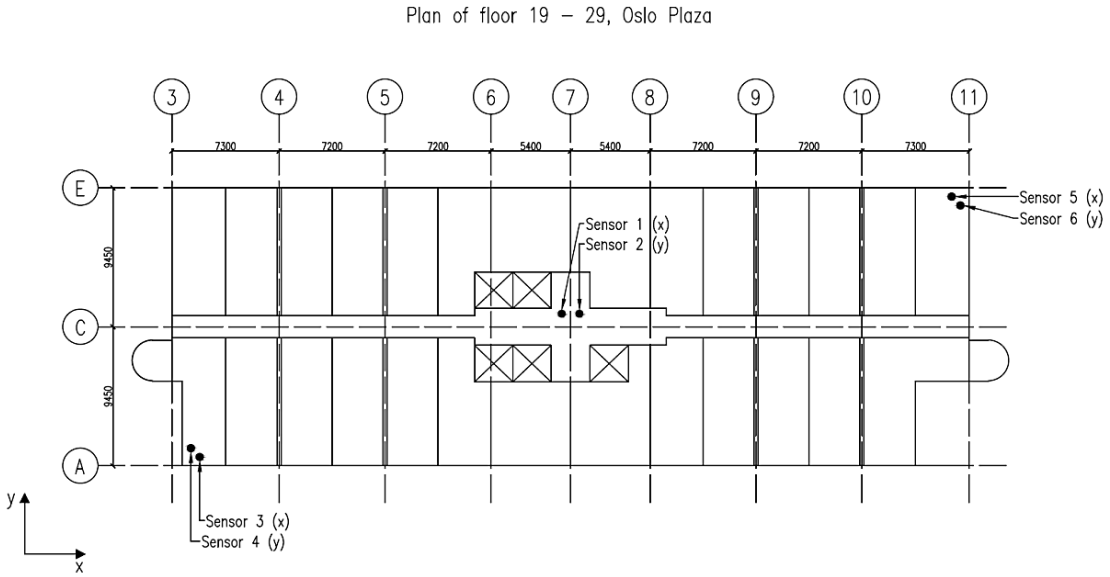

Figure 4-8: Plan of floor 19-29 with placing of the sensors.

To ensure getting sufficient data about the vibration of the structure the time range for each monitoring were set to be at least 60 min according to the prearranged plan. Due to the wind activity in the Oslo area and to various activities in the hotel this had to be adjusted during the monitoring process. It was decided during the process to keep continue monitoring on the top floor due to low vibration response in the building. Altogether, three individual measurements were performed, as indicated in table 4-3:

Table 4-3: Overview of the structural monitoring tests performed.

Test	Time length of test, t [s]	Point of time	Wind activity	Sampling frequency, [Hz]
I	3600	11.00 - 12.00	None	50
II	5400	13.00 - 14.30	None	50
III	18000	23.00 - 04.00	2 - 4 m/s	50

4.4 RESULTS

In the majority of the recordings obtained, there was no distinct natural excitation force that induced vibrations in the structure. Best data was obtained from test III, but neither the wind nor the white noise was strong enough to excite the building as much as desired. The acceleration history plot from this test is indicated in figure 4-9.

The data obtained from the first two tests resulted only in noise. After filtering out frequencies of no interest, there was no result that gave a clear indication of possible natural frequencies of vibration of the building.

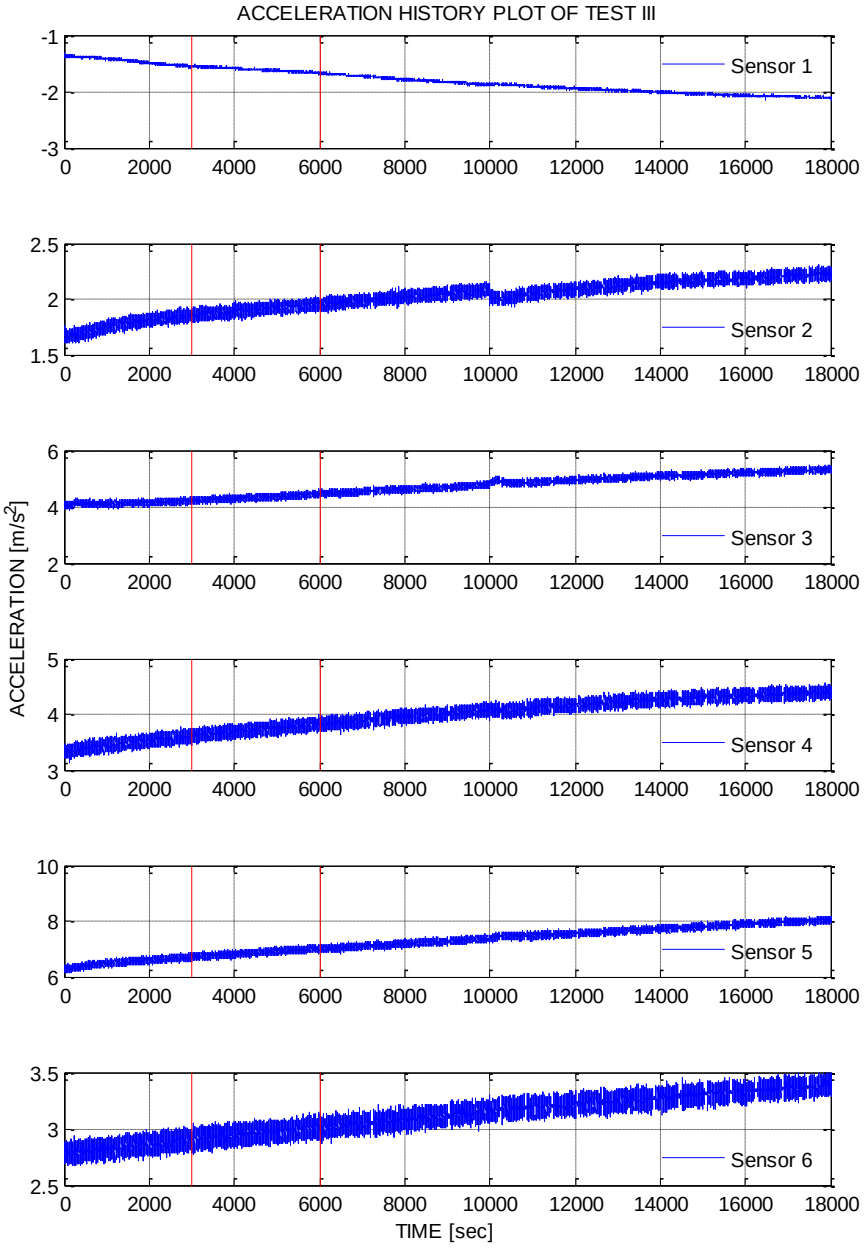

Figure 4-9: Acceleration history plots of test III from all 6 sensors.

The result obtained from test III was far from expected. A linear trend in the acceleration values about the x-axis, i.e. acceleration values of zero mean, was expected. Different acceleration values for each sensor on the y-axis are observed, and this has most likely to do with calibration problems of the sensors prior to the test. The decreasing trend in the acceleration values for sensor 1 and increasing trend for the other sensors are most likely due to great temperature changes on the top floor where

the monitoring took place. However, by extracting data from a time interval of 3000 s as depicted by the red lines in the plot and using the function `detrend` in Matlab to remove the linear trends in the acceleration-vector, the processing of the new data as indicated in figure 4-10, were used for further analyses.

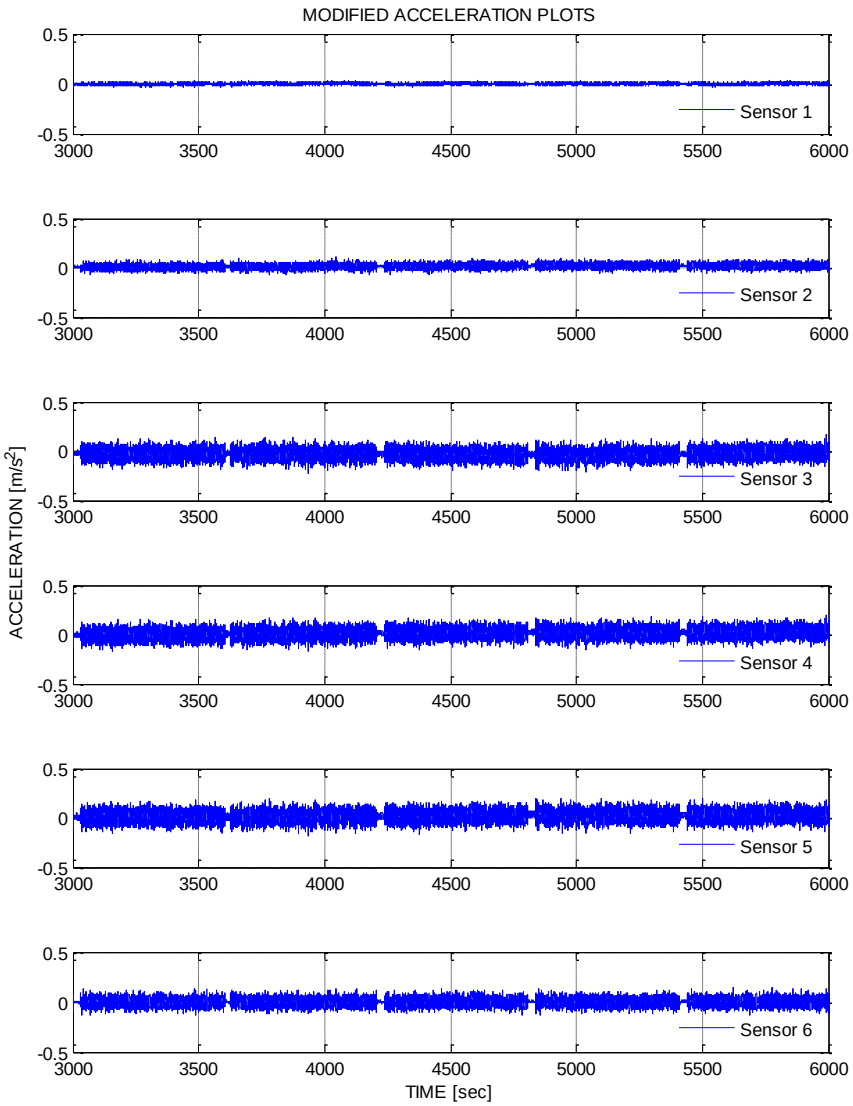

Figure 4-10: Modified acceleration plots of a segment of time for all 6 sensors.

The data indicated in figure 4-10 was analyzed using unsmoothed Fourier amplitude power spectra, i.e. periodogram, and an AR-model based on The Burg Method. Using these methods should result in a plot where the peaks are to indicate the natural frequencies of the structure. These frequencies are the ones needed in order to calibrate the element model.

Using the Burg Method, the power spectral density (PSD) is computed with an autoregressive (AR) model [34]. The order of the AR model used varied in the range of 20 - 2500 during the processing of the data. The selection of the order has to be done

with caution. A low order results in a smooth estimate whereas a high order results in including peaks that may not be statistically significant and hence indicating fake peaks. After performing analyses of all sensors, only one resulted in reasonable estimates of the natural frequency of vibration as indicated in figure 4-11. The order used for this analysis was 1500.

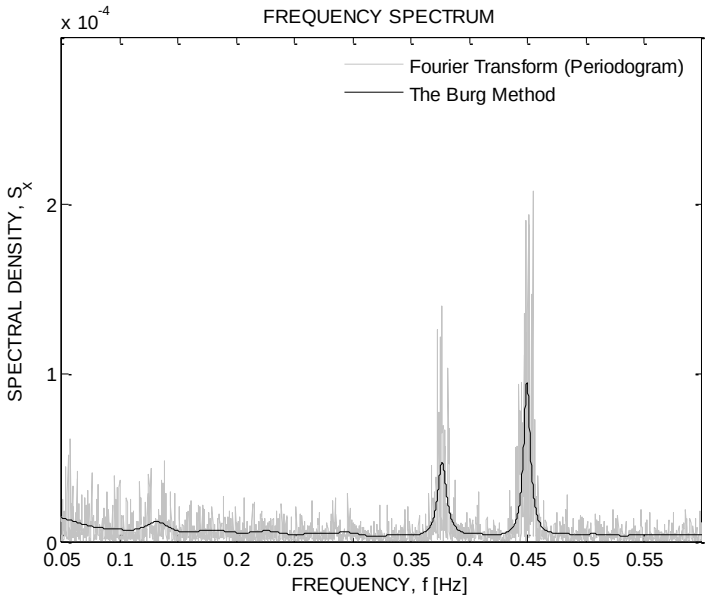

Figure 4-11: Fourier transform and The Burg Method for sensor 1.

The result of the analysis of sensor 1 is shown in figure 4-11. This sensor measures the acceleration in the x-direction of the structure as shown in figure 4-7 and gives two natural vibration frequencies of 0.4543 Hz and 0.3767 Hz. This corresponds to a natural vibration period of 2.20 s and 2.66 s respectively. Ideally, this result should indicate only the first mode, translation in the x-axis. However, it may under certain circumstances also indicate the second mode, translation in the y-direction, if the sensor is not completely aligned in the x-direction.

The results from the other sensors from the other tests did not render any information within reasonable expectations of the natural frequency of vibration. The other tests indicated white noise only, but not enough to excite the building and render natural frequencies as expected from the simulation process described in Chapter 4.1. Sensor 1 was attached to the steel frame in the top of the building. The results of the data analyzed may indicate local properties of this steel frame based on disturbances from the below floors.

As a conclusion of the results obtained from the structural monitoring process, one sensor from one test resulted in what may be considered a reasonable natural frequency of vibration for the structure. Looking at table 4-4, the fundamental period from the structural monitoring is close to the period obtained from the element model simulation. The stiffness of the real building is in general higher than the stiffness

obtained from the computational model due to the complexity of the structure contributing to increased stiffness, which is confirmed by this result.

Table 4-4: Comparison of the results obtained.

Mode	Natural vibration period, T [s]		
	Structural element model	Element model simulation	Structural monitoring
Mode 1	2.93462	2.825	2.65463
Mode 2	2.72646	2.825	2.20119

However, this is an individual result measured in one direction. There is no indication of correlation between the other sensors and there is no consistency from the other tests or sensors in which this result may be confirmed. The likelihood of several sources of error having an effect on the monitoring process leads to the conclusion of not having obtained desired parameters to fit the element model with to obtain a more realistic model for further structural and seismic analyses.

4.5 SOURCES OF ERROR

Potential sources of error during the structural monitoring process leading to undesirable results may be several. A list included of possible sources during the monitoring is provided here:

- The equipment used was laboratory equipment provided by NTNU. This kind of equipment is not as well suited for field operations due to lack of robustness. Problems with sensitivity due to environmental changes and problems with calibrating the sensors in the field are important sources of error.
- Long cables up to 45 m were used to reach the ends of the building with the sensors. Long cables such as the ones used increase the possibility of losing data.
- Little or no excitation force, such as wind, was present during the structural monitoring process to induce vibrations in the structure.
- The environmental back-ground noise in the building was not strong enough to render the natural frequencies of vibration after processing the data. Local disturbances such as human activity close to the sensors and loud music from the floors below in short periods of time during the monitoring may have caused undesirable noise.
- The structural monitoring process took place within a short period of time, i.e. within 24 hours. Ideally, structural monitoring should be performed over a long period of time to ensure good quality of the data and to increase the possibility of the structure experiencing excitation from external forces.

- The equipment applied was sensitive to temperature variations. The walls and the roof on the top floor where the monitoring took place were surrounded by a glass facade. This caused the temperature to vary 2 – 6°C, which is of great significance for the final results.

4.6 Lessons Learned

Structural monitoring of buildings requires advanced and robust equipment, good planning of the process and external forces to excite the structure. Moreover, good routines for processing the data obtained with good system identification methods to improve the element model are an essential part of the process. Field experiments do not always render satisfactory results, but the learning of performing the process and analyzing data obtained is often as important as obtaining useful results.

5 METHODS OF ANALYSIS

There are many methods of analysis for evaluation of the seismic performance of buildings. For the high-rise structure considered time-history representation analyses with emphasis on near-fault ground motion data is the main area of interest. Comparing a general response spectrum analysis according to EC8 with time-history representation analyses is of great value. This has been performed in addition to scale the time-series according to EC8 for the purpose of comparison. Simulation of time-series and rotation of time-series has been performed as well to be able to look at possible scenarios that might cause undesirable structural response. This involves modifications of the time-series, and the procedure of modification is presented in this chapter along with discussions. The chapter ends with a discussion of different methods of scaling.

In the following, it has been chosen to focus on linearly elastic representation and modeling. The investigation of whether the external loads in the form of earthquake records, hereunder near-fault earthquakes in particular, provide adequate response of an elastic structure has been emphasized. Thus, no ductility has been assigned the model of the structure, nor the response spectra. However, knowing that most building structures are designed to develop ductility in their structural elements, this has not been considered in the work of this study. The argument for this is that the peak response of the structure is of interest in performance based design when considering serviceability limit state.

5.1 MODAL RESPONSE SPECTRUM ANALYSIS

A modal response spectrum analysis involves calculating the principal modes of vibration of the structure. Using the response spectrum, the maximum response in each mode can be found. The contribution from every mode is then summed by an appropriate method as presented in Chapter 2.3.3 to produce the overall maximum response [9]. The result of the modal analysis is presented in table 3-7. As mentioned in Chapter 3.3, the total of 200 modes is included to obtain the contribution from as many modes as possible and to ensure that the modal participating mass ratio is as close to 100% as possible in all directions. By doing this, an approximation of the peak dynamic response of the structure is performed with the highest level of accuracy.

For the building considered, the modal response spectrum analysis has been performed in SAP2000 using the CQC rule for modal combination. The response spectrum has been generated by following the EC8. It has been emphasized to use the horizontal and vertical elastic response spectrum. This generally consists of excluding the behavior factor, q. This has been done with the intention of comparing the results of the EC8 response spectrum with the time-history representation analyses. However, if a ductility factor were to be assigned for the purpose of finding the seismic design forces,

$$q = 1.5 \tag{5.1}$$

is a reasonable ductility factor to implement for this building. The parameters used to generate the response spectrum are presented in table 5-1 and table 5-2. The map of seismic zones given in the National Annex (N.A.) of EC8 [15] has been used to find the reference peak ground acceleration for the location of the building; Oslo.

Table 5-1: Reference peak ground accelerations and factors by the Norwegian N.A., EC8 [15].

a_{g40Hz} [m/s^2]	a_{gR} [m/s^2]	a_g [m/s^2]	a_v [m/s^2]	γ_I
0.55	0.44	0.44	0.264	1.0

Table 5-2: Recommended values of parameters describing the response spectra by the Norwegian N.A., EC8 [15].

Component	S	T_B(s)	T_C(s)	T_D(s)
Horizontal elastic	1.6	0.15	0.45	1.50
Vertical elastic	1.0	0.05	0.20	1.20

The ground type at the site is chosen to be ground type D based on evaluations of the soil conditions. This decides the recommended values of parameters as described in table 5-2 for the horizontal elastic response spectrum. For the vertical response spectrum, EC8 recommends the soil factor S being equal to 1.0.

The response spectra generated and implemented in the modal response spectrum analysis are indicated in figure 5-1.

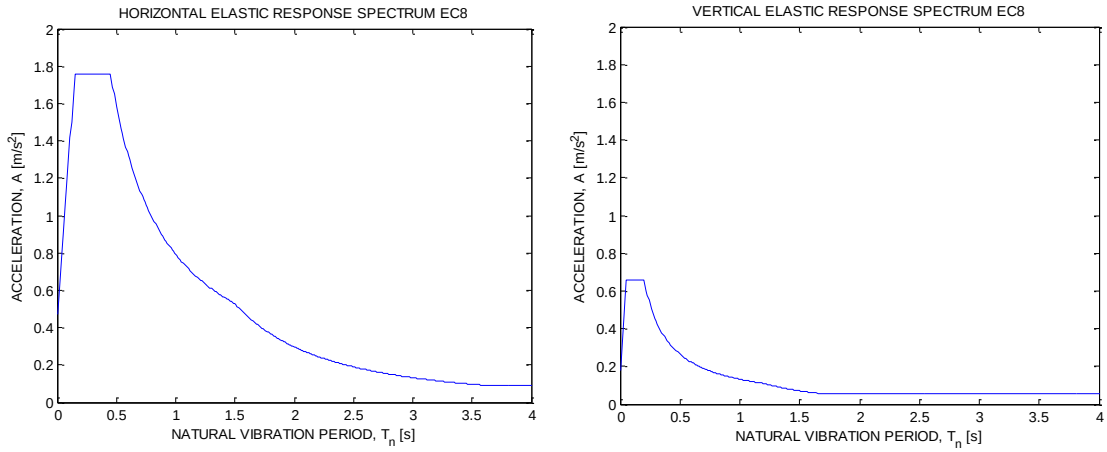

(a) **(b)**

Figure 5-1: Elastic response spectra according to EC8. (a) Horizontal response spectrum. (b) Vertical response spectrum.

The combination rules used are

$$E_1 = E_x + 0.3E_y + 0.3E_z \tag{5.2}$$

and

$$E_2 = 0.3E_x + E_y + 0.3E_z \tag{5.3}$$

Using the combination rules as stated in eq. (5.2) and eq. (5.3) for the modal response spectrum analysis rendered results for the purpose of comparison with the time-history representation analyses. It should be noted that it is not necessary to include the vertical elastic response spectrum according to EC8 [15], 4.3.3.5.2(2) since

$$a_v = 0.264\,\frac{m}{s^2} < 0.25g \tag{5.4}$$

For the purpose of comparison this has been included in the analyses since the vertical component is included in the time-history representation analyses.

5.2 Modal Time-History Representation Analysis

For a modal time-history representation analysis, seismic action is represented in the form of time-series of the ground motion. According to EC8 [15], 3.2.3.1.1(2)P, it is required that the seismic action shall consist of three simultaneously acting accelerograms. The same accelerogram may not be used simultaneously along both horizontal directions [15]. If the response is obtained from at least seven non-linear time-history analyses, the average of the response quantities from all these analyses may be used. Otherwise, the most unfavorable value of the response quantity among the analyses should be used for design purposes as a conservative approach.

At least three artificial, recorded or simulated records of earthquakes may be used as input for the representation of seismic action. This implies that pairs or triplets of different records for analysis under two or three simultaneous components of the action can be used [14], [35]. This may be stated based on an interpretation of the meaning of an accelerogram by EC8. Each ground motion record consists of three components; longitudinal (NS), transverse (EW) and vertical.

According to EC8 [15] 3.2.3.1.3(1) the values of recorded accelerograms or accelerograms generated through a physical simulation of source and fault-mechanisms may be used if the records can be regarded as representative and are scaled to $a_g S$ for the relevant site. The records given are assumed to represent ground type A. In general for the Oslo region around Oslo Plaza the scale factor

$$a_g S = 0.44 \cdot 1.6 = 0.704 \tag{5.5}$$

may be used. Proper methods of scaling will be subject for discussion in Chapter 5.4. In the analyses performed, two combinations are implemented as indicated in table 5-3.

Table 5-3: Combination of records in the time-history representation analyses.

Analysis	Component record in x-direction	Component record in y-direction	Component record in vertial direction
I	NS	EW	Vertical
II	EW	NS	Vertical

The largest response from either of these two analyses is being considered when presenting the results.

The ground motion data used in the time-history representation analyses is presented in table 5-4. Three sets of three component recorded time-histories are chosen by recommendation for the seismic zone of Norway [11].

Table 5-4: Key parameters of the ground motion data used for time-history representation analyses.

Earthquake	Recording site	Date	Type of earthquake	Fault distance [km]	Component	Magnitude	PGA [m/s^2]
Friuli, Italy	Tarcento	11.09.1976	Near-fault	19	NS	5.2	1.8985
					EW	5.2	0.8046
					Vertical	5.2	0.4689
Imperial Valley, USA	Superstition Mountain	15.10.1979	Near-fault	24	135°	5.7	1.3561
					45°	5.7	1.0431
					Vertical	5.7	0.7558
Nahanni, Canada	Site 3	23.12.1985	Far-fault	29	NS	6.9	1.2358
					EW	6.9	1.2492
					Vertical	6.9	1.2229

These records are selected for magnitudes, distances and peak accelerations which would correspond to an earthquake with low exceedance probability, but allowing for variation in the parameters as well as in the spectral content and duration. These records are representable for the seismic zone of Norway, hereunder Oslo specifically. The ground motion data have been modified in a way that the permanent drift has been removed. This means that the building will not displace or drift as a result of the ground motion. The advantage of this is to obtain a more specific structural displacement response when evaluating the seismic response of the building.

In general, a design earthquake may be defined as an earthquake with a given magnitude assumed to occur on a specific fault near a specific site [11]. The time-histories selected and presented above are not within the definition of such an earthquake. As long as the earthquake recordings, as presented in table 5-4, fit the target spectrum in a reasonable manner, the magnitudes may be within a range of possible values after proper scaling.

5.2.1 *FAR-FAULT EARTHQUAKE RECORD*

The far-fault earthquake chosen for the time-history representation analysis is the 1985 Nahanni earthquake, Canada.

Table 5-5: Key parameters for the far-fault earthquake; 1985 Nahanni earthquake, Canada.

Earthquake	Recording site	Date	Type of earthquake	Fault distance	Component	Magnitude	PGA [m/s^2]
Nahanni, Canada	Site 3	23.12.1985	Far-fault	29	NS	6.9	1.2358
					EW	6.9	1.2492
					Vertical	6.9	1.2229

The PGA values for all of the three components of this earthquake are fairly equal. The ground motion acceleration plot for all three components is indicated in figure 5-2.

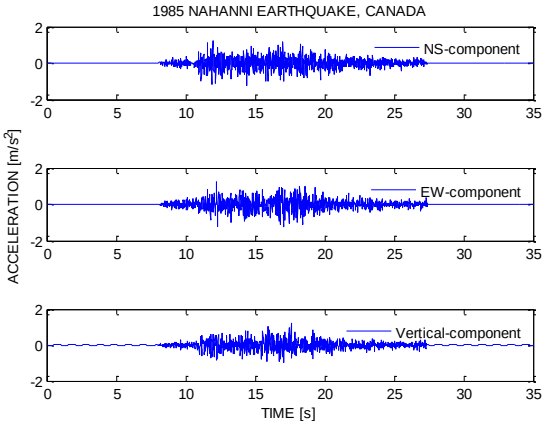

Figure 5-2: Ground motion acceleration plots for all three components of the Nahanni earthquake.

A response spectrum based on the Newmark method has been generated for this strong ground motion in particular. Plots showing the comparison of this specific response spectrum with the EC8 response spectrum are indicated in figure 5-3. As can be seen from this figure, the response spectrum for the specific earthquake is more jagged, and is in general not suitable for design purposes. The response spectrum generated for the earthquake has higher acceleration values for shorter natural vibration periods. However, the acceleration values are lower for natural vibration periods longer than approximately 0.2 s. The EC8 response spectrum is derived from statistical analyses resulting in so-called uniform hazard spectra, presented as smooth curves and straight lines and is thus preferred for design purposes [12]. The comparison of these plots is presented with the purpose and intention of comparison.

As expected, the vertical response spectrum is higher for the specific earthquake due to the fact that the vertical component can be excluded in the calculations according to EC8 as stated in eq. (5.4).

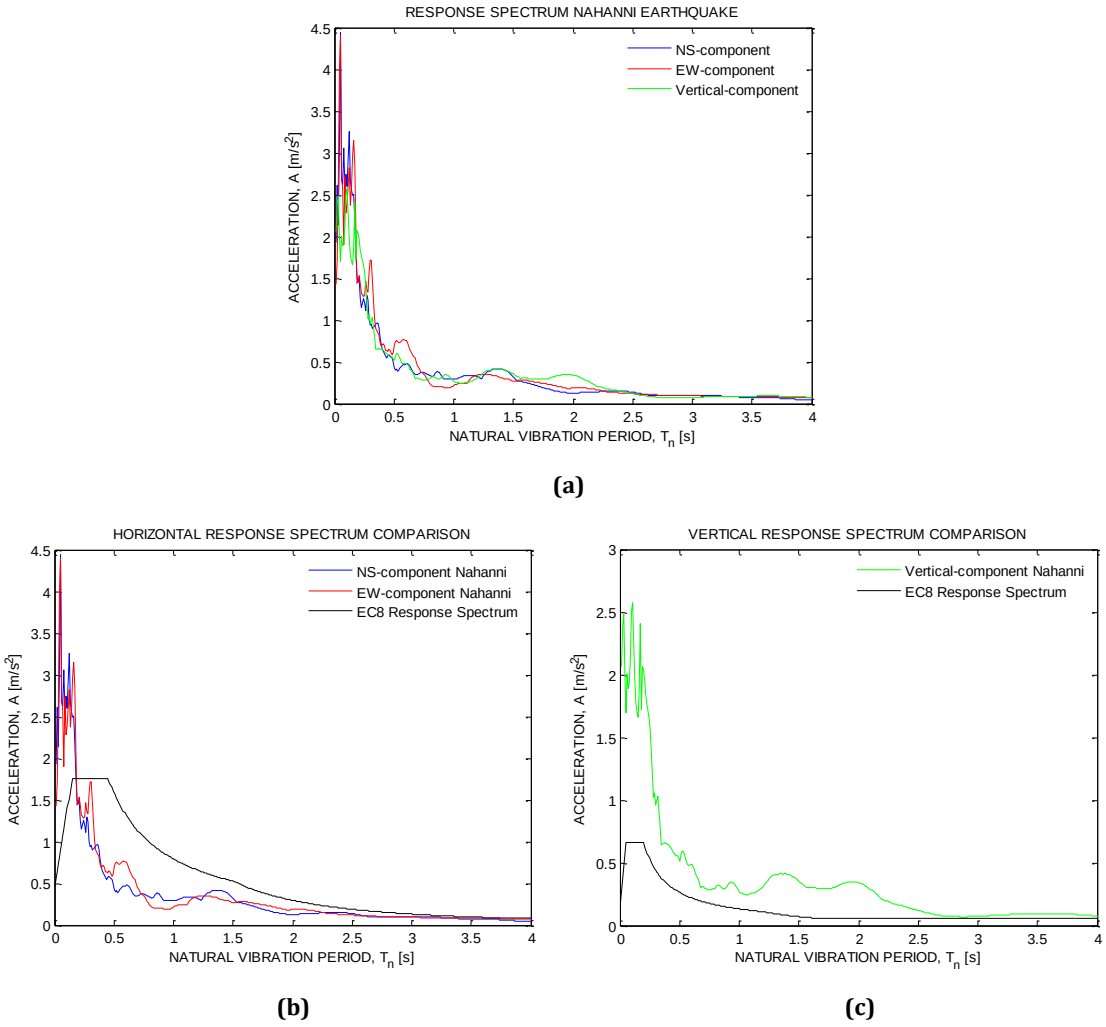

Figure 5-3: Properties of the 1985 Nahanni earthquake, Canada. (a) The response spectrum generated for the earthquake. (b) The response spectrum for the horizontal components compared to the EC8 response spectrum. (c) The response spectrum for the vertical component compared to the EC8 response spectrum.

5.2.2 NEAR-FAULT EARTHQUAKE RECORDS

The near-fault earthquake records chosen for the time-history representation analysis is the 1976 Friuli earthquake, Italy, and the 1979 Imperial Valley earthquake, USA.

Table 5-6: Key parameters for the near-fault earthquakes.

Earthquake	Recording site	Date	Type of earthquake	Fault distance [km]	Component	Magnitude	PGA [m/s^2]
Friuli, Italy	Tarcento	11.09.1976	Near-fault	19	NS	5.2	1.8985
					EW	5.2	0.8046
					Vertical	5.2	0.4689
Imperial Valley, USA	Superstition Mountain	15.10.1979	Near-fault	24	135°	5.7	1.3561
					45°	5.7	1.0431
					Vertical	5.7	0.7558

The PGA values for all of the three components of both of the earthquakes vary more than that of the far-fault earthquake. The ground motion acceleration plots for all three components are indicated in figure 5-4.

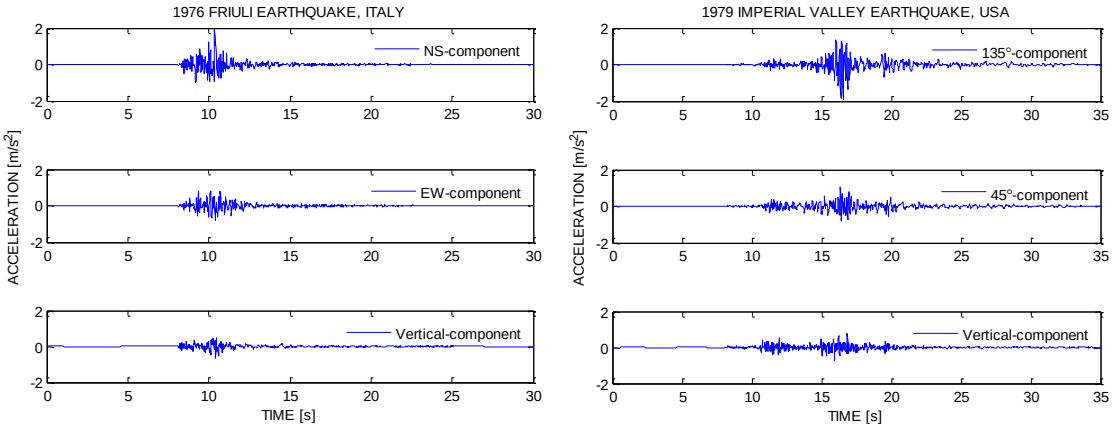

(a) **(b)**

Figure 5-4: Ground motion acceleration plots for the near-fault earthquakes. (a) 1976 Friuli earthquake, Italy. (b) 1979 Imperial Valley earthquake, USA.

Figure 5-5 shows the response spectra for the given earthquakes showing all three components in the same plot. As can be seen from these plots, the Friuli earthquake does not render as high values of acceleration for low natural vibration periods as the Imperial Valley earthquake. Figure 5-6 shows the comparison of the specific earthquakes with the EC8 response spectrum. The same general conclusions drawn from the far-fault earthquake can be stated for the near-fault earthquakes presented in this figure.

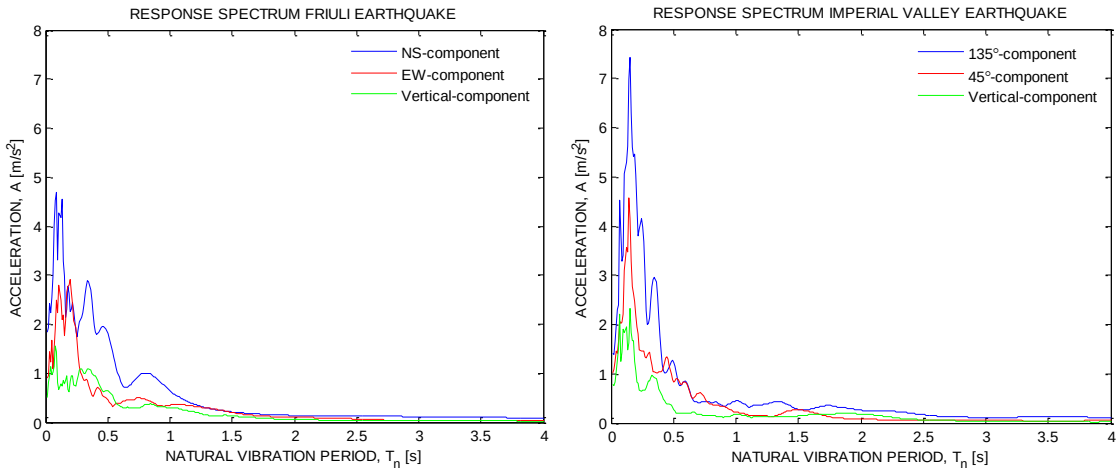

(a) **(b)**

Figure 5-5: Response spectra generated for the near-fault earthquakes. (a) Response spectrum for the 1976 Friuli earthquake, Italy. (b) Response spectrum for the 1979 Imperial Valley earthquake, USA.

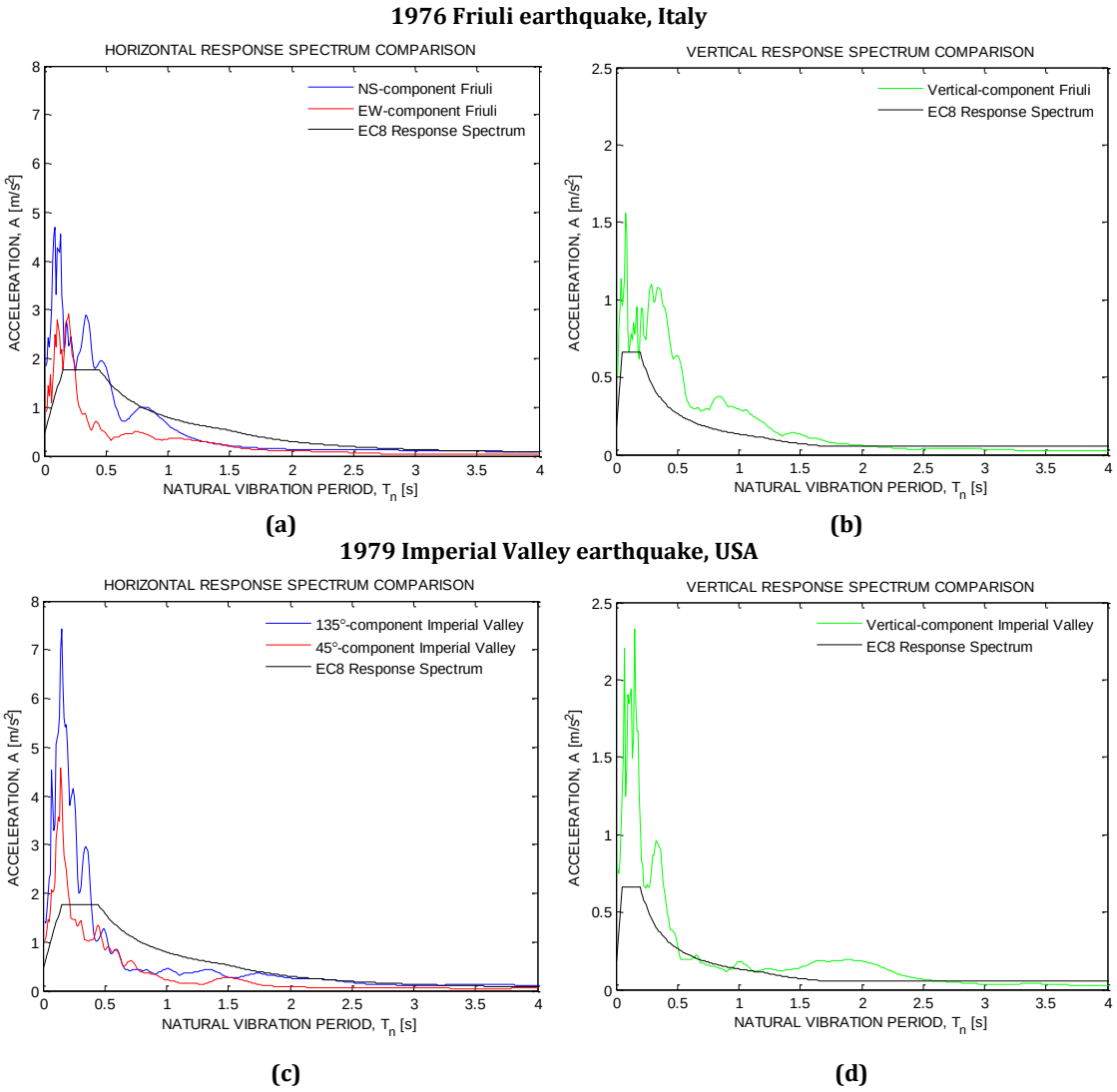

Figure 5-6: Comparison of response spectra for horizontal and vertical components to EC8. (a), (b) The response spectra for the horizontal and vertical components for the Friuli earthquake. (c), (d) The response spectra for the horizontal and vertical components for the Imperial Valley earthquake.

An important observation from the plots of figure 5-6 is how well the Friuli earthquake compares with the EC8 response spectrum. This earthquake record is considered to be a representative earthquake likely to occur in the Oslo region based on the properties of the earthquake record and data collected for the fault mechanism in the Oslo region.

The Matlab-code for the generation of the response spectra is enclosed in Appendix E.

5.3 MODIFICATIONS OF DATA

The purpose of modifying data is to obtain a good foundation to draw conclusions about the effects of near-fault earthquakes for the response of the structure considered. In order to obtain this, three different ways of modifying data have been performed; simulation of times series, rotation of time-series and correlation of time-series. How the modifications of the data used are performed is described in the following chapter.

5.3.1 SIMULATIONS

To be able to draw conclusions from the effects of near-fault earthquakes, simulations of earthquakes have been performed. The purpose of simulating and generate new ground motion data of acceleration time-series is to obtain near-fault earthquakes with similar frequency content, distance, magnitude and duration. The main difference obtained from simulating is the peak ground acceleration value and how the acceleration varies with time.

A Monte Carlo simulation of the three components of the earthquake record considered has been performed for the Friuli earthquake and the Imperial Valley earthquake. The simulations have been performed in Matlab. The simulations consist of taking the original ground motion acceleration data for each component of the earthquake and generate new ground motion data. The new ground motion data contains approximately the same value of Arias intensity, which is being plotted as a control. The time length and the time interval of each simulation of the ground motion records is indicated in table 5-7.

Table 5-7: Time length and time interval of the simulations performed.

Time-history representation	Time interval [s]	Time length [s]
Friuli simulation	7 - 22	15
Imperial Valley simulation	8 - 28	20

The time interval indicates in which time range of the original ground motion acceleration the simulation was performed. The time length indicates the length of the time range.

Figure 5-7 shows one simulation of all three components of the Friuli earthquake. The same simulation procedure has been performed for the Imperial Valley earthquake. Figure 5-8 shows the spectral density comparison of the simulation versus the original record. The intention of these plots is to see the quality of the simulation performed. Ideally, the spectral density of the simulation should not deviate from the spectral density of the original record. However, variations in the deviations are expected.

Friuli Earthquake, NS-component. PGA from simulation: 1.122 m/s²

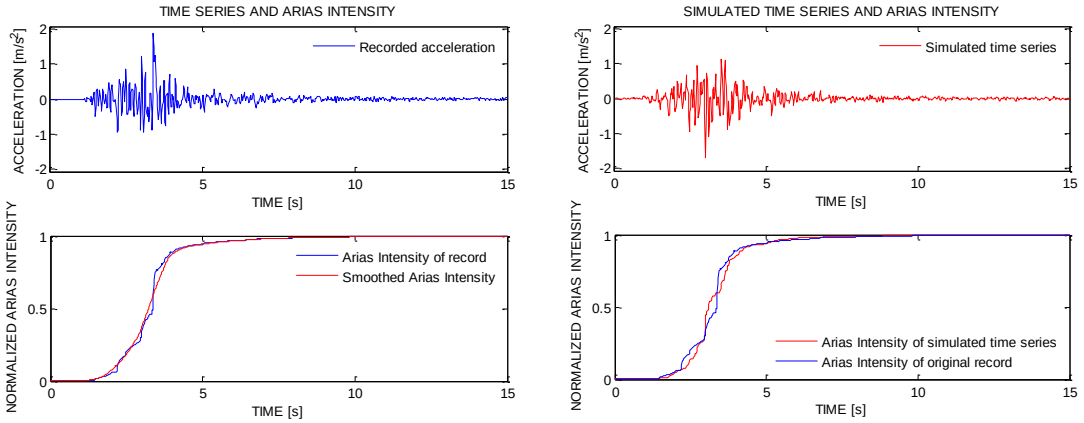

Friuli Earthquake, EW-component. PGA from simulation: 0.803 m/s2

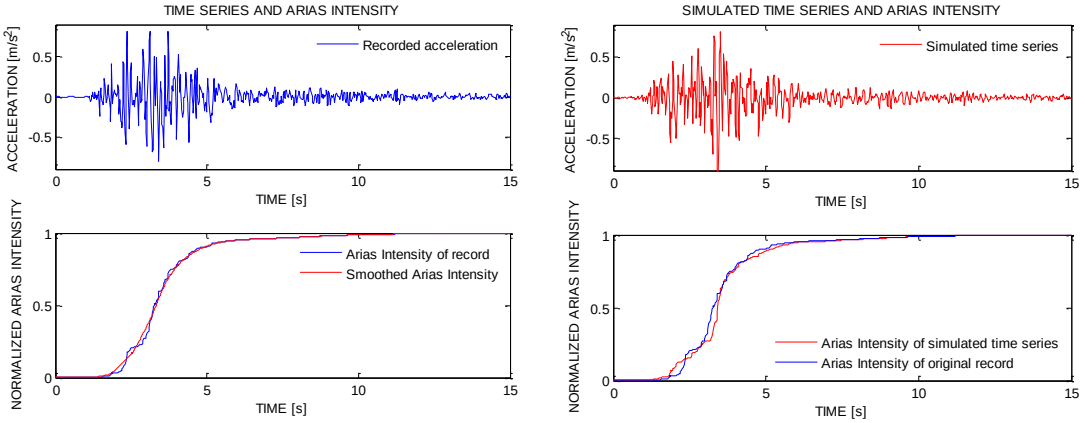

Friuli Earthquake, Vertical component. PGA from simulation: 0.632 m/s²

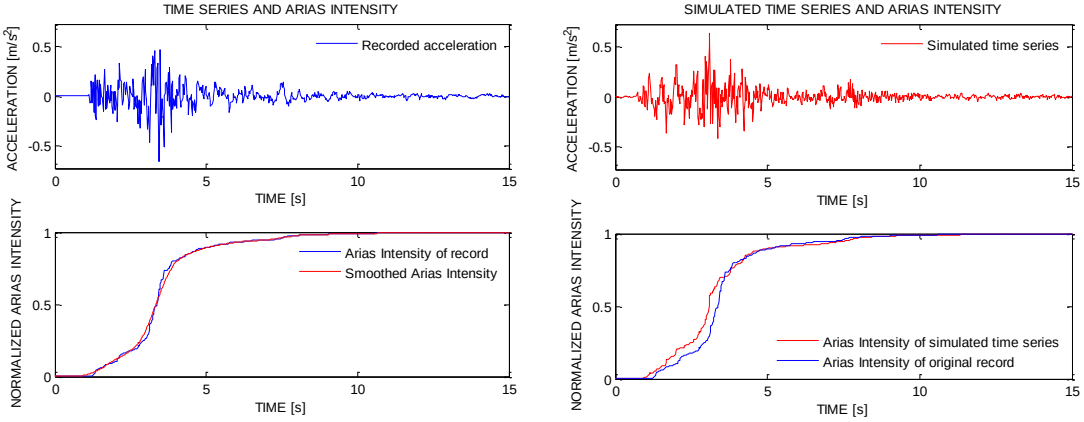

Figure 5-7: Results from simulation of all three components of the Friuli earthquake.

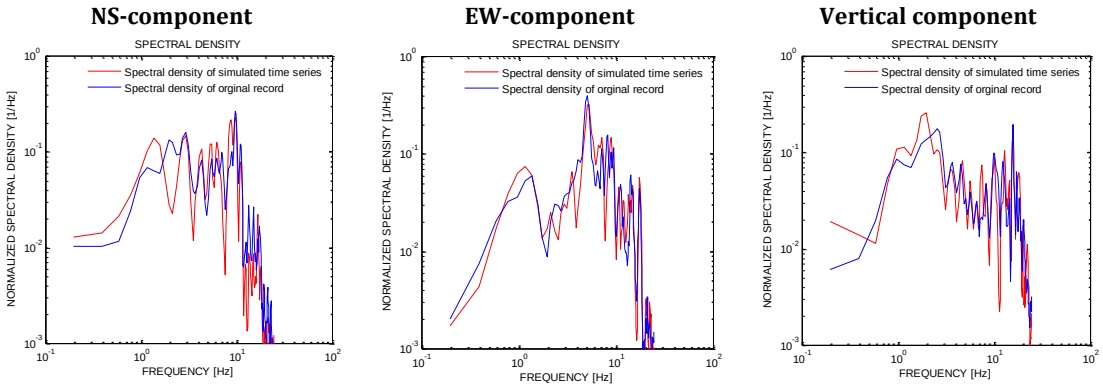

Figure 5-8: Spectral density comparison of all three components of the Friuli earthquake.

As can be seen from figure 5-7, the simulation of the earthquake records renders fairly equal ground motion records with properties as desired. The plots of Arias intensity are included as a quality check of the simulations equally as for the spectral density plots in figure 5-8. Altogether, 5 simulations of the Friuli earthquake and 5 simulations of the Imperial Valley earthquake have been performed. The results of the simulations are presented in Appendix J.

The statistical properties of the simulations are shown in table 5-8.

Table 5-8: Statistical properties of the simulations.

Simulation	Component	Mean PGA [m/s^2]	Standard deviation [m/s^2]
Friuli	NS	1.26	0.24
	EW	0.86	0.13
	Vertical	0.59	0.095
Imperial Valley	45°	0.87	0.148
	135°	1.56	0.079
	Vertical	0.59	0.087

Ideally, many simulations, typically in the range of 25 – 50, of a given earthquake record should be performed and a selection of these records within a certain confidence interval be used. By doing this a more representable distribution of the structural response of the element model would be obtained. However, performing this many analyses has not been emphasized in this work due to time limitations.

5.3.2 ROTATION

The combination rules stated in eq. (5.2) and eq. (5.3) for the modal response spectrum analysis according to EC8 states that the force in one of the horizontal directions should be multiplied with a factor of 0.3 of that in the other horizontal direction. This has been implemented in the time-series by rotating the two acceleration components by an angel, θ. By doing so it can be found when the PGA of one component is as close as possible to 0.3 of the PGA of the other component.

The procedure of rotating time-series is to rotate the NS-component and the EW-component of the given ground motion record with a fixed angle between the components (90°). The rotation is performed until the ratio between the two respective components is as close to 0.3 as possible. The time-series for the desired ratio is then found and implemented as ground motion acceleration in the element model for a combination of records as indicated in table 5-3. The combination rendering the largest response is then registered.

The angle, θ, the PGA-ratio and the corresponding time-series was found using Matlab. The Matlab-code generated to perform this is given in Appendix F. The values for the given earthquake records are stated in table 5-9.

Table 5-9: Properties of the different earthquake records as a result of rotation.

Earthquake	Rotatation angle θ [°]	PGA-ratio
Nahanni, Canada	5.7	0.772
Friuli, Italy	95.1	0.363
Imperial Valley, USA	179.3	0.404

As can be seen from table 5-9, it was not possible to rotate the components of the Nahanni earthquake to obtain a PGA-ratio of 0.3. For the near-fault earthquakes this was almost obtained and can be used for comparison with the modal response spectrum analysis.

The purpose of performing rotation of time-series is to investigate different scenarios that might result in unfortunate response in the structure considered. A rotation of the time-series is equivalent to rotating the building relative to the fault components. Doing this with the objective of obtaining a PGA-ratio of 0.3, this can easier be compared with the EC8 modal response spectrum analysis. The results are presented and discussed in Chapter 6.

5.3.3 CORRELATION

The correlation between the horizontal components of the three different ground motion records are investigated, i.e. for the far-fault earthquake record and the two near-fault earthquake records.

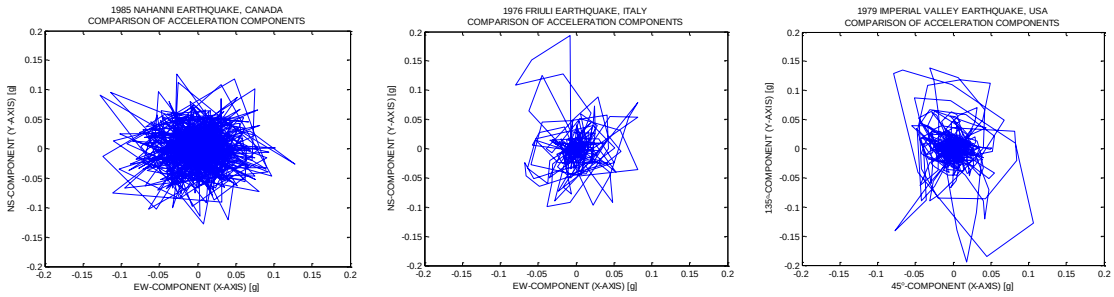

(a) **(b)** **(c)**

Figure 5-9: Correlation plots for the three different ground motion records measured in g. (a) The 1985 Nahanni earthquake, Canada. (b) The 1976 Friuli earthquake, Italy. (c) The 1979 Imperial Valley earthquake, USA.

Figure 5-9 indicates the correlation between the horizontal ground motion components for the different earthquake records. The plots simply show the acceleration in the longitudinal direction versus the acceleration in the transverse direction. As can be seen from these plots, the correlation between the components is basically 0. Zero correlation implies that there is no connection between the components investigated. If a correlation behavior were to be seen, a stretched plot with an approximately 45°-angle between the x-axis and the y-axis would typically be seen instead of a ball-shaped plot as indicated in the figure.

By assigning correlation between the components by modification of the time-series, a different earthquake scenario may be investigated. This can be implemented in the time-history representation analysis to see the effect on the seismic response of the building. This was investigated to some extent in the work of this thesis, but it was found by testing that it did not render any undesired effects on the structural response. Thus, this is not included in the results presented in Chapter 6.

5.4 SCALING OF TIME-SERIES

Whether scaling of the time-series should be performed or not is an important discussion. This strongly depends on the results of interest. The overall objective is to evaluate the consequence of a representative, possible and likely earthquake scenario considering a high-rise structure at the given location. There are mainly two approaches that decide this matter:

- Using original ground motion data from former earthquakes that has occurred other places in the world. This implies that knowledge about the seismic conditions, i.e. fault conditions, for the given location or the given site is available. By either simulating earthquake records or using earthquake records of what is considered representative for the given location results in an evaluation of a "what if"-scenario. It is important to emphasize that this can only be an approximation due to the fact that earthquakes are strongly individual regarding attenuation relationships. It is not possible to predict in an exact manner the properties of a future earthquake.

- Scaling of time-series for the purpose of structural design. Comparison of results obtained from modal response spectrum analyses versus time-history representation analyses is only meaningful given that some sort of scaling is implemented. For the industry or from a consultant engineer's point of view it is desired to obtain the lowest possible design forces according to national provisions, such as EC8. By scaling based on recommendations from provisions, the result is in a higher extent based on statistical analyses which again is based on historical data from high-seismicity areas. This may or may not result in a good representation for low-seismicity areas.

Scaling may be performed in several ways depending on the purpose of the analyses. The probability of the type of earthquakes that might occur, the reference ground acceleration at the given location and the soil conditions regarding possible soil amplification scenarios are factors that have to be taken into consideration. Based on this, a decision of whether the scaling should be performed by frequency and energy content, PGA-values, realistic acceleration values for certain natural vibration periods or requirements from national provisions such as EC8 must be done.

5.4.1 SCALING BY ACCELERATION VALUE FOR CERTAIN NATURAL PERIODS

This method of scaling is to scale based on a comparison of the response spectrum for the given earthquake record with the EC8 response spectrum. The spectral acceleration of the building can be found when the natural vibration period of the structure is known. By finding the ratio between the acceleration from the EC8 response spectrum and the response spectrum for the specific earthquake for the natural vibration period of the structure, this may be used as a ratio to scale the time-series with. As shown from the figures in Chapter 5.2, the acceleration values are very similar for the natural vibration periods between 2.5 s and 3.0 s, which are in the range of the high-rise structure considered. Thus, a scaling based on this method would render results similar to the original records. Because of this, this method of scaling is not implemented in the work presented.

5.4.2 SCALING BY FREQUENCY AND ENERGY CONTENT

Attenuation relationships may be defined as predictive relationships for parameters that decrease with increasing distance. Such relationships may be peak acceleration and peak velocity [3]. Attenuation relationships include the magnitude of the earthquake considered, and the frequency content of a ground motion is related to this magnitude. The frequency content of an earthquake record describes the distribution among different frequencies of ground motion amplitude. It strongly influences the effects of the motion; hence a method of scaling to obtain this frequency content is essential.

The scaling may be performed in different ways as explained in this chapter. However, scaling by frequency content or by energy content itself is hard to perform. Scaling to *obtain* approximately the same energy and frequency content is what is desirable. Arias intensity is a measure that includes effects of the amplitude, frequency content and duration of the ground motion record considered. By using the measure of Arias intensity one can ensure that the frequency and energy content is considered.

Three different types of scaling may be implemented [36]. (i) Scaling based on spectral acceleration ordinates is a method where the component records are scaled in such a way that that it has the same ordinates as that of the design spectrum at the fundamental period of the structure, as described in section 5.4.1. (ii) Scaling based on partial area under the acceleration spectrum is a method where the area under the acceleration spectrum of each record and that of the design spectrum between certain ranges of natural vibration periods are the same. This range of period is typically chosen for a range where the excitation motions are assumed to have the largest effects on the structural response. This is typically in a range of interest for the type of structure considered. (iii) Scaling based on full area under the acceleration spectrum is a method where the area under the acceleration spectrum of each of the records and that of the design spectrum within the entire range of period are the same.

The three methods of frequency scaling mentioned above are used for scaling with respect to the design spectrum. Even though scaling with respect to the EC8 response spectrum ensure that the frequency content is considered, this type of scaling does not include other variations different earthquake records provide. Thus, this type of scaling has not been implemented. However, Arias intensity has been used extensively to ensure that during simulations the frequency content, duration and amplitude are fairly the same.

5.4.3 SCALING BY PGA-VALUES

Scaling based on PGA-values only is an easy method to implement. By finding the ratio of the considered ground motion record compared to the reference record based on PGA, the scaling may be performed easily under the assumption of performing linear

time-history representation analyses. However, this does not take into consideration under any circumstances the frequency content, the energy content or the soil ground parameters in the earthquake record. If the PGA value of the record is very high due to an impulse-like motion with a short duration, this may result in a non-conservative scaling resulting in misleading structural response. This leads to the conclusion that scaling with PGA-values only has to be done with caution. To a certain extent it may be a suitable method of scaling for certain far-fault earthquakes rather than near-fault earthquakes.

5.4.4 SCALING BY THE EC8 PROVISION

Scaling based on the recommendation of EC8 is based on peak ground acceleration and ground type. Following this method of scaling, it is assumed that the original record is processed to represent acceleration values of ground type A. Thus, a scaling of the record taking into consideration the ground type at the given site is necessary by the use of eq. (5.6).

$$Scale\ factor = a_g S \tag{5.6}$$

Soil amplification problems are taken into consideration by some extent using this method of scaling. The disadvantage of using this method of scaling is that the frequency content and energy content of the ground motion data is changed, which may lead to inaccurate results. Nevertheless, this is the method that has been implemented in the analyses performed based on the discussion provided here. It will hereafter be referred to as scaling by EC8.

The basic problem in the discussion of scaling methods is how to perform scaling and still be able to maintain the most relevant properties of the ground motion data. A given method of scaling will provide an outcome at the expense of certain parameters regardless of the method implemented. It is important to emphasize that the method of scaling used in the work of this study has been carefully chosen for the purpose of comparison with the EC8 provision. Moreover, it is of particular interest to investigate the structural response if the maximum possible earthquake scenario occurs. As mentioned earlier, the Oslo rift zone has the potential to generate a near-fault earthquake with great magnitude. If the effects of such a near-fault earthquake on Oslo Plaza are to be investigated a representative record with approximately the same magnitude and epicentral distance may be used, yet without any methods of scaling performed. For such a scenario the Friuli earthquake has been chosen.

6 RESULTS AND COMPARISONS

The behavior and response of the structure to the seismic loading is essential. In the following chapter the response is found by looking at displacement, interstory drift and base shear. The response will be subject for discussion after a thorough comparison of the analyses is performed.

The objective of performing the analyses is divided in two parts:

- Performing analyses according to and staying within the requirements of EC8 for the purpose of comparison of the results obtained from the different methods of analyses.

- Applying strong ground motion data to the structure for a realistic scenario that might occur in the region of Oslo. The seismic response of the structure and how the high-rise structure is affected when exposed to a near-fault earthquake is subject for investigation.

The response parameter of main interest is the interstory drift ratio, IDR. IDR serves as an important indicator of damage for high-rise structures subjected to strong ground motions. It is also a parameter related to the story shears and describes local damage at the story level. The definition of IDR is stated in Chapter 2.2.2.

Displacement is related to interstory drift and vice versa. Displacement is a response parameter of importance due to problems related to pounding of buildings and due to the relative experience of comfort experienced at certain locations in high-rise structures, especially towards the top floors.

To obtain correct results for IDR the maximum value at each floor cannot be used since they do not occur at the same time step in the time-series. The procedure chosen is to find the maximum displacement of a node at the top floor as shown in figure 6-1, *when* this maximum displacement occurs and then find the displacement of the nodes representing the below floors at the same time step. The IDR-plots and the displacement plots have been generated using this procedure.

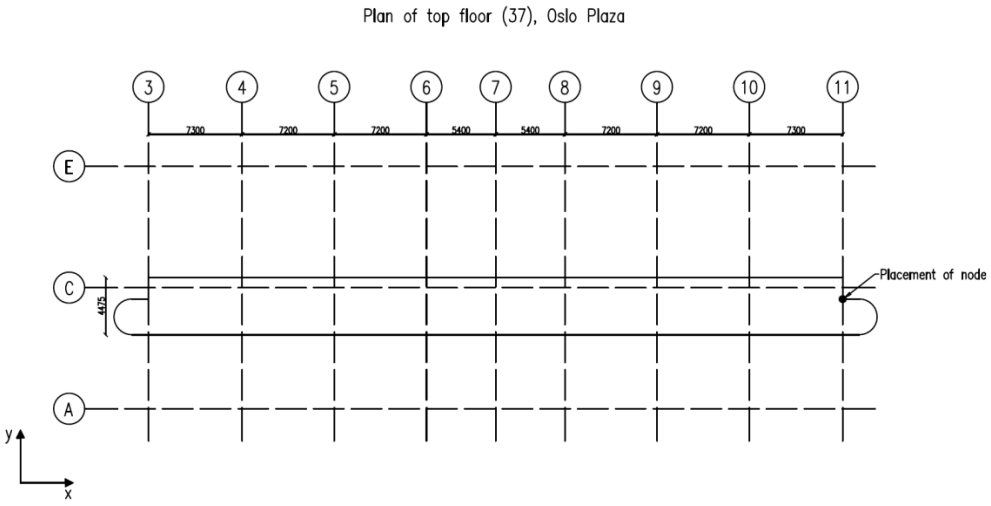

Figure 6-1: Placement of node in the element model to extract displacement values

Base shear is selected as a response parameter because it is often considered the fundamental response parameter for seismic response. It is a parameter that is easy to compare with for several methods of analyses, and it is a fundamental parameter for design purposes. Ideally, the story shear distribution describing the force distribution throughout the structure is a parameter of interest as well, but presenting such a distribution requires a thorough investigation of the structural components.

A horizontal force distribution may be calculated according to the method by EC8 [15], 4.3.3.2.3(2)P. The horizontal force acting on floor j can be computed by

$$F_j = V_b \cdot \frac{z_j \cdot m_j}{\sum z_i \cdot m_i} \tag{6.1}$$

where z_j, z_i are the heights of the story masses m_j, m_i and V_b is the base shear. The horizontal forces, F_j, are distributed to the lateral load resisting system assuming the floors are rigid in their plane. Furthermore, the shear force at a given floor j is then described by the formula

$$V_j = \sum_{k=j}^{N} F_k \tag{6.2}$$

N describes the number of floors in the structure. By looking at the formulas stated in eq. (6.1) and eq. (6.2) one can clearly see that the base shear is the only variable taken from the seismic load cases. By presenting a shear force distribution according to EC8, this would result in an equal force distribution shape of the plots, but different values for different load cases. It is obvious from the theory behind the modal analysis presented in Chapter 2.3 that the shear force distribution is different for different seismic load cases and for different foundation representations. The ideal way of presenting a shear force distribution would be to look at individual forces experienced

by structural elements at each floor for each seismic load case. Since the interstory drift is a parameter related to the story shears and describes local damage at the story level, the presentation of interstory drift describes the critical places in the structure regarding seismic response, and thus the shear force distribution is chosen not to be presented as a parameter.

SAP2000 do not have a good way of presenting the shear force distribution of the element model. Furthermore, eq. (6.1) and eq. (6.2) are mainly stated for design purposes, and is not a parameter ideal to present as force distribution throughout the structure regarding comparison of seismic load cases.

This chapter provides the results obtained from the analyses performed with emphasis on the response parameters as described above. A comparison and discussion of the results is presented as well.

6.1 RESULTS AND COMPARISON BY SCALING

The tables and figures presented here show results of the displacement response, the interstory drift ratio (IDR) and the base shear response for the method of scaling by EC8.

In all of the plots indicated in the figures the dimensionless height of the building is plotted for 37 floors, i.e. the entire height of the building including all floors. The dimensionless height is represented on the ordinate axis and the response parameter is represented on the abscissa axis. The method of scaling implemented is the method of scaling by the EC8 provision as described in Chapter 5.4.4.

6.1.1 DISPLACEMENT

In this subchapter, all the results of the structural response by displacement are presented.

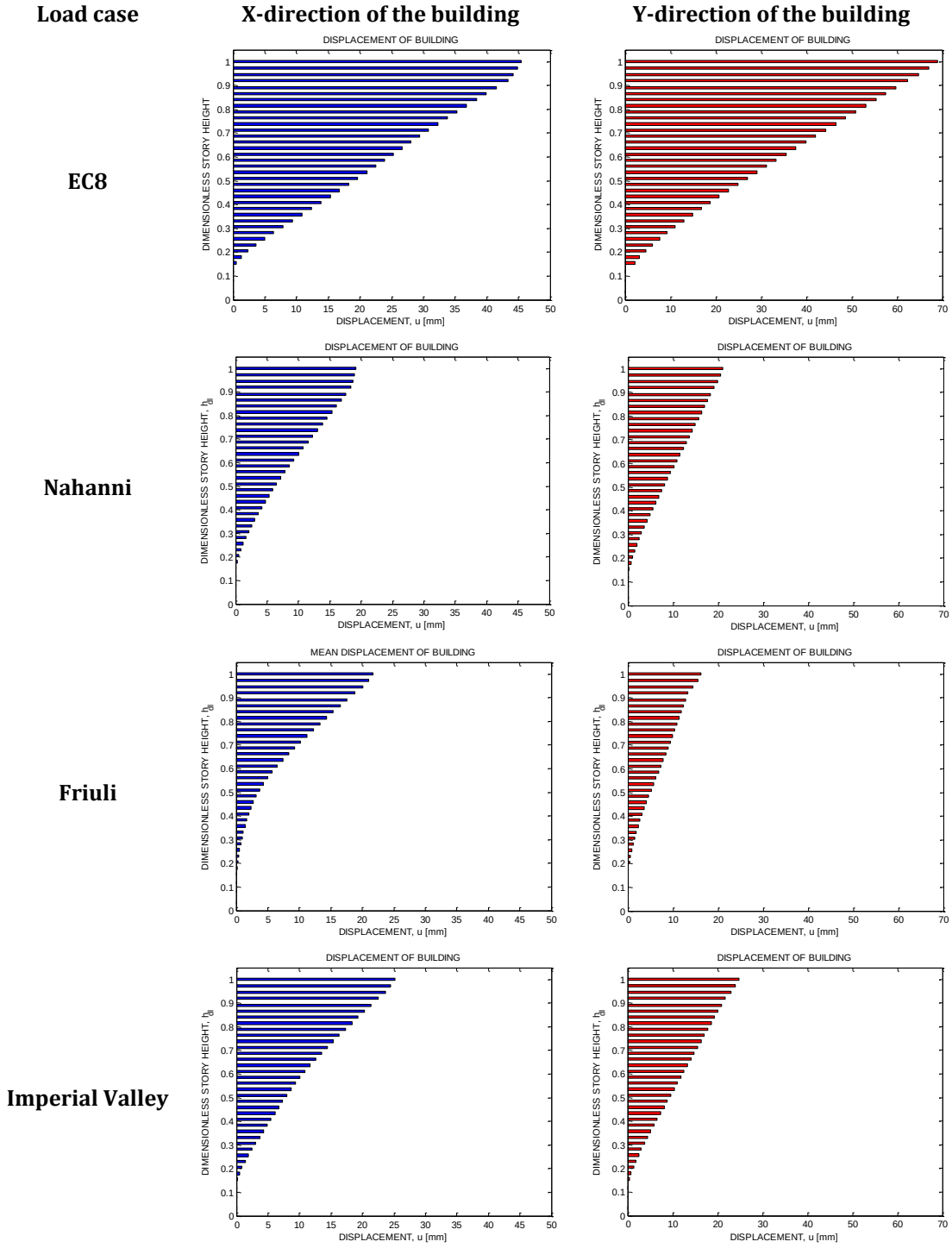

Figure 6-2: Displacement of the building according to different earthquake scenarios considered for two directions, x-direction and y-direction.

The plots presented in figure 6-2 shows the displacement of the building according to the different earthquake scenarios. Displacements along the dimensionless height of the structure are shown for the x-direction of the building and the y-direction of the building. This is the situation for the plots shown in figure 6-3 as well. In this figure, the average displacement for the Friuli earthquake and the Imperial Valley earthquake is presented. By average displacement the average of the original record, the rotated record and the simulation records are taken.

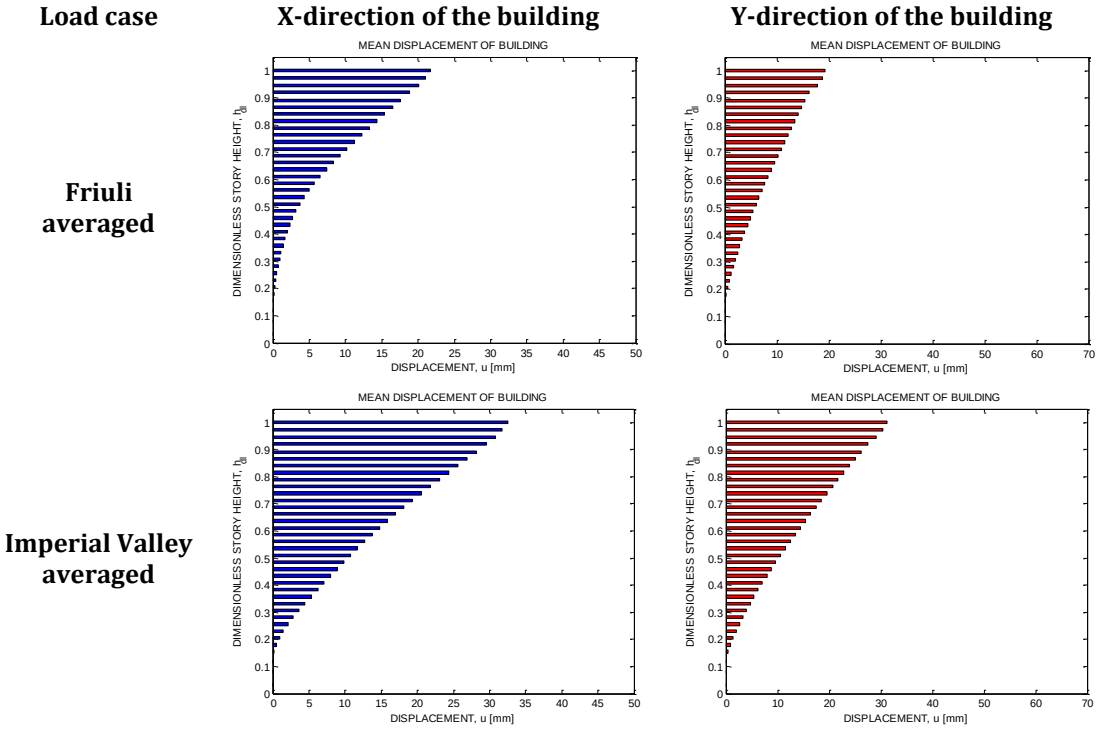

Figure 6-3: Displacement of the building according to the Friuli earthquake and the Imperial Valley earthquake for averaged values considered for two directions, x-direction and y-direction.

As expected the displacement of the building increases with height in both directions. This is confirmed by the plots in both of the figures. Table 6-1 indicates the values from the displacement response.

Table 6-1: Maximum displacement response of the building for different seismic load cases.

Load case	X-direction [mm]	Y-direction [mm]	Displacement ratio [x/y]	Load combination
EC8	45.4	68.9	0.659	Different
Nahanni	19.2	21.0	0.913	Different
Friuli	18.0	16.2	1.112	Same
Imperial Valley	25.2	24.7	1.021	Different
Friuli averaged	21.7	19.3	1.127	Different
Imperial Valley averaged	32.5	35.4	0.919	Different

As table 6-1 and figure 6-2 indicates, the maximum displacement in the x-direction and y-direction is fairly similar for all individual seismic load cases except from the EC8 load case. There are several reasons for this. For the EC8 load case, the load combination used is described by eq. (5.2) and eq. (5.3) which provides a scaling of the different direction of components by a factor of 0.3. As shown in table 6-1, the maximum displacement occurs for different load combinations, i.e. the maximum displacement is obtained in the x-direction using eq. (5.2), and the maximum displacement is obtained in the y-direction using eq. (5.3). For the specific earthquake load cases such as Nahanni, Friuli or Imperial Valley, hereafter referred to as seismic load cases, the specific component of the earthquake record is implemented without any component scaling. An exception of this is from the rotated time-series represented in the average load cases for each earthquake respectively. This leads to similar displacement values for the two directions as indicated by the displacement ratio.

The column presenting load combination indicates whether or not the maximum response in the given direction occurred for the same load combination in both x-direction and y-direction or not. As seen in the table 6-1, the Friuli earthquake rendered maximum displacement response for the same load combination.

The largest displacement response of the seismic load cases observed is obtained from the Imperial Valley earthquake. The displacement response from the seismic load cases is considerably lower than the response from the EC8 load case. The averaged value of the Friuli earthquake and the Imperial Valley earthquake indicates larger response than the individual load cases. Regardless, the displacement response is far less for the averaged cases than for the EC8 load case, insinuating that the EC8 load case is conservative for this response parameter.

The following plots presented in figure 6-4 shows the displacement of the building according to the simulations of the Friuli earthquake and the Imperial Valley earthquake performed.

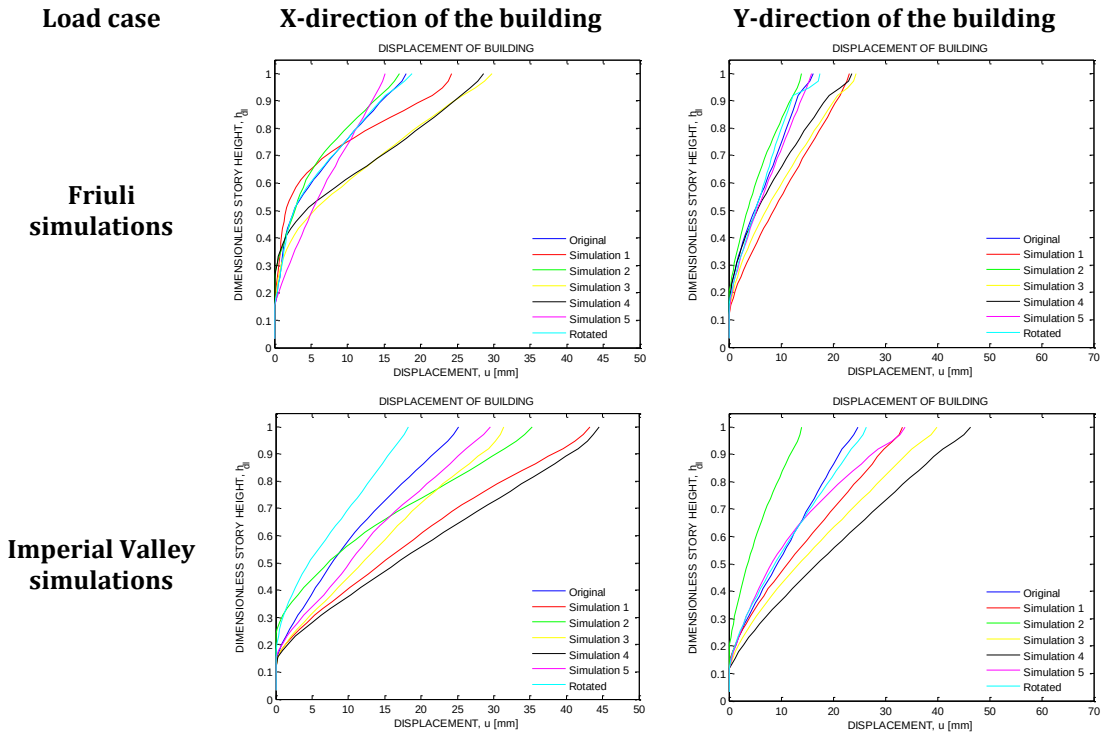

Figure 6-4: Displacements results of the simulations performed for the Friuli earthquake and the Imperial Valley earthquake.

Included in the plots in figure 6-4 are the results from the rotated records and the original records. The displacement response from the Imperial Valley earthquake is larger than for the Friuli earthquake. A possible explanation of this might be the method of scaling. A scaling of the earthquake record by the method of EC8 is performed as explained previously. Looking at the ground motion plots indicated in figure 5-4 in Chapter 5, the Friuli records have few peaks with great magnitude in the acceleration plots, whereas the Imperial Valley records have numerous peaks with acceleration values of less magnitude. In addition, the duration of the Friuli earthquake is less than the Imperial Valley earthquake. The method of scaling by EC8 results in a better approximation of the Imperial Valley earthquake than the Friuli earthquake due to the fact that the overall scaling of the Imperial Valley earthquake downsizes the earthquake record in a better way than for the Friuli earthquake. This method of scaling is better for far-fault earthquakes than for near-fault earthquakes, moreover the Imperial Valley ground motion relates better to a far-fault earthquake than the Friuli ground motion. Another method of scaling could have been considered to obtain a better comparison of the response.

The difference in the response is greater for the Imperial Valley earthquake simulations than for the Friuli earthquake simulations. A statistical approach was performed to investigate this as indicated in table 6-2.

Table 6-2: Statistical properties of the simulations of the displacement response performed for the averaged seismic load cases.

Load case	Average standard deviation in x-direction [mm]	Average standard deviation in y-direction [mm]
Friuli	2.29	1.96
Imperial Valley	4.58	4.79

The standard deviation of the simulations is larger for the Imperial Valley earthquake than for the Friuli earthquake. For the response generated by the simulations performed, all but the response from one simulation are higher than the response obtained from the original record for the Imperial Valley earthquake. The simulations performed for the Friuli earthquake appears to be better than for the Imperial Valley earthquake. Thus, the displacement response of the Friuli earthquake simulation case is closer to the single seismic load case than the same situation for the Imperial Valley earthquake is. This is also one of the reasons for using the Friuli earthquake as the realistic scenario.

6.1.2 INTERSTORY DRIFT RATIO (IDR)

In this subchapter, all the results of the structural response by interstory drift ratio (IDR) are presented. The plots presented in figure 6-5 shows the IDR of the building according to the different earthquake scenarios.

In the plots indicated in the following figures, IDR along the dimensionless height of the structure are shown for the x-direction of the building and the y-direction of the building.

Load case	X-direction of the building	Y-direction of the building
EC8	N.A.	N.A.
Nahanni	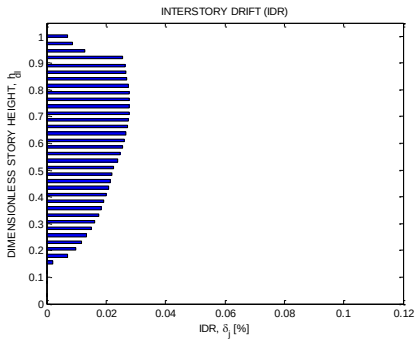	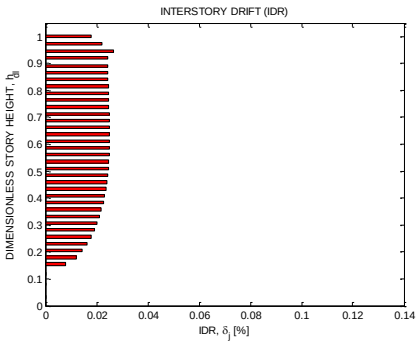
Friuli	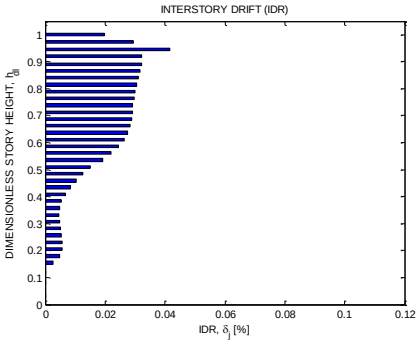	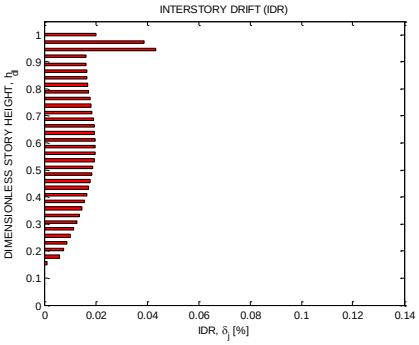
Imperial Valley	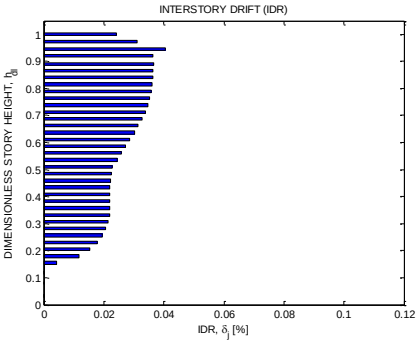	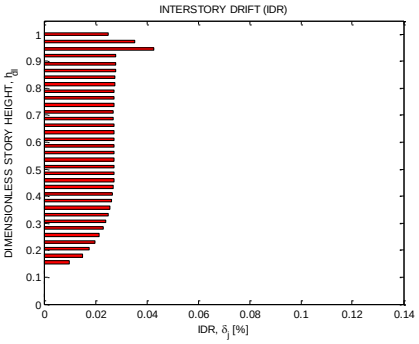

Figure 6-5: IDR of the building according to different earthquake scenarios considered for two directions, x-direction and y-direction.

The IDR for the EC8 load case is not available due to the fact that the results stems from a response spectrum analysis and not a time-history representation analysis.

As can be seen from the plots of figure 6-5, the far-fault earthquake does not produce a peak IDR at the location of floor 34-35 in x-direction like the near-fault earthquakes do. This supports the explanation stated in the introduction (Chapter 1) that high-rise structures are vulnerable to pulse excitations such as the ones caused by near-fault earthquakes. Near-fault earthquakes may cause percent-wise larger displacement at critical floors with reduced stiffness than what far-fault earthquakes may do. Recall that the concrete shear wall system ends at the transition of floor 34-35 resulting in a story mechanism occurrence as confirmed by the plots. In the y-direction of the far-fault

earthquake, the IDR distribution is fairly equal for the stories of the upper half of the building. The IDR distribution for the near-fault earthquakes is fairly as expected.

In figure 6-6 the average IDR for the Friuli earthquake and the Imperial Valley earthquake is presented. By average IDR the average of the original record, the rotated record and the simulation records are taken.

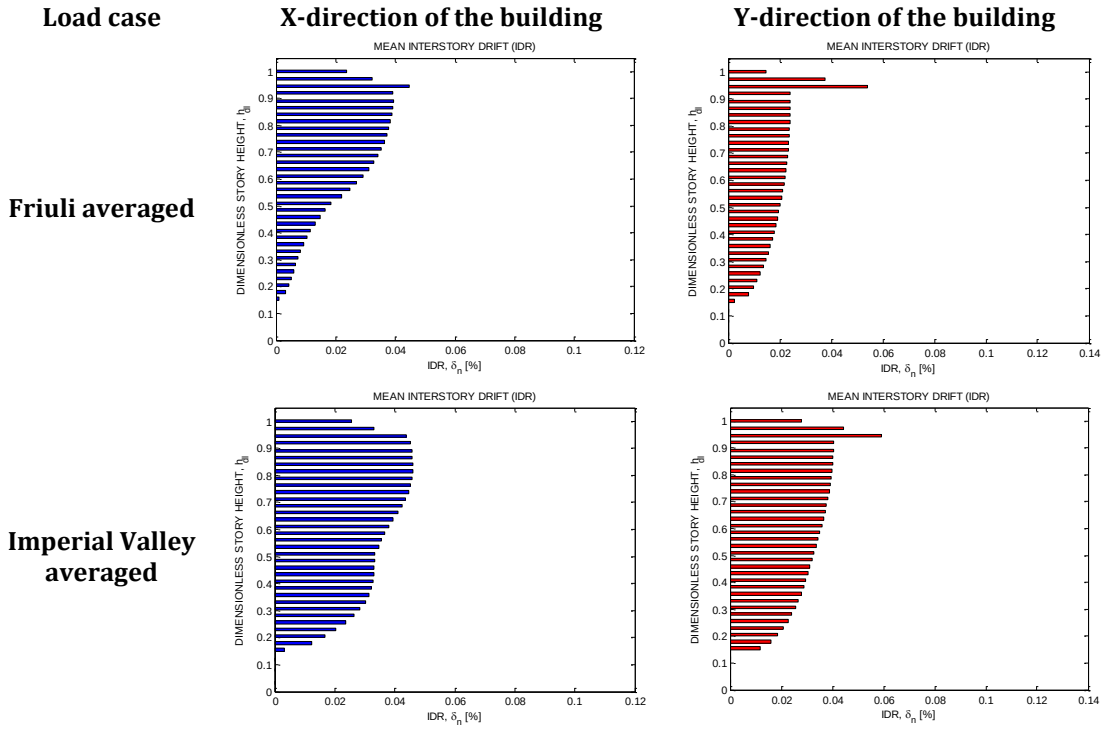

Figure 6-6: IDR of the building according to the Friuli earthquake and the Imperial Valley earthquake for averaged values considered for two directions, x-direction and y-direction.

Table 6-3 indicates the values for the IDR of the seismic load cases.

Table 6-3: Maximum IDR of the building for different seismic load cases.

Load case	X-direction		Y-direction		IDR ratio
	IDR [%]	Floor	IDR [%]	Floor	[x/y]
Nahanni	0.028	27-28	0.027	34-35	1.037
Friuli	0.042	34-35	0.043	34-35	0.977
Imperial Valley	0.040	34-35	0.043	34-35	0.930
Friuli averaged	0.045	34-35	0.054	34-35	0.833
Imperial Valley averaged	0.046	30-31	0.059	34-35	0.780

As can be seen from table 6-3 and the plots of figure 6-6, the Imperial Valley earthquake results in larger IDR than the Friuli earthquake for the averaged case. One of the reasons for this may be due to the fact that the simulations for Imperial Valley were not as good

as the simulations for Friuli, as mentioned before. In addition, all the simulations for the Imperial Valley earthquake resulted in larger response than the original record did. The maximum IDR of Imperial Valley occurs in the transition of floor 30-31 in the x-direction, whereas for the other plots of figure 6-6 it occurs in the transition of floor 34-35, except from the Nahanni load case as mentioned before.

An important factor to consider is the stiffness of the building. The building is stiffer in the x-direction (about the y-axis) than in the y-direction (about the x-axis). The IDR ratio is lower for the averaged load cases, whereas for the regular seismic load cases the ratio is very close to 1.0 indicating that the IDR is equal for both directions.

The following plots presented in figure 6-7 shows the IDR of the building according to the simulations of the Friuli earthquake and the Imperial Valley earthquake performed.

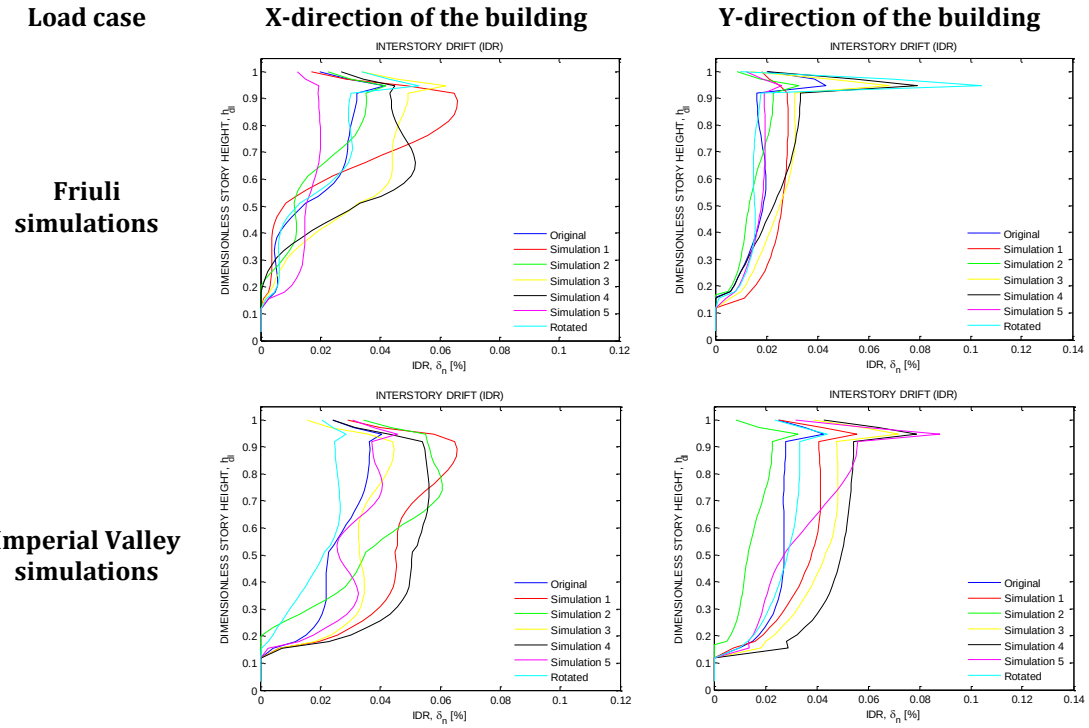

Figure 6-7: IDR results of the simulations performed for the Friuli earthquake and the Imperial Valley earthquake.

As can be seen from table 6-3 and partly from the plots of figure 6-7, the IDR is slightly larger for the Imperial Valley simulations than for the Friuli simulations. Compared with the difference in the displacement response of the same two earthquake simulations, the difference is much smaller regarding the IDR. A statistical approach was performed to investigate the difference between these simulations in a similar way as for the displacement response, and the result is given in table 6-4.

The statistical approach show that the average standard deviation for the Friuli simulations is about twice the average standard deviation for the Imperial Valley

simulations. This indicates once again that the simulations performed for the Friuli earthquake were better.

Table 6-4: Statistical properties of the simulations of IDR performed for the averaged load cases.

Load case	Average standard deviation in x-direction [%]	Average standard deviation in y-direction [%]
Friuli	0.0059	0.0059
Imperial Valley	0.0107	0.0109

An important observation is that the response for the Friuli earthquake is larger than the Imperial Valley earthquake regarding IDR, but not for displacement. One of several possible reasons for this may be that the NS-component of the Friuli ground motion has the largest PGA-value of all the records considered in this study. In addition, the Friuli earthquake is considered a more impulse-like near-fault earthquake than the Imperial Valley earthquake is considered. The Imperial Valley earthquake have a longer duration but with more peaks of high acceleration values. This supports the fact that interstory drift is a critical structural response parameter regarding near-fault earthquakes.

6.1.3 BASE SHEAR

In this subchapter, all the results of the structural response by base shear are presented.

Table 6-5: Maximum base shear response of the building for different seismic load cases

Load case	X-direction [kN]	Y-direction [kN]	Base shear ratio [x/y]	Load combination
EC8	2929	8257	0.355	Same (eq. 5.3)
Nahanni	1345	3538	0.380	Different
Friuli	1885	6204	0.304	Same (combination I)
Imperial Valley	2151	5882	0.366	Different
Friuli averaged	2356	6786	0.347	Varies
Imperial Valley averaged	2651	7333	0.362	Different

As can be seen from table 6-5, the base shear from the EC8 load case is largest as for the displacement response shown in Chapter 6.1.1. The same arguments used previously that this is due to the method of scaling and that the EC8 load case may be conservative applies here. Other observations made are that the Nahanni earthquake renders the smallest response and the Friuli earthquake and the Imperial Valley earthquake renders fairly equal base shear response.

The average base shear for the Friuli earthquake and the Imperial Valley earthquake is presented in table 6-5. By average base shear the average of the original record, the rotated record and the simulation records are taken. The two seismic load cases representing averaged values results in similar base shear response. This leads to an important observation that base shear response is not affected as much by the simulations as displacement response and IDR are. The averaged seismic load cases results in a slightly larger response than the original scaled seismic load cases.

The base shear ratio is almost equal for all the seismic load cases as indicated in the table. Due to the structural system it is obvious that the shear wall construction takes a lot more forces than the other structural components.

A statistical approach was performed to investigate the difference between the results of base shear of the simulations performed, in a similar way as for the displacement response and IDR. The result is given in table 6-6.

Table 6-6: Statistical properties of the simulations of base shear performed for the averaged load cases.

Load case	Average standard deviation in x-direction [kN]	Average standard deviation in y-direction [kN]
Friuli	354	791
Imperial Valley	400	1125

The statistical approach show that the average standard deviation for the Imperial Valley simulations is higher compared to the average standard deviation for the Friuli simulations. However, the observation made previously that base shear response is not affected as much by the simulations as displacement response and IDR are is still valid.

By inspecting the IDR plots presented in the previous subchapter a conclusion of that an increase in the story shears on the 4th floor and the 34th floor will occur. The increase in the story shear corresponds to when sudden structural changes occur. The main building reaches the 4th floor leaving the tower to rise up. This is the explanation for the first change. On the 34th floor the concrete shear wall construction is replaced by a steel frame construction supporting the top part of the structure. This is the explanation for the second change. These are the main reasons for the sudden shear force changes in the structure.

6.2 Results By Realistic Earthquake Scenario

The tables and figures presented here show results of the displacement response, the IDR and the base shear response of the structure for a realistic earthquake scenario, i.e. no scaling is introduced for the ground motion data. The earthquake chosen is the Friuli earthquake.

6.2.1 Displacement

The following plots presented in figure 6-8 shows the displacement of the building according to the Friuli earthquake as a realistic scenario, the averaged load case and for the simulations.

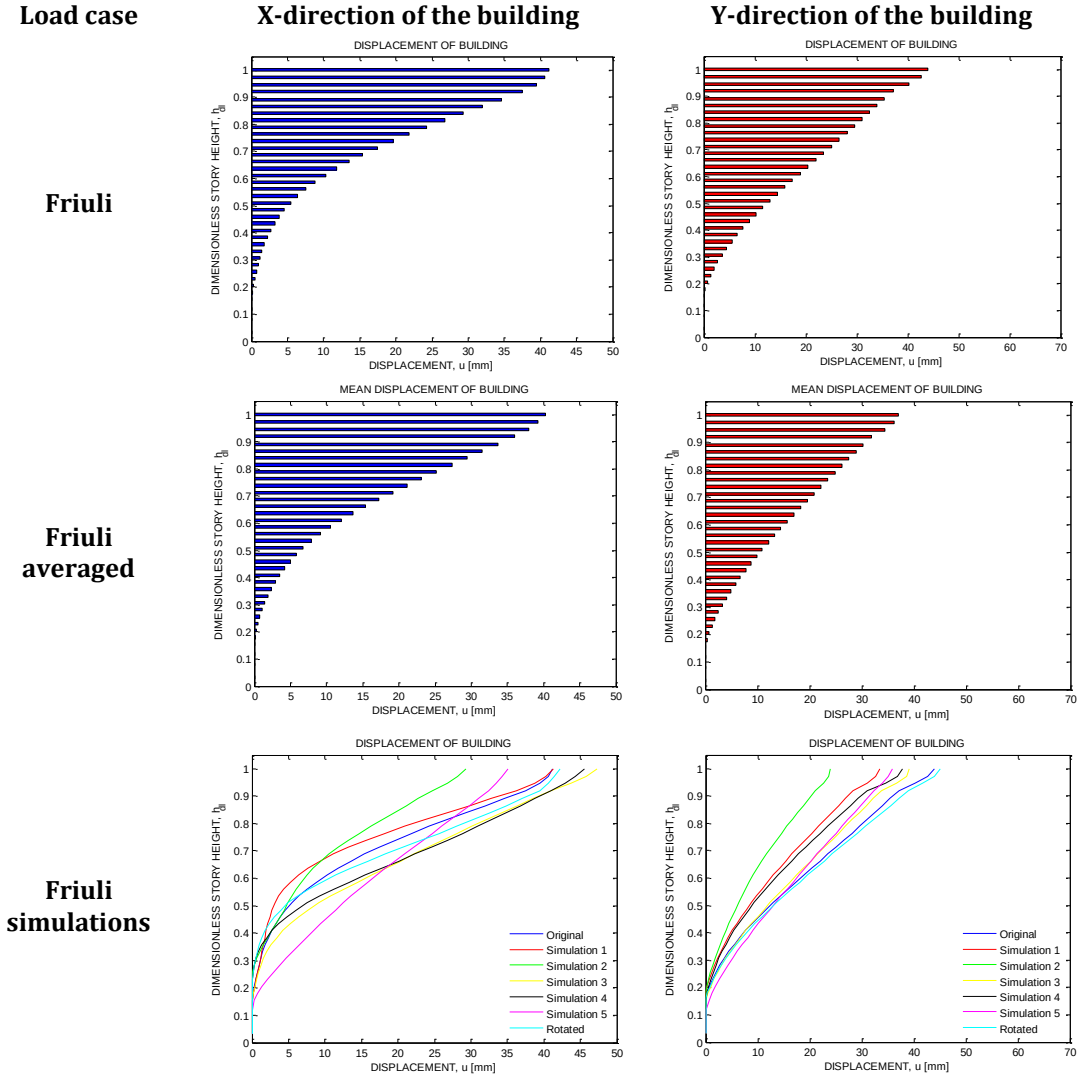

Figure 6-8: Displacement of the structure in the two different directions for the Friuli earthquake based on the individual case, on averaged values and on simulations for a realistic earthquake scenario.

As can be seen from table 6-7 and the plots in figure 6-8, the displacement values are similar for the given directions. The shape of the displacement plot for the y-direction has a linear trend whereas the shape of the displacement in the x-direction has an exponential trend.

Table 6-7: Comparison of maximum displacement response of the building for the scaled and the realistic Friuli earthquake scenario.

Load case	X-direction [mm]	Y-direction [mm]	Displacement ratio [x/y]	Load combination
EC8	45.4	68.9	0.659	Different
Friuli scaled	18.0	16.2	1.112	Same (combination II)
Friuli RS*	41.2	43.9	0.938	Different
Ratio	*0.437*	*0.369*		
Friuli scaled averaged	21.7	19.3	1.127	Different
Friuli RS averaged	40.3	37.0	1.088	Different
Ratio	*0.539*	*0.520*		

*RS indicates the realistic scenario.

The difference in the displacement response of the building for the scaled and the realistic case scenario is indicated by the ratio in table 6-7. This is an interesting parameter. The ratio increases for the averaged case scenarios compared to the single individual case scenarios. As mentioned before, the averaged seismic case scenario represents the average of the original record, the rotated record and the simulation records. If an earthquake scenario like the Friuli earthquake were to happen in Oslo, the maximum displacement response of the building would be approximately twice the magnitude compared to the response of the scaled scenario. Recall that the EC8 load case rendered maximum displacement values of 45.4 mm and 68.9 mm in the x-direction and y-direction respectively as shown in the table. This supports the statement that for the maximum displacement response, the EC8 case is conservative regarding displacement response.

Table 6-8: Statistical properties of the simulations of the displacement response performed for the averaged seismic load cases for the scaled scenario and the realistic scenario.

Load case	Average standard deviation in x-direction [mm]	Average standard deviation in y-direction [mm]
Friuli	2.29	1.96
Friuli RS*	2.09	2.18

*RS indicates the realistic scenario.

Table 6-8 indicates the statistical properties and compares the standard deviation for the realistic case scenario with the scaled scenario. The average standard deviations are fairly similar.

6.2.2 INTERSTORY DRIFT RATIO (IDR)

The following plots presented in figure 6-9 shows the IDR of the building according to the Friuli earthquake as a realistic scenario, the averaged load case and for the simulations.

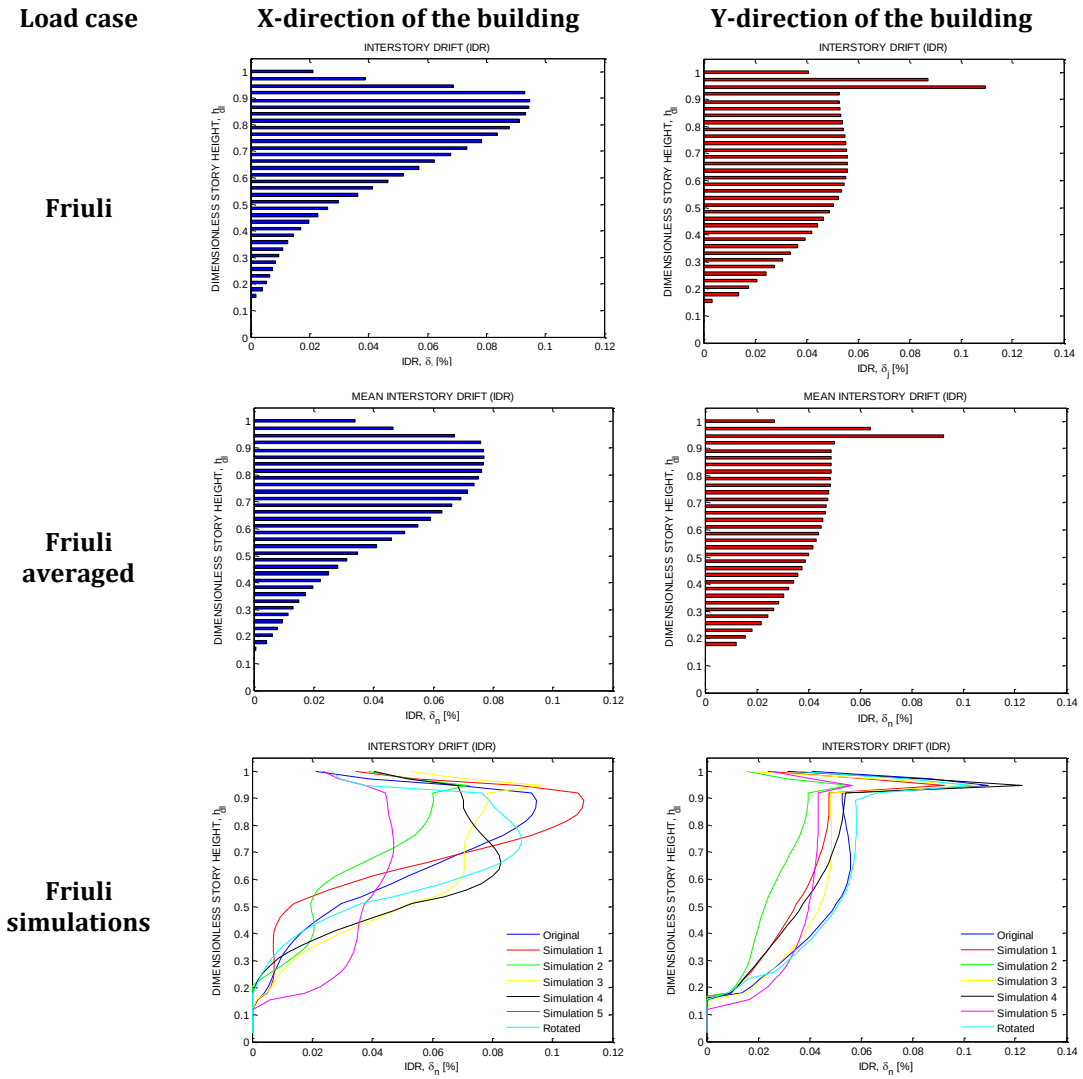

Figure 6-9: IDR of the structure in two different directions for the Friuli earthquake based on the individual case, on averaged values and on simulations for a realistic earthquake scenario.

As can be seen from table 6-9 and the plots in figure 6-9, IDR values are greater for the y-direction than for the x-direction. The shape of the IDR plots for the given directions are different.

Table 6-9: Comparison of maximum IDR of the building for the scaled and the realistic Friuli earthquake scenario.

Load case	X-direction		Y-direction		IDR ratio
	IDR [%]	Floor	IDR [%]	Floor	[x/y]
Friuli scaled	0.042	34-35	0.043	34-35	0.977
Friuli RS*	0.095	32-33	0.110	34-35	0.865
Ratio	*0.444*		*0.393*		
Friuli scaled averaged	0.045	34-35	0.054	34-35	0.833
Friuli RS averaged	0.077	32-33	0.092	34-35	0.834
Ratio	*0.584*		*0.585*		

*RS indicates the realistic scenario.

The difference in IDR of the building for the scaled and the realistic case scenarios are indicated by the ratios in table 6-9. The respective ratios are practically the same as for the displacement response ratios.

Table 6-10: Statistical properties of the simulations of IDR performed for the averaged seismic load cases for the scaled scenario and the realistic scenario.

Load case	Average standard deviation in x-direction [%]	Average standard deviation in y-direction [%]
Friuli	0.0059	0.0059
Friuli RS*	0.0065	0.0047

*RS indicates the realistic scenario.

Table 6-10 indicates the statistical properties and compares the average standard deviation for the realistic case scenario with the scaled scenario. The average standard deviations are fairly similar here as they are for the displacement response indicated in table 6-8, meaning that they do not differ much from each other for the scaled scenario versus the realistic scenario. This is positive indicating that the simulations performed are reliable.

6.2.3 BASE SHEAR

In this subchapter, all the results of the structural response by base shear of the building according to the Friuli earthquake for the scaling by EC8, the realistic scenario and the averaged load case are presented.

As can be seen from table 6-11 the base shear values are greater for the y-direction than for the x-direction.

Table 6-11: Comparison of maximum base shear response of the building for the scaled and the realistic Friuli earthquake scenario.

Load case	X-direction [kN]	Y-direction [kN]	Base shear ratio [x/y]	Load combination
EC8	2929	8257	0.355	Same (eq. 5.3)
Friuli scaled	1885	6204	0.304	Same (combination I)
Friuli RS*	3455	11361	0.304	Different
Ratio	*0.546*	*0.546*		
Friuli scaled averaged	2356	6786	0.347	Varies
Friuli RS averaged	3955	11480	0.345	Varies
Ratio	*0.596*	*0.591*		

*RS indicates the realistic scenario.

The differences in the base shear response of the building for the scaled and the realistic case scenarios are indicated by the ratios in table 6-11. The respective ratios are higher than for the displacement response ratios and the IDR ratios. The result obtained for the base shear response is interesting. The Friuli earthquake renders much higher base shear than the EC8 load case does. This is confirmed by the result from the averaged load case. However, for the scaled load case the base shear obtained are lower than what obtained by the EC8 load case. Based on this, characterizing the EC8 load case as conservative or non-conservative as insinuated earlier must be done with caution. Another method of scaling could render much higher values of base shear than the method of scaling implemented here does. This yields for displacement response and IDR as well.

Table 6-12: Statistical properties of the simulations of the maximum base shear response performed for the averaged seismic load cases for the scaled scenario and the realistic scenario.

Load case	Average standard deviation in x-direction [kN]	Average standard deviation in y-direction [kN]
Friuli	354	791
Friuli RS*	714	1282

*RS indicates the realistic scenario.

Table 6-12 indicates the statistical properties and compares the standard deviation for the realistic case scenario with the scaled scenario. The standard deviations differs a lot which is obvious due to the fact that the response is much larger for the realistic case scenario than for the scaled scenario. This is standard deviation of the maximum base shear obtained.

7 CASE STUDY

In the presented research of Chapter 6 the response of Oslo Plaza as a high-rise structure exposed to different seismic load cases relevant for the location of Oslo was investigated. The motivation for the following case study is to evaluate *how* the structure performs based on the obtained results.

In this case study, it has been emphasized to follow the recommendations of EC8. However, comparison and evaluation of the behavior according to recommendations stated in other literature has been included as well. Important parameters such as interstory drift and displacement, the P-Δ effect, the effect of soil-structure interaction and the difference of near-fault earthquakes and far-fault earthquakes regarding response of the structure have been emphasized.

7.1 INTERSTORY DRIFT AND DISPLACEMENT

The introduction of interstory drift and displacement as performance requirements are mostly due to avoid structural collapse. Collapse may initiate at any level in the structure. Local failure of supporting members, excessive foundation movement and lateral or torsional structural displacement are among the most important factors. The nature of earthquake ground motion inevitably leads to differential movements between structural components. The forming of story-mechanisms must be avoided.

Soft-story floors are obtained if the horizontal resistance is strongly reduced on or above a certain floor. This may typically be if the lateral bracing is weakened or omitted. A ground soft-story floor is when the bracing elements, typically walls that are available in the upper floors, are omitted in the ground floor and replaced by columns [37]. This phenomenon is illustrated in figure 7-1.

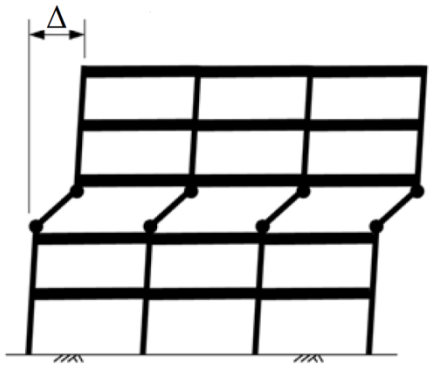

Figure 7-1: Illustration of a story mechanism.

Damage on columns is caused by cyclic displacements. Plastic hinges are formed at both ends of the columns leading to a story mechanism.

There are numerous reasons why deflections must be limited during earthquakes, thus adequate stiffness of the building must be ensured. Non-structural elements such as cladding and partitions must withstand the deflections imposed without failure. Internal structural damage such as blockage of escape routes and ruptured pipework are other parameters that result in serious safety implications. Large displacement may have effects on structural members such as columns in particular, and failure of load-bearing members is highly critical. It is important that the code requirements regarding stiffness are met since this criterion, rather than the strength criterion, often determines the sections sizes in tall buildings [9].

Relative horizontal deflections within the building, known as interstory drift, is an important parameter regarding seismic design. Interstory drift and displacements are both parameters that are described in relation to each other. According to EC8 [15], 4.4.3.2, the limitations of interstory drift are given for buildings categorized in three ways regarding non-structural elements.

1. For buildings having non-structural elements of brittle materials attached to the structure:

$$d_r \nu_{EC8} \leq 0.005h \tag{7.1}$$

2. For buildings having ductile structural elements:

$$d_r \nu_{EC8} \leq 0.0075h \tag{7.2}$$

3. For buildings having non-structural elements fixed in a way so as not to interfere with structural deformations, or without non-structural elements:

$$d_r \nu_{EC8} \leq 0.01h \tag{7.3}$$

d_r is the design interstory drift, h is the story height and ν_{EC8} is the reduction factor which takes into account the lower return period of the seismic action associated with the damage limitation requirement.

According to the National Annex of EC8 [15], NA.4.4.3.2, there is no requirement of damage control in Norway. Thus, the recommended value $\nu_{EC8} = 0.5$ may be used for the purpose of investigating the requirements stated above. It should be noted that throughout the calculations and comparisons, the use of the ductility factor, q, has not been implemented for the purpose of comparison.

Table 7-1: Maximum values of interstory drift obtained for Oslo Plaza compared to the EC8 provision.

Maximum interstory drift, $d_r v_{EC8}$			
Realistic scenario		EC8 requirement	
X-direction	Y-direction	X-direction	Y-direction
$0.00095h$	$0.0011h$	$0.005h$	$0.005h$

As can be seen from table 7-1, Oslo Plaza is within the recommended interstory drift limits. The realistic scenario of the Friuli earthquake rendered the largest interstory drift. It is the glass facade on Oslo Plaza that determines the interstory drift requirement according to EC8. In this case, this is categorized under the first requirement stated in eq. (7.1).

The maximum interstory drift occurs in the transition of floor 34-35. As mentioned previously, this is due to the sudden change in the structural stiffness. The concrete shear wall system ends at this transition resulting in a story mechanism. This is by far one of the most critical points of the building. As confirmed by table 7-1 this is not a structural problem to consider. The other possible critical point is in the transition of floor 4-5. This is where the main concrete shear walls are substituted by large columns. However, this does not render a story-mechanism to consider because the tower is supported by the rest of the building, leaving negligible displacements and interstory drift at this floor.

The maximum displacement of the top of the building is also a parameter of importance to discuss. EC8 does not provide a specific requirement of displacement other than what is incorporated in the interstory drift requirements. As indicated in table 6-7, the maximum displacement was found to be 45.4 mm and 68.9 mm in the x-direction and the y-direction of the building respectively, according to the response spectrum analysis by EC8. However, these displacements do not occur simultaneously as they are found for different load cases. The Friuli earthquake rendered maximum displacements of 41.2 mm and 43.9 mm in the x-direction and the y-direction respectively. None of these results indicate large displacements considering the height of the building. The possibility that lateral forces generated by wind may induce larger top displacement of the building is likely. It should be noted that this has not been emphasized to investigate in this study.

7.2 THE P-Δ EFFECT

Seismic forces lead to lateral displacement of the structure and this may result in gravity-induced moments. These moments are normally small, but in cases where the product of the relative displacement and the gravity load give significant contribution to

the seismic overturning moment, P-Δ effects should be accounted for. The P-Δ effect is illustrated in figure 7-2.

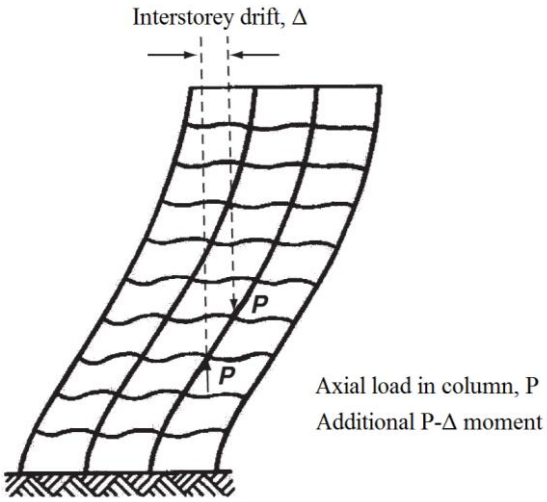

Figure 7-2: Illustration of the P-Δ effect.

Whether or not this effect should be accounted for is subject for discussion. EC8 [15], 4.4.2.2(2) states that the second-order effects do not need to be taken into account for if the following condition is fulfilled in all stories:

$$\theta_{EC8} = \frac{P_{tot} \cdot d_r}{V_{tot} \cdot h} \leq 0.10 \tag{7.4}$$

θ_{EC8} is the is the interstory drift sensitivity coefficient, P_{tot} is the total gravity load at and above the story considered in the seismic design, d_r is the design interstory drift as explained previously, V_{tot} is the total seismic story shear and h is the interstory height.

Furthermore, if $0.1 \leq \theta_{EC8} \leq 0.2$, the second-order effects may approximately be taken into account by multiplying the relevant seismic action effects by a factor equal to $1/(1 - \theta_{EC8})$. The value of θ_{EC8} should not exceed 0.3.

For the realistic scenario of the Friuli earthquake, the P-Δ effects were investigated for the x-direction and the y-direction. The result obtained is shown in table 7-2.

Table 7-2: Sensitivity coefficient for the two directions calculated for the Friuli earthquake.

Sensitivity coefficient, θ_{EC8}	
X-direction	Y-direction
0.964	0.293

For detailed calculations it is referred to Appendix H. As can be seen from table 7-2, the sensitivity coefficient exceeds the upper limit of 0.3 in the x-direction, and is very close to this limit in the y-direction. This indicates that the P-Δ effect might cause problems

resulting in large overturning base moments. By closer inspection of eq. (7.4), it can be seen that the sensitivity coefficient depends on the interstory drift. As shown in table 7-1, the interstory drift is well within the limits provided by EC8 for the building. Thus, P_{tot} and V_{tot} are the parameters that affects the formula the most. The mass of the building is large due to the fact that this is a high-rise structure, resulting in a high value for the total gravity load. However, the total seismic story shear is low despite the great mass of the building. This leads to a high sensitivity ratio that can be defined as

$$r_s = \frac{P_{tot}}{V_{tot}} \tag{7.5}$$

Considering the interstory drift obtained for the structure, it is questionable whether or not P-Δ effects can be calculated by eq. (7.4) as indicated in EC8. It might not be applicable to high-rise structures such as the one considered. Taking into consideration the fact that it is mainly the shear wall construction that takes most of the gravity loads in the structure, considering P-Δ effects this way will not be correct. It should be noted that it has not been emphasized to find a better representation to check for P-Δ effects for high-rise structures in this study. However, it can be stated that P-Δ effects have a great influence on postyield response of structures. P-Δ effects have little influence of the earthquake response of a structure considered that the structure remains elastic during the ground motion. This is due to the fact that P-Δ effects only slightly reduce the initial elastic stiffness of a structure [12]. Staying within the limits of interstory drift seems the most appropriate conclusion after performing the investigation of this parameter, especially since only linearly elastic representation and modeling has been performed in this study.

7.3 SOIL-STRUCTURE INTERACTION

Considerable effort in analyzing the foundation of Oslo Plaza was performed without considering a full direct analysis of the soil-structure interaction effects using numerical solutions. The foundation was modeled using springs as boundary conditions by a substructure analysis.

Moreover, based on the description of the foundation work as described in Chapter 3, the foundation of Oslo Plaza is considered a point bearing foundation. Piles and concrete foundation walls are connected to the bedrock through softer layers of soil between the bedrock and the slab foundation. This has led to a minimization of soil-structure interaction for this case in particular. Oslo Plaza was the first high-rise structure higher than 100 m built in Norway on difficult soil conditions such as the Oslo area consists of. In addition, a subway is led through the foundation work beneath the structure itself. These two factors are probably the main reason for making the bearing capacity of the foundation what may be considered as conservative, and the foundation considered

rigid. This has led to the investigation of how an alternative foundation approach would affect the seismic response of the building.

The question in matter is really how important the foundation work is for the seismic response of this building in particular. A scenario investigating the seismic response of the building assuming the foundation consists of an embedded foundation represented by soil springs has been carried out. The intention is to compare with the existing foundation work for the realistic scenario of the Friuli earthquake.

The foundation was modeled and represented by a substructure analysis according to the theory presented in Chapter 2.4. The results of the analysis with the new embedded foundation are compared with the existing foundation throughout this presentation. In the tables and figures the model with the existing foundation is referred to as Model 1, and the model with the new foundation representation is referred to as Model 2.

The embedded foundation is represented by 155 soil springs in the vertical direction and 216 soil springs in each horizontal direction. The stiffness assigned to each spring is indicated in table 7-3. For detailed calculations it is referred to Appendix I.

Table 7-3: Spring stiffness for the horizontal and vertical direction assigned to the element model.

Horizontal stiffness [N/m]		Vertical stiffness [N/m]
X-direction	Y-direction	
5.25E+07	6.55E+07	1.27E+08

For the purpose of comparison, all the soil parameters are the same for the new foundation representation as for the existing foundation representation, including using ground type D. As expected, the spring stiffness for the new foundation representation is lower than for the existing foundation. The result of the modal analysis is indicated in table 7-4.

Table 7-4: Modal analysis results from SAP2000 of the numerical FE-model for different foundation representations.

Mode	Frequency, f [Hz]		Period of vibration, T [s]		Participating Mass Ratio					
					Sum X		Sum Y		Sum Z	
	Model 1	Model 2	Model 1	Model 2	Model 1	Model 2	Model 1	Model 2	Model 1	Model 2
1	0.3408	*0.2869*	2.9346	*3.4853*	0.44	*0.08*	0.03	*0.43*	0.0002	*0.0011*
2	0.3668	*0.3109*	2.7265	*3.2169*	0.47	*0.47*	0.47	*0.52*	0.0015	*0.0012*
3	0.4307	*0.4171*	2.3218	*2.3976*	0.47	*0.47*	0.49	*0.52*	0.0015	*0.0014*
4	1.3092	*1.2837*	0.7638	*0.7790*	0.58	*0.59*	0.49	*0.52*	0.0016	*0.0022*
5	2.2162	*1.7610*	0.4512	*0.5679*	0.58	*0.59*	0.64	*0.53*	0.0050	*0.2800*
6	2.2310	*1.9222*	0.4482	*0.5202*	0.58	*0.59*	0.64	*0.57*	0.0588	*0.6200*
7	2.4269	*1.9576*	0.4121	*0.5108*	0.58	*0.59*	0.66	*0.73*	0.0616	*0.6300*
8	2.7619	*2.4011*	0.3621	*0.4165*	0.62	*0.59*	0.66	*0.73*	0.0730	*0.6300*
9	3.1595	*2.6517*	0.3165	*0.3771*	0.62	*0.59*	0.66	*0.73*	0.2000	*0.8000*
10	3.2497	*2.6796*	0.3077	*0.3732*	0.62	*0.65*	0.66	*0.73*	0.2100	*0.8000*

As expected, the new foundation representation resulted in higher natural vibration periods of the structure. This is a result of the representation of soil springs with lower stiffness than in the existing foundation. Table 7-4 also indicates that the first and second modes have switched translational direction. It is also worth noticing the increased modal participating mass ratio in the z-direction. Reduced foundation stiffness leads to higher modal mass participating in the vertical direction.

To investigate the difference in seismic response of the structure with the new foundation representation, an analysis with the original Friuli earthquake record was performed. The results of this compared with the seismic response of the structure with the existing foundation are presented in the following figures and tables.

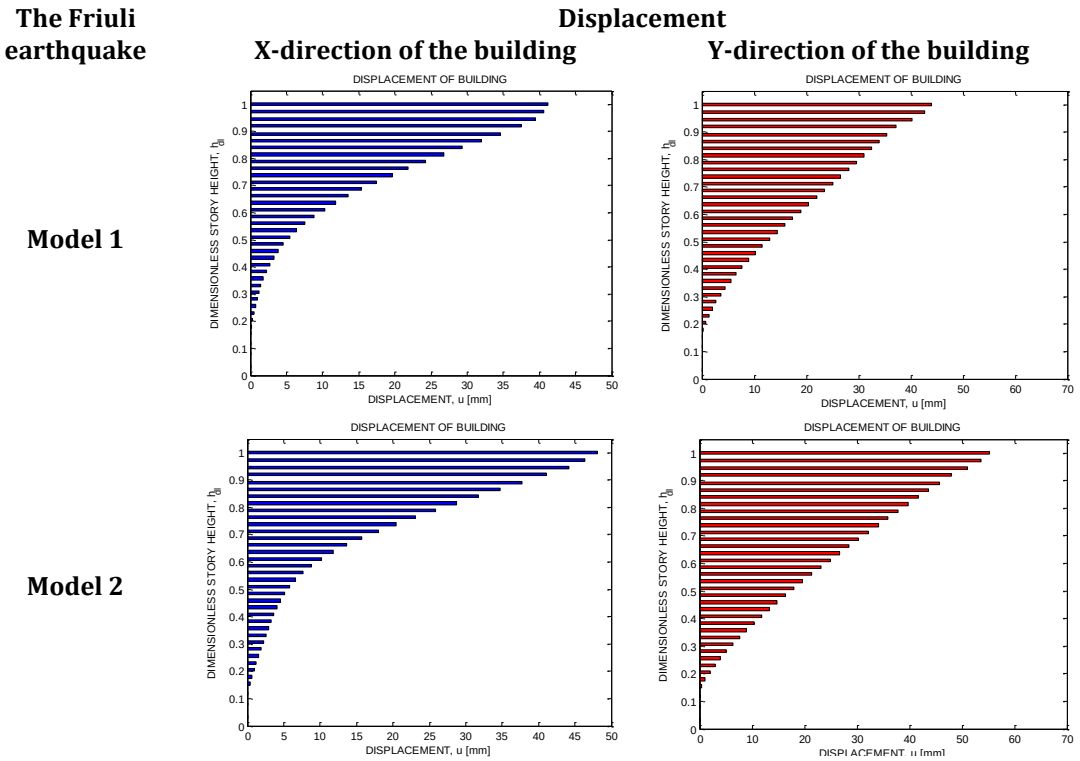

Figure 7-3: Maximum displacement response of the two models for the Friuli earthquake.

The maximum displacement of the building, i.e. the top displacement, is larger for the model with the new foundation representation. The increase of displacement is approximately 17% in the x-direction and approximately 26% in the y-direction. This is a considerable increase. However, the displacement response is still less than what obtained for the EC8 response spectrum load case for model 1.

Table 7-5: Maximum displacement response of the two models for the Friuli earthquake.

The Friuli earthquake	Displacement [mm]		Displacement ratio [x/y]
	X-direction	Y-direction	
Model 1	41.2	43.9	0.938
Model 2	48.1	55.2	0.871

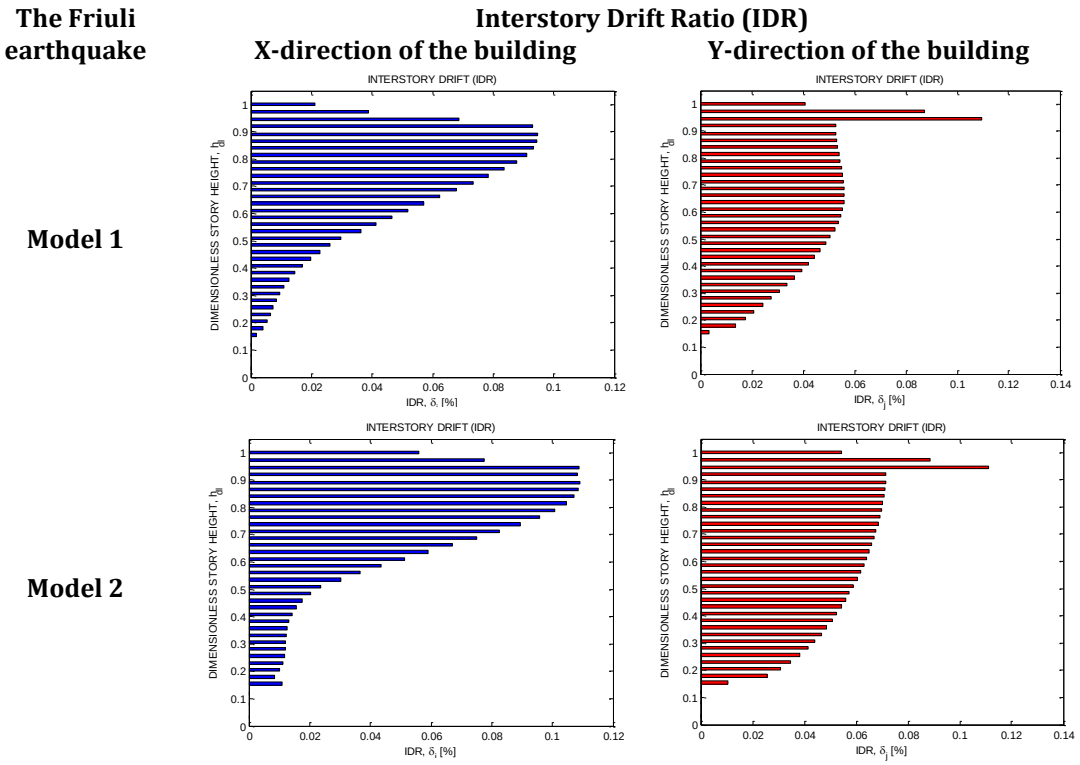

Figure 7-4: IDR of the two models for the Friuli earthquake.

The interstory drift is larger for the model with the new foundation representation. The interstory drift has increased in the x-direction and the location for the maximum drift has shifted two floors up for the model with the new foundation representation. The increase in IDR is approximately 15% for the x-direction and 1% for the y-direction. The interstory drift is still within the requirements by EC8.

Table 7-6: IDR of the two models for the Friuli earthquake.

The Friuli earthquake	X-direction		Y-direction		IDR ratio
	IDR [%]	Floor	IDR [%]	Floor	[x/y]
Model 1	0.095	32-33	0.110	34-35	0.864
Model 2	0.109	34-35	0.111	34-35	0.982

The largest increase in seismic response is found in the base shear. The base shear values are indicated in table 7-7.

The base shear is considerably larger for the model with the new foundation representation. The base shear has increased with 63% in the x-direction and approximately 27% in the y-direction. Without the piles and the concrete foundation walls the seismic response increase and the structure with the new foundation representation will be less able to withstand overturning moments. As mentioned before the soil conditions in the area considered are hard to classify, but a ground type categorized worse than ground type D might be realistic. This leads to the conclusion that some sort of foundation representation with piles is inevitable to avoid failure.

Table 7-7: Base shear obtained for the two models for the Friuli earthquake.

The Friuli earthquake	Base shear [kN]		Base shear ratio [x/y]
	X-direction	Y-direction	
Model 1	3 455	11 361	0.304
Model 2	5 613	14 422	0.389

The results obtained were partly as expected. The new foundation representation leading to softer soil springs results in higher natural vibration periods of the building. This results in a more flexible structure implying higher displacement as seismic response. This is obvious. However, it is not as obvious that the base shear should increase as much as indicated in table 7-7. In general, the base shear depends on the acceleration value taken from the response spectrum. Higher natural vibration periods lead to a smaller acceleration values. In this case, the increase in the natural vibration periods does not affect the acceleration value much according to the response spectrum for the Friuli earthquake indicated in figure 5-6. Thus, based on this one should expect some, but not considerable changes in the base shear. One explanation for the considerable increase in base shear could be that due to the more flexible foundation a larger modal participating mass ratio is obtained in the modal analysis. This was confirmed in table 7-4. The reason for this is that due to a more flexible foundation, a larger part of the mass is included in the modes and hence the modal participating mass ratio increases. However, only 20 modes were included in the modal analysis for model 2 whereas 200 modes were included in the modal analysis for model 1. This was done to obtain equal *total* modal participating mass ratio in each direction for each model to be able to compare results correctly. However, the difference in the model with the new foundation representation from the model with the existing foundation representation is that a larger part of the modal participating mass is included in the lower modes. Lower modes contribute more to base shear than higher modes, and thus the base shear for the already flexible building exposed to a realistic earthquake scenario such as the Friuli earthquake increase. This is one explanation for the increase in base shear for the new foundation representation. In addition, the first and second modes have switched translational direction as was seen from the modal analysis. Last, considering the response spectrum and the time-history representation of the Friuli earthquake, some of the natural vibration periods from the new model (model 2) may occur at peaks in the response spectrum leading to unrealistically high base shear values for some modes.

However, this should have been reflected in the displacement response as well. Regardless, the response in displacement, IDR and base shear have increased for the new foundation representation compared to the existing foundation representation.

The results obtained lead to the conclusion that the existing foundation is a good foundation based on the analyses obtained for the simplified foundation representation. Using piles in the foundation work is inevitable. However, a combination of the two methods may be a reasonable approach. By using piles instead of concrete foundation walls for the tower foundation and fewer piles underneath the structure foundation could have resulted in a less conservative foundation representation, but still within reasonable requirements of the EC8. It must be emphasized to include many modes in the analyses performed for a model with a stiff foundation (equivalent of modeling on rock) to be able to obtain a total modal participating mass ratio that includes as much mass as possible in the calculations performed.

7.4 NEAR-FAULT GROUND MOTIONS VS. FAR-FAULT GROUND MOTIONS

The difference of near-fault earthquakes and far-fault earthquakes regarding response of the structure is of particular interest. For the method of scaling the results have been presented in Chapter 6 with the intention of comparing with the EC8 response spectrum analysis. In this subchapter, emphasis is placed in comparing the Nahanni far-fault earthquake with the Friuli near-fault earthquake.

As stated in Chapter 6.1, the Nahanni earthquake and the Friuli earthquake rendered fairly similar results of maximum displacement, but indeed lower than the EC8 response spectrum analysis. This is summarized in table 7-8.

Table 7-8: Maximum displacement response of the building for different load cases.

Load case	Displacement [mm]		Displacement ratio [x/y]
	X-direction	Y-direction	
EC8	45.4	68.9	0.659
Nahanni	19.2	21.0	0.913
Friuli	18.0	16.2	1.112

The results from the Friuli earthquake rendered much higher IDR-values than the results rendered from the Nahanni earthquake. This is summarized in table 7-9. This is the first indication of the difference in near-fault earthquakes versus far-fault earthquakes regarding seismic response of the high-rise structure.

Table 7-9: Maximum IDR of the building for the near-fault and far-fault load cases.

Load case	X-direction		Y-direction		IDR ratio
	IDR [%]	Floor	IDR [%]	Floor	[x/y]
Nahanni	0.028	27-28	0.027	34-35	1.037
Friuli	0.042	34-35	0.043	34-35	0.977

The IDR for the Friuli earthquake is 50% larger in x-direction and 59% larger in the y-direction than for the Nahanni earthquake. IDR is an important damage parameter, and only considering the far-fault earthquake in this situation would be non-conservative. For Oslo Plaza the IDR for the near-fault earthquake and the far-fault earthquake are within acceptable limits for the method of scaling by EC8.

As indicated in table 7-10, the base shear obtained for the Nahanni earthquake are lower than the base shear obtained for the Friuli earthquake. The difference is largest in the y-direction of the building, where the base shear is 75% larger for the Friuli earthquake. In the x-direction the base shear is 40% larger.

Table 7-10: Maximum base shear of the building for different load cases.

Load case	Base shear [kN]		Base shear
	X-direction	Y-direction	ratio [x/y]
EC8	2 929	8 257	0.355
Nahanni	1 345	3 538	0.380
Friuli	1 885	6 204	0.304

By scaling the ground motion records as performed in this study the properties of the near-fault ground motion and the far-fault ground motion changes. As mentioned earlier, scaling by the method of EC8 according to PGA and ground type may be better suited for far-fault ground motion compared to near-fault ground motion. This affects the original ground motion records which again affects the seismic response of the building. Nevertheless, the results presented here support the conclusion that design according to seismic response obtained by the EC8 response spectrum analysis will be sufficient.

The uncertainty of how the scaling of the time-series affects the structure considered has led to investigating the seismic response when exposed to the original Friuli earthquake and the original Nahanni earthquake. For these two load cases, no modifications of the ground motion acceleration data have been performed. The result obtained is given in the following tables and figures.

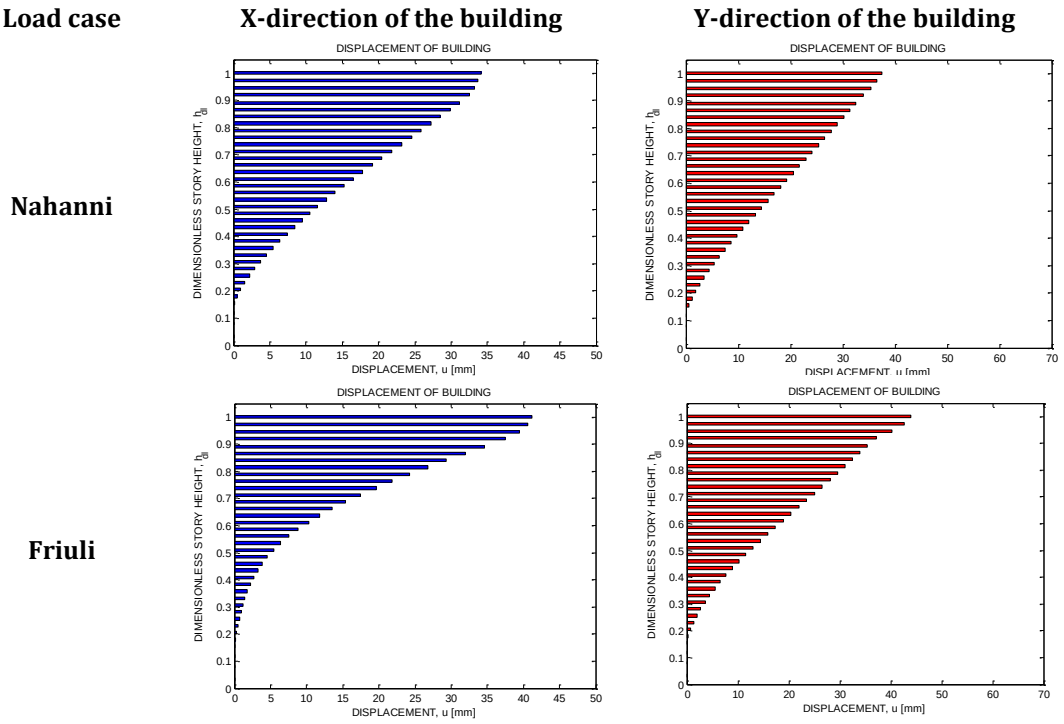

Figure 7-5: Maximum displacement response for the near-fault and the far-fault load case.

As figure 7-5 and table 7-11 indicates, the Friuli earthquake renders larger maximum displacement response than the Nahanni earthquake even though the magnitude is smaller for the Friuli earthquake, see table 5-4 in Chapter 5. However, these displacement values may be considered reasonable, and neither of the values is problematic due to any requirements.

Table 7-11: Maximum displacement response for the near-fault and far-fault load case.

Load case	Displacement [mm]		Displacement ratio [x/y]
	X-direction	Y-direction	
Nahanni	34.1	37.5	0.909
Friuli	41.2	43.9	0.938

The results from the Friuli earthquake render much higher IDR-values than the Nahanni earthquake. This is summarized in table 7-12. This is the same indication of the difference in near-fault earthquakes versus far-fault earthquakes regarding seismic response of the high-rise structure as seen for the results rendered by scaling after the method of EC8. The IDR for the Friuli earthquake is approximately 94% larger in the x-direction, and approximately 116% larger in the y-direction than the Nahanni earthquake.

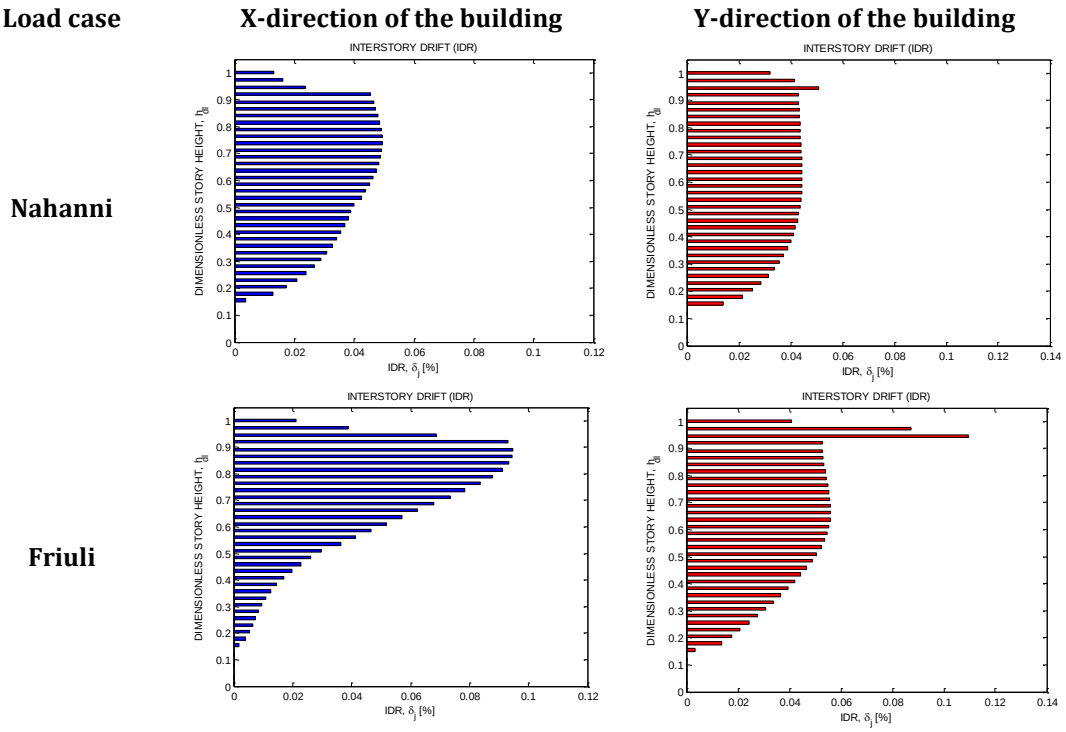

Figure 7-6: Maximum IDR for the near-fault and far-fault load case.

The plots in figure 7-6 show the difference in IDR throughout the dimensionless height of the building. As can be seen clearly, the near-fault ground motion results in a significant IDR distribution that might cause problems with interstory drift requirements. However, for this earthquake it is not a problem as concluded with previously. In a general situation where a far-fault ground motion would result in response close to the limits of the requirements, near-fault ground motion could cause problems for high-rise structures considering IDR as seismic response parameter.

Table 7-12: Maximum IDR for the near-fault and the far-fault load case.

Load case	X-direction		Y-direction		IDR ratio
	IDR [%]	Floor	IDR [%]	Floor	[x/y]
Nahanni	0.049	27-28	0.051	34-35	0.961
Friuli	0.095	32-33	0.110	34-35	0.864

Table 7-13 shows the result obtained for the base shear response. As indicated in the table, the same general observation regarding base shear is obtained for the two load cases here as for the results obtained in the method by scaling. The base shear is approximately 45% larger in the x-direction and approximately 79% larger in the y-direction for the Friuli earthquake than for the Nahanni earthquake. This supports the conclusion of the structural response regarding near-fault ground motion versus far-fault ground motion.

Table 7-13: Base shear obtained for the near-fault and far-fault load case.

Load case	Base shear [kN]		Base shear ratio [x/y]
	X-direction	Y-direction	
Nahanni	2 390	6 346	0.377
Friuli	3 455	11 361	0.304

The results from the time-history representation analyses of far-fault and near-fault ground motion records correspond well to the theory presented in Chapter 2. Near-fault earthquakes have larger deformation and strength demand than far-fault earthquakes, especially considering high-rise structures.

This has been confirmed by looking at ground motion data for two specific earthquakes, one representing near-fault ground motion and one representing far-fault ground motion for the high-rise structure.

8 CONCLUDING REMARKS

In the presented research a numerical element model of a high rise structure located in the seismic area of Oslo was created using the structural analysis program SAP2000. The modeling was performed based on construction and architectural drawings of Oslo Plaza in addition to building inspections. An analysis of the foundation work with the intention of obtaining a good soil-structure interaction representation of the structure was carried out. To obtain this, research of the foundation work of Oslo Plaza in addition to research in the general theory behind SSI was performed.

Structural monitoring of the building was performed with the intention of calibrating the numerical element model. The application of structural response measurements for calibration is a powerful tool in dynamic analysis. Unfortunately, due to the limited time to perform the structural monitoring and due to the lack of excitation of the building the results of the monitoring process did not render any information within reasonable expectations of the natural vibration periods of the structure. Thus, no calibration of the numerical FE-model was performed.

For the time-history representation analyses performed, strong ground motion data from one far-fault record and two near-fault records were used. For this purpose strong ground motion records from the 1985 Nahanni earthquake, the 1979 Imperial Valley earthquake and the 1976 Friuli earthquake was chosen. The ground motion data were analyzed and modified for the purpose of comparison with the modal response spectrum analysis according to EC8 and for the purpose of investigating the effects of realistic earthquake scenarios. Simulations and modifications of the near-fault ground motion records were performed. The purpose of this was to obtain statistically more reliable ground motion representation for investigation of the seismic response of the structure considered.

The behavior and response of the structure to the seismic loading was thoroughly investigated with emphasis on response parameters considered important for high-rise structures. The response parameters of main interest were displacement, interstory drift and base shear. These parameters were investigated for two reasons; staying within the requirements of EC8 for the purpose of comparison of results obtained from the analyses and applying strong ground motion data to the structure for a realistic earthquake scenario that might occur in the region of Oslo. A case study of the structure regarding these parameters including the evaluation of a different foundation representation was carried out. The main findings and conclusions drawn from the analyses results and the case study are summarized in the following list:

- The structural response indicates that the simulations based on the Friuli earthquake are better than the simulations of the Imperial Valley earthquake.

This is indicated through the statistical properties of the structural response parameters.

- For the method of scaling by EC8, the modal response spectrum analysis results in larger displacement response and base shear than the ground motion from the time-history representation analyses. The near-fault earthquakes render larger IDR than the far-fault earthquake. The maximum interstory drift occurs in the transition of floor 34-35 due to the sudden change in the structural stiffness.

- For the non-modified ground motion records, i.e. the realistic case scenarios, the response from the near-fault earthquake records render larger interstory drift at the critical floors with reduced stiffness than what the far-fault earthquake record does. This corresponds well to what is stated in the literature regarding high-rise structures.

- If an earthquake scenario like the Friuli earthquake were to happen in Oslo, the maximum displacement response would be less than the results obtained from the EC8 response spectrum analysis, but the base shear would be larger.

- The top displacement of the building is small considering the total height of the building. The maximum top displacement obtained from a realistic earthquake scenario is estimated to be in the range of 40 – 45 mm. The explanation of this is most likely due to the fact that the building and its foundation is considered stiff.

- Oslo Plaza is within the recommended interstory drift limits according to EC8. The control for P-Δ effects performed according to EC8 resulted in a sensitivity factor that exceeds the upper limit for Oslo Plaza. A conclusion stating that this requirement by eq. (7.4) is not applicable to high-rise structures such as the one considered can be drawn from this.

- The foundation work is important regarding seismic response, especially for a high-rise structure like Oslo Plaza. The existing point bearing foundation resulted in less response than the alternative foundation representation. The existing foundation performs well in the seismic analyses. However, a combination of the existing foundation representation and the alternative representation could be a reasonable approach considered less conservative.

- Near-fault earthquakes have larger deformation and strength demands than far-fault earthquakes. All the response parameters from the analyses of the unmodified ground motion data resulted in higher values for the near-fault earthquake than for the far-fault earthquake. The main difference between near-fault and far-fault earthquakes is that near-fault earthquakes are dominated by one or few strong pulses. Using modal response spectrum analysis for seismic

analyses and design may lead to underestimation of forces and displacement in the structure.

- If an earthquake scenario with approximately the same attenuation relationships as the Friuli earthquake were to happen in Oslo, Oslo Plaza would perform well. It is emphasized that this statement is based only on the response parameters investigated. In the work of this study, no design checks have been performed for the structural elements of the building.

- A seismic design according to EC8 and the National Annex of Norway is sufficient for high-rise structures like Oslo Plaza. However, the requirement of P-Δ effects may be difficult to fulfill, and an alternative approach for taking these effects into consideration should be performed.

9 FURTHER WORK

Many of the most important aspects regarding the evaluation of the seismic response of a high-rise structure have been covered in this thesis. The difference between far-fault ground motion and near-fault ground motion with emphasis on the latter has been investigated.

This chapter contains a proposal for further work of how to better understand and learn the behavior of high-rise structures exposed to near-fault ground motions:

- Introduce ductility in the numerical element model and investigate the effect of material non-linearity to gain more insight in the element behavior of the structure.

- Introduce continuous structural monitoring of Oslo Plaza for an extended period to obtain exact result of the dynamic behavior of the building. This also monitors and reports the changes that might occur in the dynamic behavior of the structure over time.

- Increase the number of simulations and include more ground motion records from other representative earthquakes for the seismic zone of Oslo to obtain a statistical better representation of the seismic situation.

- Perform a direct analysis in a finite element approach to obtain a full representation of the foundation and the soil conditions for the structure. This would gain better insight in the understanding of the soil-structure interaction in the global dynamic response of the building.

- Design of the building in accordance with the EC8 provision of the existing structural system for the different seismic scenarios. Perform seismic design of alternative structural systems in concrete and in steel.

BIBLIOGRAPHY

[1] S. Molina and C. Lindholm, "A logic tree extension of the capacity spectrum method developed to estimate seismic risk in Oslo, Norway," *Journal of Earthquake Engineering,* pp. 877-897, 4 September 2008.

[2] H. M. Westergaard, "Earthquake-shock transmission in tall buildings," *Engineering News Record,* pp. 654-656, 1933.

[3] S. L. Kramer, Geotechnical Earthquake Engineering, Washington: Pearson College Div, 1996.

[4] NORSAR, «jordskjelv.no: Om jordskjelv,» NORSAR, 20 Juli 2010. [Internett]. Available: http://www.jordskjelv.no. [Funnet 7 Mars 2012].

[5] R. W. Clough and J. Penzien, Dynamics of Structures, Berkeley, USA: Computers & Structures Inc., 2003.

[6] A. Chopra and C. Chintanapakdee, "Comparing response of SDF systems to near-fault and far-fault earthquake motions in the context of spectral regions," *Earthquake Engineering and Structural Dynamics,* pp. 1770-1789, 19 March 2001.

[7] P. G. Sommerville, «Engineering characterization of near fault ground motions,» i *2005 NZSEE Conference*, Pasadena, CA, USA, 2005.

[8] R. Rupakhety and R. Sigbjörnsson, "Can Simple Pulses Adequately Represent Near-Fault Ground Motions?," *Journal of Earthquake Engineering,* pp. 1260-1272, 4 February 2011.

[9] E. Booth and D. Key, Earthquake design practice for buildings, London: Thomas Telford Publishing, 2006.

[10] R. Rupakhety, S. Sigurdsson, A. Papageorgiou and R. Sigbjörnsson, "Quantification of ground-motion parameters and response spectra in the near-fault region," *Bulletin of Earthquake Engineering,* pp. 894 - 930, 18 March 2011.

[11] NFR / NORSAR, "Seismic Zonation For Norway," NORSAR / Norwegian Geotechnical Institute, Oslo, 1998.

[12] A. K. Chopra, Dynamics of Structures. Theory and Applications to Earthquake Engineering, 3 red., Upper Saddle River, New Jersey: Pearson Prentice Hall, 2007.

[13] A. Rönnquist, "Lecture notes: TKT4201 Structural Dynamics," Trondheim, Norway, The Norwegian University of Science and Technology. Department of Structural Engineering, 2012.

[14] M. Fardis, Designers' Guide to Eurocode 8: Design of Structures for Earthquake Resistance., Thomas Telford Limited., 2009.

[15] European committee for standardization, Eurocode 8: Design of structures for earthquake resistance - Part 1: General rules, seismic actions and rules for buildings, Oslo: Standards Norway, 2004.

[16] S. L. Kramer and J. P. Stewart, "Earthquake Engineering: From Engineering Seismology to Performance-Based Engineering," in *Chapter 4.5 - Soil-Foundation-Structure Interaction*, CRC Press LLC, 2004.

[17] R. Tuladhar, "Seismic behavior of concrete pile foundation embedded in cohesive soil," PhD Dissertation, Saitama University, Japan, Saitama, 2006.

[18] G. Mylonakis, S. Nikolaou and G. Gazetas, "Footings under seismic loading: Analysis and design issues with emphasis on bridge foundations," *Soil Dynamics and Earthquake Engineering,* pp. 824 - 853, 9 December 2005.

[19] A. Pecker, "Soil Structure Interaction," in *Advanced Earthquake Engineering Analysis*, Palaiseau, Springer, 2007, pp. 33 - 42.

[20] European committee for standardization, Eurocode 8: Design of structures for earthquake resistance - Part 5: Foundations, retaining structures and geotechnical aspects, Oslo: Standards Norway, 2004.

[21] A. Kaynia, "Lecture notes: TKT4108 Advanced Structural Dynamics. Sessions 4 & 5. Soil-Structure Interaction," Trondheim, The Norwegian University of Science and Technology. Department of Structural Engineering., 2011.

[22] A. S. Veletsos and Y. T. Wei, "Lateral and rocking vibrations of footings," Proc. ASCE Jnl. SM and Founds. Div., Houston, U.S, 1971.

[23] W. Shiming and G. Gang, "Dynamic Soil-Structure Interaction For High-Rise Buildings," *Developments in Geotechnical Engineering,* pp. 203 - 216, 10 May 2007.

[24] T. Söderström and P. Stoica, System Identification, Uppsala (Sweden), Bucharest (Romania): Prentice Hall International (UK) Ltd, 1989.

[25] R. Sigbjörnsson, *Conversations and guidance through meetings at NTNU for TKT4195 - Computational Mechanics, Master Thesis,* Trondheim, 2012.

[26] The Mathworks Inc., «Matlab R2011a User Guide and Product Documentation,» 2012. [Internett]. Available: http://www.mathworks.se/. [Funnet Januray - June 2012].

[27] E. Kreyszig, "Chapter 11 - Fourier Series, Integrals and Transforms," in *Advanced Engineering Mathematics*, Ohio, John Wiley & Sons, Inc, 2006, pp. 478 - 534.

[28] E. Strømmen, Theory of Bridge Aerodynamics, Trondheim: Springer Verlag, 2010.

[29] A. Kaynia, "Lecture notes: TKT4108 Advanced Structural Dynamics," Trondheim, Norway, The Norwegian University of Science and Technology. Department of Structural Engineering, 2011.

[30] Radisson Blu Plaza Hotel Oslo, Technical Engineer Svein Willadsen., "Building facts," Radisson Blu Plaza Hotel Oslo, Oslo, 2012.

[31] E. Thorn, «Fundamentering av Norges høyeste bygg - Oslo Plaza Hotel - på slisseveggpaneler til bratt fjell,» i *Norsk forening for fjellsprengningsteknikk-fjellsprengningskonferanse*, 1988.

[32] Hottinger Baldwin Messtechnik GmbH (HBM), "User Guide and Product Documentation," 2012. [Online]. Available: http://www.hbm.com. [Accessed April 2012].

[33] E. F. Taylor and J. A. Wheeler, "Spacetime Physics," in *The Clock Paradox III*, San Francisco, W. H. Freeman and Company, 1966, pp. 97 - 98.

[34] L. Ljung, System Identification: Theory for the User (2nd Edition), Prentice Hall, 1998.

[35] B. T. Svendsen, "Analysis of a Building Subject To Earthquake-Induced Motion," NTNU / Tapir, Trondheim, 2011.

[36] N. Naumoski, M. Saatcioglu and K. Amiri-Hormozaki, "Effects of Scaling of Earthquake Excitations On The Dynamic Response of Reinforced Concrete Frame Buildings.," *World Conference on Earthquake Engineering,* pp. 1 - 15, August 2004.

[37] H. Bachmann, Seismic Conceptual Design of Buildings - Basic principles for engineers, architects, building owners, and authorities, Zurich: Swiss Federal Office for Water and Geology; Swiss Agency for Development and Cooperation, 2002.

[38] E. L. Wilson, "Chapter 16 - Soil Structure Interaction," in *Three-Dimensional Static and Dynamic Analysis of Structures*, Berkeley,California, Computers and Structures, Inc., 2002.

[39] G. Mylonakis and G. Gazetas, "Seismic Soil-Structure Interaction: Beneficial or Detrimental?," *Journal of Earthquake Engineering ,* pp. 277 - 301, 30 April 2008.

[40] California Insitute of Technology, «Caltech Media relations,» 10 August 2006. [Internett]. Available: http://media.caltech.edu/press_releases/12883. [Funnet 21 May 2012].

[41] Betongelementforeningen, Dimensjonering for jordskjelv, bind H, Oslo: Betongelementforeningen, 2011.

[42] Computers and Structures, Inc. (CSI), "SAP2000 User Manual," 2012. [Online]. Available: http://www.csiberkeley.com/. [Accessed January - June 2012].

APPENDIX A – MATLAB CODE FOR WHITE NOISE

```
%MASTER THESIS.
%NTNU 2012. Bjørn Th. Svendsen.

%This program generates a random time-series representing white
%noise, and exports the data to a .txt file.

clear all
clc
close all

% Defining variables and vectors
T = [0:0.005:45];
A = randn(length(T),1)';

disp('The standard deviation of the white noise matrix is')
std(A)
disp('The peak value of the white noise is')
max(abs(A))

A = A./max(abs(A));

% Plotting the result
figure(1)
plot(T,A)
title('WHITE NOISE')
xlabel('TIME [s]')
ylabel('ACCELERATION [m/s^2]')
set(gca,'YTick',-1:0.5:1);
grid on

% Exporting matrix to textfile
data = [T; A];
fileID = fopen('WhiteNoise.txt','w');
fprintf(fileID,'%5s %10s\n','T','A');
fprintf(fileID,'%5.3f %5.7f\n',data);
fclose(fileID);
```

APPENDIX B – SSI CALCULATIONS

In this appendix the calculations for the spring stiffness used for boundary conditions in the numerical FE-model of Oslo Plaza in SAP2000 is presented.

The horizontal stiffness of the piles is taken from EC8 [20]. The pile stiffness is defined as the force to be applied to the pile head to produce a unit displacement along the same direction as the direction of the force applied. The horizontal stiffness is

$$\frac{K_{H,p}}{d_p \cdot E_s} = 1.08\left(\frac{E_p}{E_s}\right)^{0.21} \tag{B.1}$$

where d_p is the pile diameter (0.275 m), E_p is Young's modulus of the pile material which in this case is concrete C75 $\left(3.9 \cdot 10^{10}\,\frac{N}{m^2}\right)$ and E_s is defined as

$$E_s = (1 + 2\nu)G_s \tag{B.2}$$

$$G_s = \rho V_s^2 \tag{B.3}$$

ν is Poisson's ratio, V_s is the shear wave velocity of the soil at the location (180 m/s) and ρ is the bulk density of the soil (1700 kg/m^3). Thus $K_{H,p}$ is the pile stiffness per pile, and becomes

$$K_{H,p} = 1.08\left(\frac{3.9 \cdot 10^{10}}{1.102 \cdot 10^{8}}\right)^{0.21} \cdot 0.275m \cdot (1.102 \cdot 10^{8})\frac{N}{m^2} \tag{B.4}$$

$$K_{H,p} = 1.12 \cdot 10^{8}\frac{N}{m} \tag{B.5}$$

With 700 piles located in the structure foundation divided on the total number of 76 springs in each horizontal direction, the horizontal stiffness becomes

$$K_{H,p\ tot} = \frac{700 \cdot K_H}{76} \tag{B.6}$$

$$\underline{K_{H,p\ spring} = 1.03 \cdot 10^{9}\frac{N}{m}} \tag{B.7}$$

This spring stiffness is applied in both the x-direction and the y-direction in the element model.

The vertical stiffness of a pile is given by

$$K_{V,p} = \frac{EA}{l} = \frac{3.9 \cdot 10^{10} \frac{N}{m^2} \cdot 0.275m^2}{17.4m} \tag{B.8}$$

$$K_{V,p} = 1.7 \cdot 10^8 \frac{N}{m} \tag{B.9}$$

where l is the average length of the piles. With 700 piles located in the structure foundation divided on the total number of 76 springs in the vertical direction, the vertical stiffness becomes

$$\underline{K_{V,p\ spring} = 1.56 \cdot 10^9 \frac{N}{m}} \tag{B.10}$$

The concrete foundation walls representing the tower foundation may also be represented by horizontal and vertical springs. The horizontal stiffness representing the walls in the in-plane direction is

$$K_{Hy,w} = \frac{GA}{l} \tag{B.11}$$

In this case

$$A = 1.2m \cdot 2.8m = 3.36m^2 \tag{B.12}$$

$$G = \frac{E_c}{1 + 2v} = \frac{3.6 \cdot 10^{10} \frac{N}{m^2}}{1 + 2 \cdot 0.2} \tag{B.13}$$

$$G = 2.57 \cdot 10^{10} \frac{N}{m^2} \tag{B.14}$$

To find the horizontal stiffness in the out-of-plane direction the walls are represented with equivalent piles. The thickness of the wall is 1.2 m and this is chosen as the equivalent pile diameter. Each wall has a length of 2.8 m, i.e. 2.33 equivalent piles. Hence

$$K_{H,w} = 2.33 \cdot 1.08 \left(\frac{3.9 \cdot 10^{10}}{1.102 \cdot 10^8} \right)^{0.21} \cdot 0.275m \cdot (1.102 \cdot 10^8) \frac{N}{m^2} \tag{B.15}$$

$$\underline{K_{H,w} = 1.12 \cdot 10^9 \frac{N}{m}} \tag{B.16}$$

The vertical stiffness is given by

$$K_{v,w} = \frac{EA}{l} \tag{B.17}$$

To represent the stiffness of the foundation in the best possible way, 6 springs are assigned along the y-axis of the tower varying linearly with depth, see table B-1. The stiffness of all the springs in each direction is indicated in the table as well.

Table B-1: Spring stiffness for concrete foundation walls.

Spring number	y-coordinate [m]	Wall length [m]	Vertical stiffness [m]	Horizontal stiffness	
				In-plane	Out-of-plane
1	7500	12	1.01E+10	7.20E+09	1.12E+09
2	10720	15.6	7.75E+09	5.54E+09	1.12E+09
3	13940	19.2	6.30E+09	4.50E+09	1.12E+09
4	17160	22.8	5.31E+09	3.79E+09	1.12E+09
5	20380	26.4	4.58E+09	3.27E+09	1.12E+09
6	23600	30	4.03E+09	2.88E+09	1.12E+09

The width of the tower is approximately 18.9 m, that is from y = 6.1 m to y = 25 m in the tower coordinate system. It is desired to place the first spring half a wall width from both of the ends of the building (y = 7.5 m and y = 23.6 m) with approximately 3.22 m distance between each spring.

APPENDIX C – ESTIMATION OF MASS AND SECOND MOMENT OF INERTIA

In this appendix the calculations for the estimation of the natural vibration period for Oslo Plaza is carried out for the purpose of comparison with the numerical FE-model obtained in SAP2000.

Estimation of mass

The mass of the slabs, m_s, may be calculated by

$$m_s = t_s \cdot y \cdot x \cdot \rho_{concrete} \cdot n_f \tag{C.1}$$

where t_s is the thickness of the slab, y is the width of the slab, x is the length of the slab and n_f is the amount of floors.

$$m_s = 0.22m \cdot 18.9m \cdot 54.2m \cdot 2500\frac{kg}{m^3} \cdot 36 \tag{C.2}$$

$$m_s = 20\ 282\ 724kg \tag{C.3}$$

The mass of the walls, m_w, may be calculated by

$$m_w = t_w \cdot y \cdot h_{tot} \cdot \rho_{concrete} \cdot n_w \tag{C.4}$$

where t_w is the thickness of the wall, y is as described previously, h_{tot} is the height of the building and n_w is an equivalent approximation of the amount of walls.

$$m_w = 0.3m \cdot 18.9m \cdot 117m \cdot 2500\frac{kg}{m^3} \cdot 6 \tag{C.5}$$

$$m_w = 9\ 950\ 850kg \tag{C.6}$$

The number of walls is set to 6 to account for the 4 main walls, plus the shear walls. This is a rough estimate. The total mass is then

$$m_{TOT} = m_s + m_w = 30\ 233\ 574kg \tag{C.7}$$

$m(x)$ has units of kg/m and is obtained by dividing by the total height, $x = h_{tot}$, of the building:

$$\underline{m(x) = 258\ 406\frac{kg}{m}} \tag{C.8}$$

Estimation of second moment of inertia, I_X

This calculation provides the estimation of the second moment of inertia about the y-axis (in the x-direction).

In general

$$I = \frac{1}{12} b h_i^3 + A d_c^2 \tag{C.9}$$

The shear wall contribution is calculated as

$$I_1 = 2\left(\frac{1}{12} \cdot 18.9 \cdot 0.3^3 + 18.9 \cdot 0.3 \cdot 12.6^2\right) m^4 = 1800 m^4 \tag{C.10}$$

$$I_2 = 2\left(\frac{1}{12} \cdot 18.9 \cdot 0.3^3 + 18.9 \cdot 0.3 \cdot 19.8^2\right) m^4 = 4446 m^4 \tag{C.11}$$

The contribution from the elevator cores is calculated as

$$I_3 = 4 \cdot 0.25 \cdot 5.775 \cdot 5.4^2 = 168 m^4 \tag{C.12}$$

The total estimated second moment of inertia is

$$\underline{I_{TOTx} = 6414 m^4} \tag{C.13}$$

Estimation of second moment of inertia, I_Y

This calculation provides the estimation of the second moment of inertia about the x-axis (in the y-direction).

The shear wall contribution is calculated as

$$I_1 = 4\left(\frac{1}{12} \cdot 0.3 \cdot 18.9^3\right) m^4 = 675 m^4 \tag{C.14}$$

The contribution from the elevator cores is calculated as

$$I_2 = 4\left(\frac{1}{12} \cdot 0.25 \cdot 5.775^3 + 0.25 \cdot 5.775 \cdot 6.56^2\right) m^4 = 265 m^4 \tag{C.15}$$

The elevator core element contributions from elements in the y-direction is

$$I_3 = 8\left(\frac{1}{12} \cdot 0.25 \cdot 2.475^3 + 0.25 \cdot 2.475 \cdot 1.89^2\right) m^4 = 20 m^4 \tag{C.16}$$

The total estimated second moment of inertia is

$$\underline{I_{TOTy} = 960m^4} \tag{C.17}$$

APPENDIX D – MATLAB CODE FOR FOURIER ANALYSIS AND THE BURG METHOD

```
%MASTER THESIS.
%NTNU 2012. Bjørn Th. Svendsen and Karin Harnæs Hoel.

%This program reads a .txt file consisting of two columns of data;
%the first column represents time and the second column represents
%acceleration. The program plots the Fourier Amplitude Spectrum and
%The Burg Method in order to recognize the eigenfrequencies rendered
%from the input data.

clc
clear all
close all

% Importing data and defining variables
data = importdata('Accelerationdata.txt');
T = data(:,1);
A = data(:,2);

% Performing a routine to avoid overflow results from the data
for i = 1:length(A)
    if abs(A(i)) > 10
        A(i) = A(i-1);
    end
end

A = detrend(A);              % Removes linear trends in the plot
w = tukeywin(length(A),0.4);
A_tk = w.*A;

% Plotting the acceleration history
figure(1)
plot(T,A)
title('ACCELERATION HISTORY PLOT OF SENSOR 1')
xlabel('TIME [s]');
ylabel('ACCELERATION, [m/s^2]');
xlim([0 45]);
ylim([-15 15]);

% FOURIER AMPLITUDE SPECTRUM
dt = T(2) - T(1);
Fs = 1/dt;
n = length(A_tk);
nyf = Fs/2;
f = linspace(0,nyf,n/2);
aVf = A_tk - mean(A_tk);
fftavf = (2*(fft(aVf)))/n;
ck = abs(fftavf);

% POWER SPECTRAL DENSITY (PSD) USING PERIODOGRAM
Hf = spectrum.periodogram;
l = psd(Hf,A,'Fs',Fs);
```

```
% THE BURG METHOD
order = 2000;
Hs = spectrum.burg(order);
h = psd(Hs,A,'Fs',Fs);

% Plotting the result
figure(3)
hold on
%plot(f,ck(1:n/2),'color',[0.765,0.765,0.765]) %FA Spectrum
plot(l.Frequencies,l.Data,'color',[0.765,0.765,0.765]) %PSD Spectrum
plot(h.Frequencies,h.Data,'color',[0,0,0]) %The Burg Method
title('FREQUENCY SPECTRUM')
xlim([0 0.8]);
ylim([0 24]);
xlabel('FREQUENCY, f [Hz]')
ylabel('SPECTRAL DENSITY, S_x')
legend('Fourier Transform (Periodogram)','The Burg Method');
set(legend,'box','off');
set(legend,'location','NorthWest')
set(gca,'box','on');

%Finding peaks and corresponding values to render eigenfrequencies
[pks,loks] =
findpeaks(ck(1:n/2),'minpeakdistance',2,'npeaks',5,'SORTSTR','descen
d')
j = length(loks);
frek = loks;

for i=1:1:j
    frek(i) = f(loks(i));
end

% Displaying data
disp('The natural frequencies are: ')
Frequency = frek
disp('The natural vibration periods are: ')
NaturalPeriod = 1./frek
```

APPENDIX E – MATLAB CODE FOR GENERATION OF RESPONSE SPECTRA

In this appendix the Matlab-code for the generation of response spectra according to Eurocode 8 and for a specific strong ground motion is carried out. In this appendix it is exemplified by the generation of the Friuli response spectrum. The program uses a function to generate the response spectra by The Newmark Method, which is also enclosed.

```
%MASTER THESIS.
%NTNU 2012. Bjørn Th. Svendsen and Karin Harnæs Hoel.

%This program use Newmarks Method to make a response spectrum. It
%also compares to the EC8 Response Spectrum. The program plots for
%different ground motion components.

clear all
clc
close all

% Importing data for the provided earthquake record.
EQData_NS = importdata('Friuli_NScompCor_Matlab.txt');
EQData_EW = importdata('Friuli_EWcompCor_Matlab.txt');
EQData_Z = importdata('Friuli_VertCompCor_Matlab.txt');

% Defining variables
t_NS = EQData_NS(:,1);
P_NS = EQData_NS(:,2);
t_EW = EQData_EW(:,1);
P_EW = EQData_EW(:,2);
t_Z = EQData_Z(:,1);
P_Z = EQData_Z(:,2);
M = 1; gam = 0.5; beta = 0.25;
u0 = 0; udot0 = 0;
ksi = 0.05;
Tn = [0:0.01:5];

% Running Newmarks Method to generate response spectrum
for i = 1:length(Tn)
    C = (2*ksi)*((2*pi)/Tn(i));
    K = (2*pi/Tn(i))^2;
    u_NS = Newmark_Method_NS(t_NS,M,C,K,P_NS,gam,beta,u0,udot0);
    u_EW = Newmark_Method_EW(t_EW,M,C,K,P_EW,gam,beta,u0,udot0);
    u_Z = Newmark_Method_Z(t_Z,M,C,K,P_Z,gam,beta,u0,udot0);
    PGD_NS(i) = abs(max(u_NS));
    PGD_EW(i) = abs(max(u_EW));
    PGD_Z(i) = abs(max(u_Z));
    PGA_NS(i) = ((2*pi/Tn(i))^2)*PGD_NS(i);
    PGA_EW(i) = ((2*pi/Tn(i))^2)*PGD_EW(i);
    PGA_Z(i) = ((2*pi/Tn(i))^2)*PGD_Z(i);
end
```

```
% Creating the horizontal EC8 Response Spectrum
ag_40Hz = 0.55;
ag_R = 0.8*ag_40Hz;
vy_1 = 1.0;
ag = ag_R;
S = 1.6;
q = 1.0; % q can be set to a desired value here.
beta2 = 0.20;
Tb = 0.15; Tc = 0.45; Td = 1.50;
Sd = zeros(1,length(Tn));

% Calculating the horizontal elastic EC8 response spectrum
for j = 1:length(Tn)
    if (Tn(j) >= 0) & (Tn(j) <= Tb)
        Sd(j) = ag*S*((2/3) + ((Tn(j)/Tb)*((2.5/q)-(2/3))));
    elseif (Tn(j) >= Tb) & (Tn(j) <= Tc)
        Sd(j) = ag*S*(2.5/q);
    elseif (Tn(j) >= Tc) & (Tn(j) <= Td)
        Sd(j) = ag*S*(2.5/q)*(Tc/Tn(j));
        if (Sd(j) <= (beta2*ag))
            Sd(j) = beta2*ag;
        end
    else
        Sd(j) = ag*S*(2.5/q)*((Tc*Td)/(Tn(j)^2));
        if (Sd(j) <= (beta2*ag))
            Sd(j) = beta2*ag;
        end
    end
end

% Calculating the vertical elastic EC8 response spectrum
a_vg = 0.6*ag;
vy_1 = 1.0;
S_vg = 1.0;
q_vg = 1.0; % q can be set to a desired value here.
beta2_vg = 0.20;
Tb_v = 0.05; Tc_v = 0.20; Td_v = 1.20;
S_ve = zeros(1,length(Tn));

for j = 1:length(Tn)
    if (Tn(j) >= 0) & (Tn(j) <= Tb_v)
        S_ve(j) = a_vg*S_vg*((2/3) + ((Tn(j)/Tb_v)*((2.5/q_vg)-
(2/3))));
    elseif (Tn(j) >= Tb_v) & (Tn(j) <= Tc_v)
        S_ve(j) = a_vg*S_vg*(2.5/q_vg);
    elseif (Tn(j) >= Tc_v) & (Tn(j) <= Td_v)
        S_ve(j) = a_vg*S_vg*(2.5/q_vg)*(Tc_v/Tn(j));
        if (S_ve(j) <= (beta2_vg*a_vg))
            S_ve(j) = beta2_vg*a_vg;
        end
    else
        S_ve(j) = a_vg*S_vg*(2.5/q_vg)*((Tc_v*Td_v)/(Tn(j)^2));
        if (S_ve(j) <= (beta2_vg*a_vg))
            S_ve(j) = beta2_vg*a_vg;
        end
    end
end
```

```
% Plotting the HORIZONTAL RESPONSE SPECTRUM COMPARISON
figure(1)
%hold on
plot(Tn,PGA_NS,'b',Tn,PGA_EW,'r',Tn,Sd,'k')
%plot(Tn,Sd,'color',[0.765,0.765,0.765]);
title('HORIZONTAL RESPONSE SPECTRUM COMPARISON')
xlabel('NATURAL VIBRATION PERIOD, T_n [s]');
ylabel('ACCELERATION, A [m/s^2]');
xlim([0 4]);
ylim([0 8]);
legend('NS-component Friuli','EW-component Friuli','EC8 Response
Spectrum')
set(legend,'box','off')

% Plotting the VERTICAL RESPONSE SPECTRUM COMPARISON
figure(2)
%hold on
plot(Tn,PGA_Z,'g',Tn,S_ve,'k')
%plot(Tn,Sd,'color',[0.765,0.765,0.765]);
title('VERTICAL RESPONSE SPECTRUM COMPARISON')
xlabel('NATURAL VIBRATION PERIOD, T_n [s]');
ylabel('ACCELERATION, A [m/s^2]');
xlim([0 4]);
ylim([0 2.5]);
legend('Vertical-component Friuli','EC8 Response Spectrum')
set(legend,'box','off')

% Plotting the RESPONSE SPECTRUM FRIULI EARTHQUAKE
figure(3)
plot(Tn,PGA_NS,'b',Tn,PGA_EW,'r',Tn,PGA_Z,'g')
title('RESPONSE SPECTRUM FRIULI EARTHQUAKE')
xlabel('NATURAL VIBRATION PERIOD, T_n [s]');
ylabel('ACCELERATION, A [m/s^2]');
xlim([0 4]);
ylim([0 8]);
legend('NS-component','EW-component','Vertical-component')
set(legend,'box','off')

% Plotting the EC8 HORIZONTAL RESPONSE SPECTRUM
figure(4)
plot(Tn,Sd)
title('HORIZONTAL ELASTIC RESPONSE SPECTRUM EC8')
xlabel('NATURAL VIBRATION PERIOD, T_n [s]');
xlim([0 4]);
ylim([0 2]);
ylabel('ACCELERATION, A [m/s^2]');

% Plotting the EC8 VERTICAL RESPONSE SPECTRUM
figure(5)
plot(Tn,S_ve)
title('VERTICAL ELASTIC RESPONSE SPECTRUM EC8')
xlabel('NATURAL VIBRATION PERIOD, T_n [s]');
ylabel('ACCELERATION, A [m/s^2]');
xlim([0 4]);
ylim([0 2]);
```

The function that implements the Newmark Method is shown in the following Matlab-code.

```
function u_NS = Newmark_Method_NS(t_NS,M,C,K,P_NS,gam,beta,u0,udot0)

%Newmarks Direct Integration Method
%-------------------------------------------------------------------
-------
% OUTPUT
% u = Displacemente Response   [n,2]
% n = number of time steps

% INPUT
% t =       Time vector         [1,n]
% M =       Mass matrix         [1,1]
% C =       Damping matrix      [1,1]
% K =       Stiffness matrix    [1,1]
% P =       load vs. time       [2,n] Denne skal være kun load som
Acc.
% gam =     Gamma (constant)
% beta =    Beta  (constant)
% u0 =      Initial displacements
% udot0 =   Initial velocity

%-------------------------------------------------------------------
-------
% beta = 0,     gamma = 1/2 -> explicit central difference method
% beta = 1/4,   gamma = 1/2 -> undamped trapezoidal rule (implicit)

% 1.0 INITIAL CONDITIONS
u_NS = u0;
udot = udot0;
u2dot = (P_NS(1) - (C*udot0) - (K*u0))/M;
dt = t_NS(2) - t_NS(1);
k_hat = K + (gam*C)/(beta*dt) + M/(beta*(dt^2));
a = M/(beta*dt) + (gam*C)/beta;
b = M/(2*beta) + (dt*C)*((gam/(2*beta))-1);

% 2.0 CALCULATIONS FOR EACH TIME STEP, i
for i = 1:(length(t_NS)-1)
    dP = (P_NS(i+1)-P_NS(i)) + (a*udot) + (b*u2dot);
    du_i = dP/k_hat;
    dudot_i = ((gam*du_i)/(beta*dt)) - ((gam*udot)/beta) +
((dt*u2dot)*(1-(gam/(2*beta))));
    du2dot_i = (du_i/(beta*(dt^2))) - (udot/(beta*dt)) -
(u2dot/(2*beta));
    u_NS(i+1) = du_i + u_NS(i);
    udot = dudot_i + udot;
    u2dot = du2dot_i + u2dot;
end
```

APPENDIX F – MATLAB CODE FOR ROTATION OF GROUND MOTION

```
%MASTER THESIS.
%NTNU 2012. Bjørn Th. Svendsen and Karin Harnæs Hoel.

%This program imports the ground motion acceleration data for the
%three component records of the given earthquake, and rotates the
%two horizontal components. The PGA-ratio is plotted with respect to
%the angle of rotation.

clc
clear all
close all

% Importing data and defining variables
EQData_NS = importdata('NS-component_earthquake.txt');
EQData_EW = importdata('EW-component_earthquake.txt');
EQData_Z = importdata('Vertical-component_earthquake.txt');
T_NS = EQData_NS(:,1);
A_NS = EQData_NS(:,2);
T_EW = EQData_EW(:,1);
A_EW = EQData_EW(:,2);
T_Z = EQData_Z(:,1);
A_Z = EQData_Z(:,2);
theta =0:0.01:2*pi;

% Rotating the time-series
for i = 1:length(theta)
transform = [cos(theta(i)) sin(theta(i)); -sin(theta(i))
cos(theta(i))];
Atrans = [A_NS,A_EW]*transform;
PGA_1(i) = abs(max(Atrans(:,1)));
PGA_2(i) = abs(max(Atrans(:,2)));
a(i) = PGA_1(i)/PGA_2(i);
end

% Plotting the result
figure(1)
plot(theta,a)
xlabel('Angle \theta')
ylabel('PGA ratio')

[pks,loks] = findpeaks(1./a,'npeaks',1);

% Displaying data
disp('The angle of rotatino is: ')
Angle = theta(loks)*(180/pi)
disp('The PGA-ratio is: ')
Ratio = min(a)

% Writing the new time-series
trans = [cos(theta(loks)) sin(theta(loks)); -sin(theta(loks))
cos(theta(loks))];
```

```
A_new =[A_NS,A_EW]*trans;
disp('PGA of the rotated NS-component: ')
PGA_1 = abs(max(A_new(:,1)))
disp('PGA of the rotated EW-component: ')
PGA_2 = abs(max(A_new(:,2)))
```

APPENDIX G – MATLAB CODE FOR CORRELATION MATRIX

```
%MASTER THESIS.
%NTNU 2012. Bjørn Th. Svendsen and Karin Harnæs Hoel.

%This program generates a correlation matrix between ground motion
%data components and plot the result.

clc
clear all
close all

% Import data
EQData_NS = importdata('Friuli_NS.txt');
EQData_EW = importdata('Friuli_EW.txt');
T_NS = EQData_NS(:,1);
A_NS = EQData_NS(:,2);
T_EW = EQData_EW(:,1);
A_EW = EQData_EW(:,2);

Covar = cov(A_NS,A_EW);
[phi,om]= eig(Covar);
Atrans =[A_NS,A_EW]*phi;

% Plotting the result
hold on
plot(T_NS,Atrans(:,2))
plot(T_NS,A_EW,'r')

CO = cov(Atrans(:,1),Atrans(:,2))
```

APPENDIX H – CALCULATIONS OF THE P-Δ EFFECTS

In this appendix the calculations of the P-Δ effects by the interstory drift sensitivity coefficient, θ_{EC8}, are performed for the Friuli earthquake as a realistic scenario.

The total mass of the building is 39 200 000 kg, the floor mass is assumed 1 059 459 kg for simplicity. This is a conservative approach.

The calculations of the interstory drift sensitivity coefficient for the x-direction is shown in table H-1. The base shear for this direction is 3 455 000 N.

Table H-1: Calculations of the interstory drift sensitivity coefficient, θ_{EC8}, for the x-direction.

Floor	Height	Interstory height, h	SFD-ratio	SFD [N]	P [N]	P_{tot} [N]	Displacement d [mm]	Interstory drift, d_r [mm]	Sensitivity coefficient, θ
37	108 300		0.00486	16 791	10 393 297	10 393 297	41.2		
36	105 300	3 000	0.03403	117 574	10 393 297	20 786 595	40.6	0.632	0.037
35	102 500	2 800	0.04840	167 222	10 393 297	31 179 892	39.5	1.091	0.073
34	99 650	2 850	0.05827	201 323	10 393 297	41 573 189	37.5	1.958	0.142
33	96 500	3 150	0.08079	279 129	10 393 297	51 966 486	34.6	2.931	0.173
32	93 750	2 750	0.03867	133 605	10 393 297	62 359 784	32.0	2.604	0.442
31	91 000	2 750	0.03542	122 376	10 393 297	72 753 081	29.4	2.598	0.562
30	88 250	2 750	0.03438	118 783	10 393 297	83 146 378	26.8	2.569	0.654
29	85 500	2 750	0.03334	115 190	10 393 297	93 539 676	24.3	2.505	0.740
28	82 750	2 750	0.03231	111 631	10 393 297	103 932 973	21.9	2.413	0.817
27	80 000	2 750	0.03127	108 038	10 393 297	114 326 270	19.6	2.297	0.884
26	77 250	2 750	0.03169	109 489	10 393 297	124 719 568	17.4	2.159	0.894
25	74 500	2 750	0.03201	110 595	10 393 297	135 112 865	15.4	2.016	0.896
24	71 750	2 750	0.03088	106 690	10 393 297	145 506 162	13.5	1.866	0.925
23	69 000	2 750	0.02974	102 752	10 393 297	155 899 459	11.8	1.716	0.947
22	66 250	2 750	0.02860	98 813	10 393 297	166 292 757	10.3	1.568	0.960
21	63 500	2 750	0.02747	94 909	10 393 297	176 686 054	8.8	1.423	0.964
20	60 750	2 750	0.02633	90 970	10 393 297	187 079 351	7.6	1.280	0.957
19	58 000	2 750	0.02519	87 031	10 393 297	197 472 649	6.4	1.139	0.940
18	55 250	2 750	0.02383	82 333	10 393 297	207 865 946	5.4	0.996	0.915
17	52 500	2 750	0.02325	80 329	10 393 297	218 259 243	4.6	0.821	0.811
16	49 750	2 750	0.02229	77 012	10 393 297	228 652 541	3.9	0.722	0.779
15	47 000	2 750	0.02113	73 004	10 393 297	239 045 838	3.3	0.630	0.750
14	44 250	2 750	0.01996	68 962	10 393 297	249 439 135	2.7	0.545	0.716
13	41 500	2 750	0.01880	64 954	10 393 297	259 832 432	2.2	0.468	0.680
12	38 750	2 750	0.01764	60 946	10 393 297	270 225 730	1.8	0.400	0.645
11	36 000	2 750	0.01647	56 904	10 393 297	280 619 027	1.5	0.343	0.615
10	33 250	2 750	0.01531	52 896	10 393 297	291 012 324	1.2	0.297	0.593
9	30 500	2 750	0.01415	48 888	10 393 297	301 405 622	0.9	0.259	0.581
8	27 750	2 750	0.01298	44 846	10 393 297	311 798 919	0.7	0.229	0.579
7	25 000	2 750	0.01182	40 838	10 393 297	322 192 216	0.5	0.203	0.582
6	22 250	2 750	0.01066	36 830	10 393 297	332 585 514	0.3	0.178	0.584
5	19 500	2 750	0.00949	32 788	10 393 297	342 978 811	0.2	0.150	0.570
4	16 750	2 750	0.00833	28 780	10 393 297	353 372 108	0.1	0.113	0.506
3	12 750	4 000	0.03752	129 632	10 393 297	363 765 405	0.0	0.067	0.047
2	8 580	4 170	0.02205	76 183	10 393 297	374 158 703	0.0	0.000	0.000
1	3 500	5 080	0.01960	67 718	10 393 297	384 552 000	0.0	0.000	0.000
0	-200	3 700	0.01107	38 247	10 393 297	394 945 297	0.0	0.000	0.000
	Control by sum:		**1.00000**	**3455000**			**Maximum sensitivity of all floors =**		**0.964**

The calculations of the interstory drift sensitivity coefficient for the y-direction is shown in table H-2. The base shear for this direction is 11 361 000 N.

Table H-2: Calculations of the interstory drift sensitivity coefficient, θ, for the y-direction.

Floor	Height	Interstory height, h	SFD-ratio	SFD [N]	P [N]	P_{tot} [N]	Displacement d [mm]	Interstory drift, d_r [mm]	Sensitivity coefficient, θ
37	108 300		0.00486	55 214	10 393 297	10 393 297	41.2		
36	105 300	3 000	0.03403	386 615	10 393 297	20 786 595	40.6	0.632	0.011
35	102 500	2 800	0.04840	549 872	10 393 297	31 179 892	39.5	1.091	0.022
34	99 650	2 850	0.05827	662 005	10 393 297	41 573 189	37.5	1.958	0.043
33	96 500	3 150	0.08079	917 855	10 393 297	51 966 486	34.6	2.931	0.053
32	93 750	2 750	0.03867	439 330	10 393 297	62 359 784	32.0	2.604	0.134
31	91 000	2 750	0.03542	402 407	10 393 297	72 753 081	29.4	2.598	0.171
30	88 250	2 750	0.03438	390 591	10 393 297	83 146 378	26.8	2.569	0.199
29	85 500	2 750	0.03334	378 776	10 393 297	93 539 676	24.3	2.505	0.225
28	82 750	2 750	0.03231	367 074	10 393 297	103 932 973	21.9	2.413	0.248
27	80 000	2 750	0.03127	355 258	10 393 297	114 326 270	19.6	2.297	0.269
26	77 250	2 750	0.03169	360 030	10 393 297	124 719 568	17.4	2.159	0.272
25	74 500	2 750	0.03201	363 666	10 393 297	135 112 865	15.4	2.016	0.272
24	71 750	2 750	0.03088	350 828	10 393 297	145 506 162	13.5	1.866	0.281
23	69 000	2 750	0.02974	337 876	10 393 297	155 899 459	11.8	1.716	0.288
22	66 250	2 750	0.02860	324 925	10 393 297	166 292 757	10.3	1.568	0.292
21	63 500	2 750	0.02747	312 087	10 393 297	176 686 054	8.8	1.423	0.293
20	60 750	2 750	0.02633	299 135	10 393 297	187 079 351	7.6	1.280	0.291
19	58 000	2 750	0.02519	286 184	10 393 297	197 472 649	6.4	1.139	0.286
18	55 250	2 750	0.02383	270 733	10 393 297	207 865 946	5.4	0.996	0.278
17	52 500	2 750	0.02325	264 143	10 393 297	218 259 243	4.6	0.821	0.247
16	49 750	2 750	0.02229	253 237	10 393 297	228 652 541	3.9	0.722	0.237
15	47 000	2 750	0.02113	240 058	10 393 297	239 045 838	3.3	0.630	0.228
14	44 250	2 750	0.01996	226 766	10 393 297	249 439 135	2.7	0.545	0.218
13	41 500	2 750	0.01880	213 587	10 393 297	259 832 432	2.2	0.468	0.207
12	38 750	2 750	0.01764	200 408	10 393 297	270 225 730	1.8	0.400	0.196
11	36 000	2 750	0.01647	187 116	10 393 297	280 619 027	1.5	0.343	0.187
10	33 250	2 750	0.01531	173 937	10 393 297	291 012 324	1.2	0.297	0.180
9	30 500	2 750	0.01415	160 758	10 393 297	301 405 622	0.9	0.259	0.177
8	27 750	2 750	0.01298	147 466	10 393 297	311 798 919	0.7	0.229	0.176
7	25 000	2 750	0.01182	134 287	10 393 297	322 192 216	0.5	0.203	0.177
6	22 250	2 750	0.01066	121 108	10 393 297	332 585 514	0.3	0.178	0.178
5	19 500	2 750	0.00949	107 816	10 393 297	342 978 811	0.2	0.150	0.173
4	16 750	2 750	0.00833	94 637	10 393 297	353 372 108	0.1	0.113	0.154
3	12 750	4 000	0.03752	426 265	10 393 297	363 765 405	0.0	0.067	0.014
2	8 580	4 170	0.02205	250 510	10 393 297	374 158 703	0.0	0.000	0.000
1	3 500	5 080	0.01960	222 676	10 393 297	384 552 000	0.0	0.000	0.000
0	-200	3 700	0.01107	125 766	10 393 297	394 945 297	0.0	0.000	0.000
	Control by sum:		**1.00000**	**11361000**			**Maximum sensitivity of all floors =**		**0.293**

APPENDIX I – SOIL SPRING CALCULATIONS

In this appendix the calculations of the stiffness for the soil springs of the new foundation representation is performed according to the theory presented in Chapter 2.4. This calculation is performed in Matlab. The various coefficients used are described in the following Matlab-code presented.

```
%MASTER THESIS.
%NTNU 2012. Bjørn Th. Svendsen and Karin Harnæs Hoel.

%This program calculates the horizontal and vertical spring
%stiffness according to the theory presented in Chapter 2.4 in the
%master thesis document.

clear all
clc
close all

% Defining variables
T = 3.485;      % Natural vibration period.
rho = 1700;     % Soil density.
V = 180;        % Shear wave velocity.
L = 105/2;      % Foundation length.
B = 53/2;       % Foundation breadth.
D = 3.7;        % Depth of foundation embedment.
d = 0.5;        % Assumed foundation thickness.
v = 0.5;        % Poisson's ratio.
nz = 155;       % Amount of vertical soil springs.
nv = 216;       % Amount of horizontal soil springs.
w = (2*pi)/T;   % Natural circular frequency.
a0 = w*B/V;     % Dimensionless parameter.
G = rho*(V^2);  % Shear modulus of soil.

% Static stiffness coefficients.
K_z = (3.3*G*L)/(1-v);
K_vx = (4.9*(1-1.4*v)*G*L)/((2-v)*(0.75-v));
K_vy = (6.8*G*L)/(2-v);
k_z = (1+0.16*(D/L))*(1+0.42*(d/L)^(2/3));
k_horizontal = (1+0.2*sqrt((D/L)))*(1+(d/L)^(0.8));

% Total spring stiffness
K_zembedded = K_z*k_z;
K_yembedded = K_vy*k_horizontal;
K_xembedded = K_vx*k_horizontal;

% Dynamic stiffness coefficient.
dyn_s = 1-0.09*(D/B)^(3/4)*(a0^2);

% Spring stiffness.
disp('The dynamic stiffnes for the different directions are: ')
kz = (K_zembedded/nz)*dyn_s
kx = (K_xembedded/nv)*dyn_s
ky = (K_yembedded/nv)*dyn_s
```

APPENDIX J – SIMULATIONS

In the following appendix the simulations of the Friuli earthquake and the Imperial Valley earthquake are presented. Altogether, 5 simulations of each earthquake are performed.

The Friuli earthquake – Spectral density comparison of all three components obtained from the simulations

Simulation 1

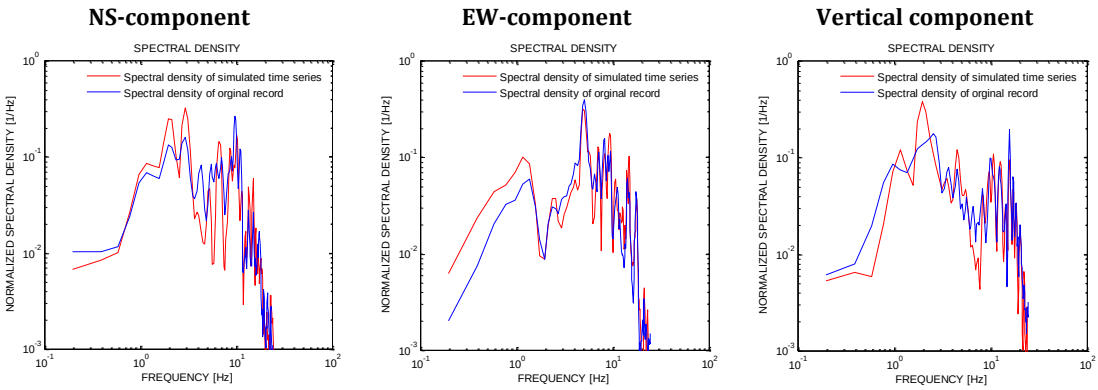

Figure J-1: Spectral density comparison of all three components, simulation 1 Friuli earthquake.

Simulation 2

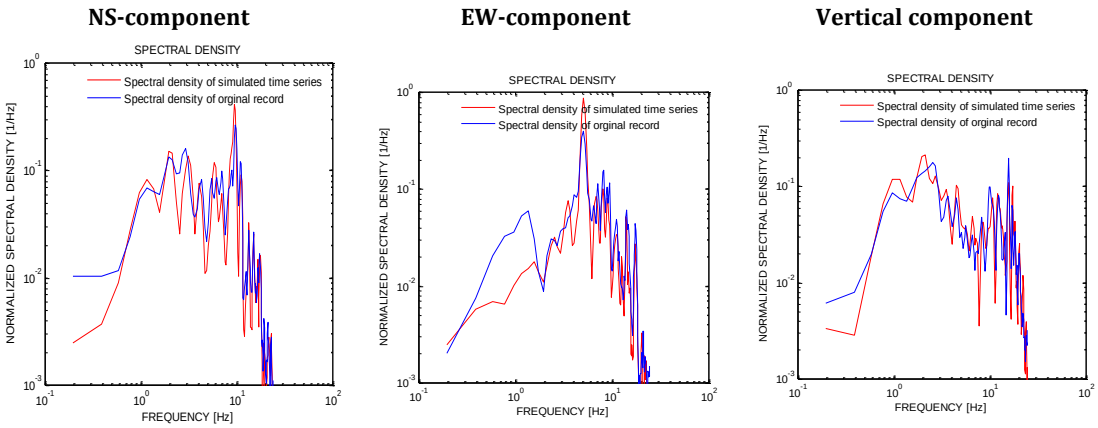

Figure J-2: Spectral density comparison of all three components, simulation 2 Friuli earthquake.

Simulation 3

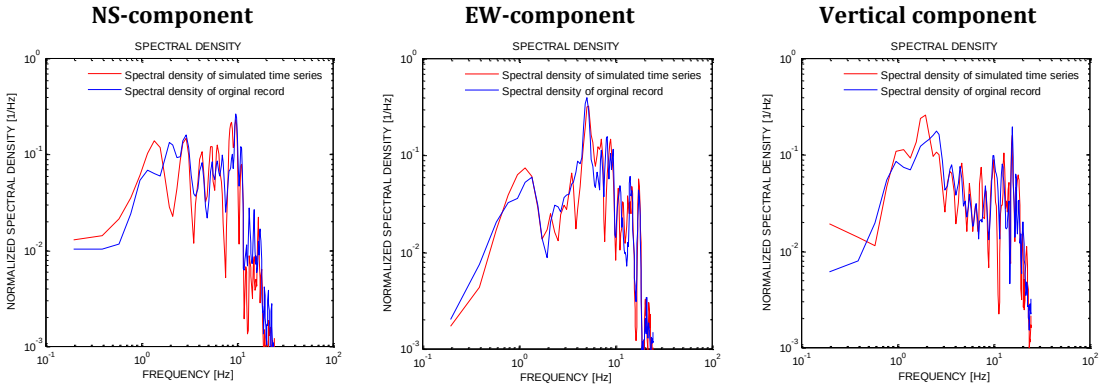

Figure J-3: Spectral density comparison of all three components, simulation 3 Friuli earthquake.

Simulation 4

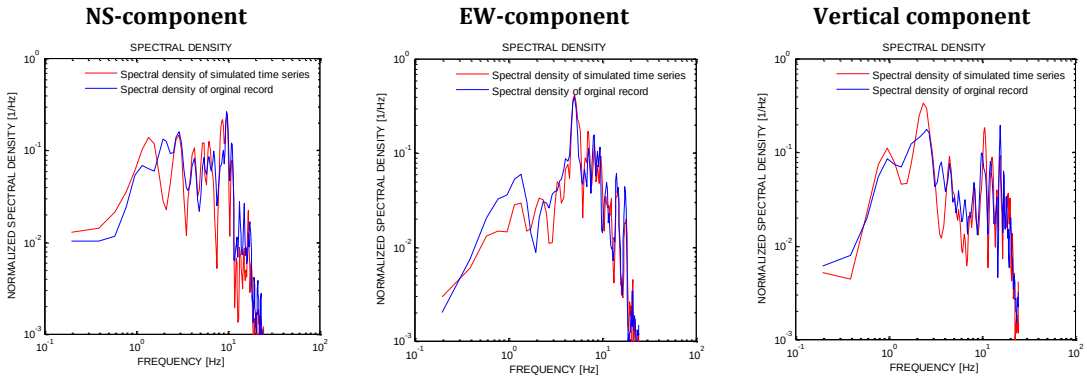

Figure J-4: Spectral density comparison of all three components, simulation 4 Friuli earthquake.

Simulation 5

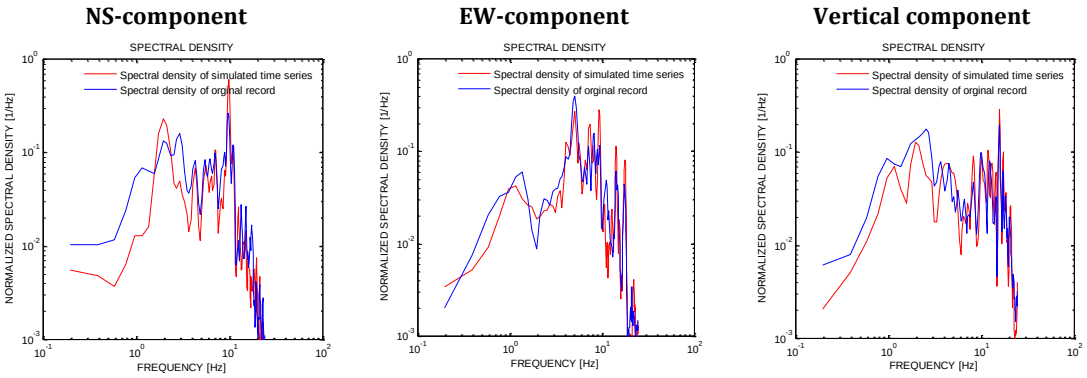

Figure J-5: Spectral density comparison of all three components, simulation 5 Friuli earthquake.

Simulation 1 – The Friuli earthquake

Friuli Earthquake, NS-component. PGA from simulation: 1.180 m/s²

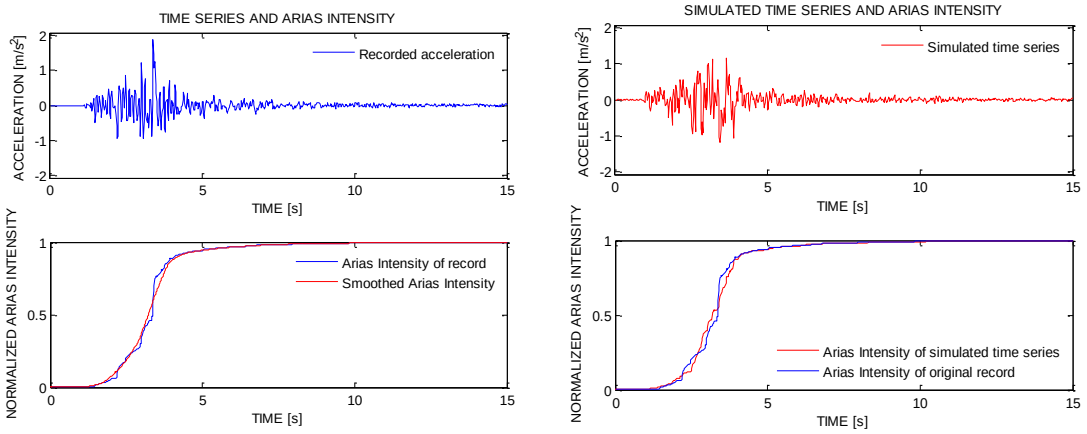

Friuli Earthquake, EW-component. PGA from simulation: 0.843 m/s2

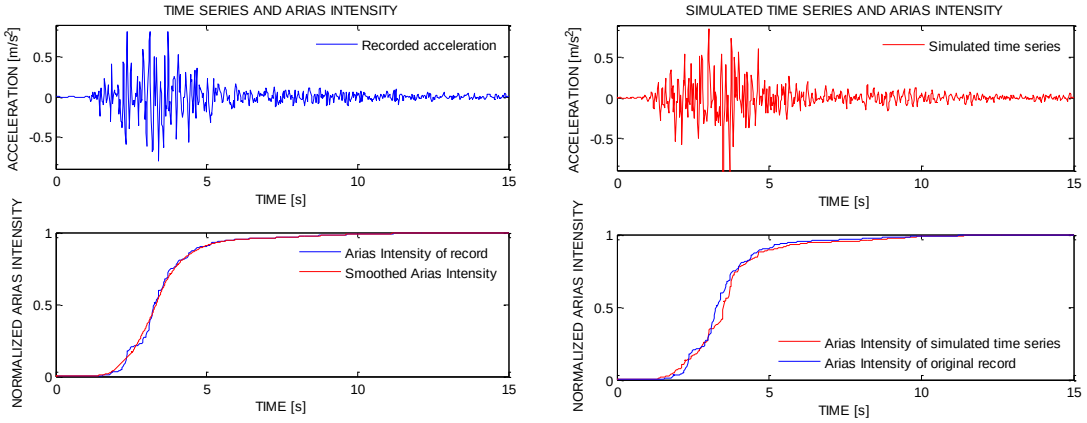

Friuli Earthquake, Vertical component. PGA from simulation: 0.537 m/s²

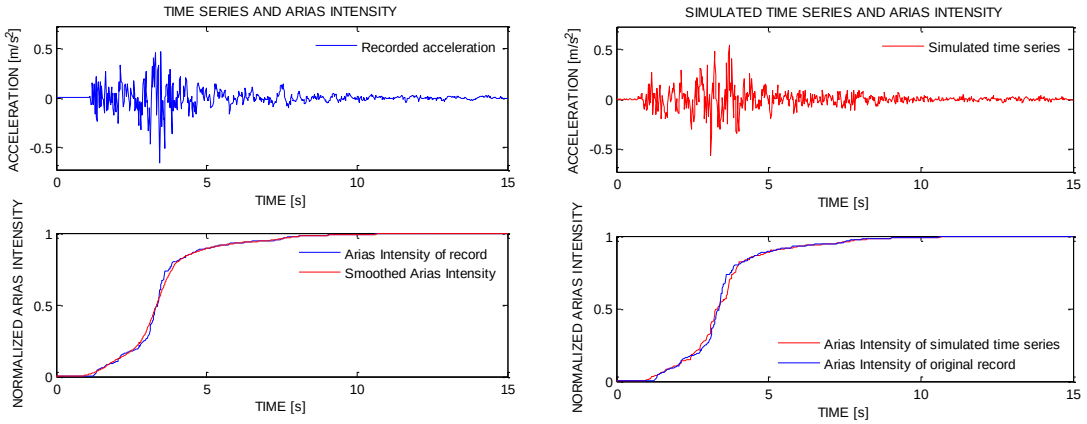

Figure J-6: Results from simulation of all three components, simulation 1 Friuli earthquake.

Simulation 2 – The Friuli earthquake

Friuli Earthquake, NS-component. PGA from simulation: 1.206 m/s²

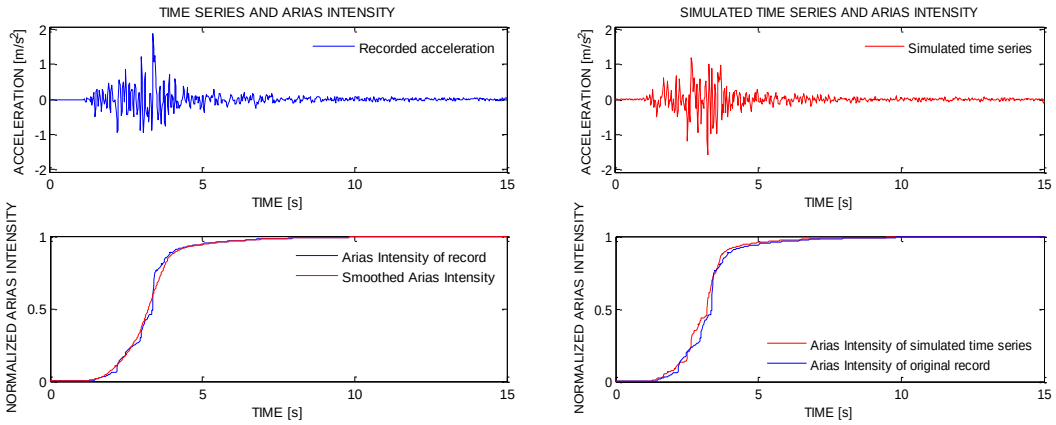

Friuli Earthquake, EW-component. PGA from simulation: 1.060 m/s2

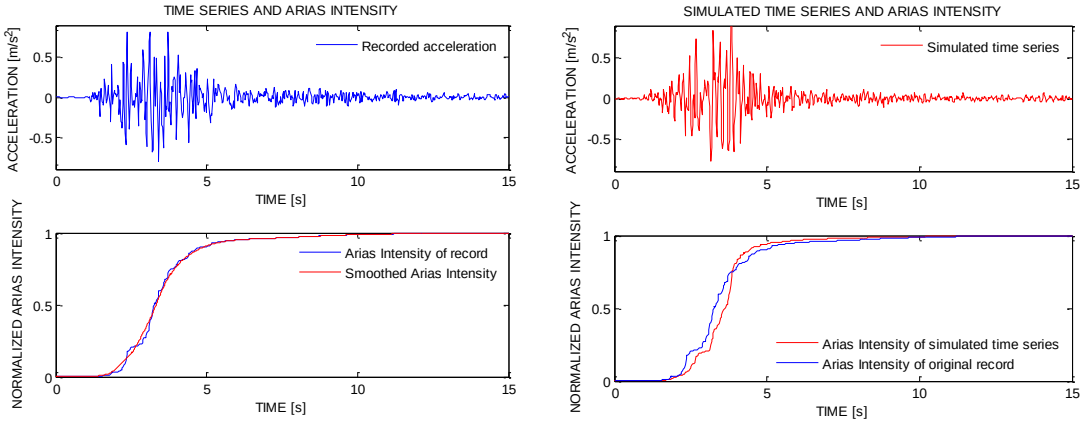

Friuli Earthquake, Vertical component. PGA from simulation: 0.573 m/s²

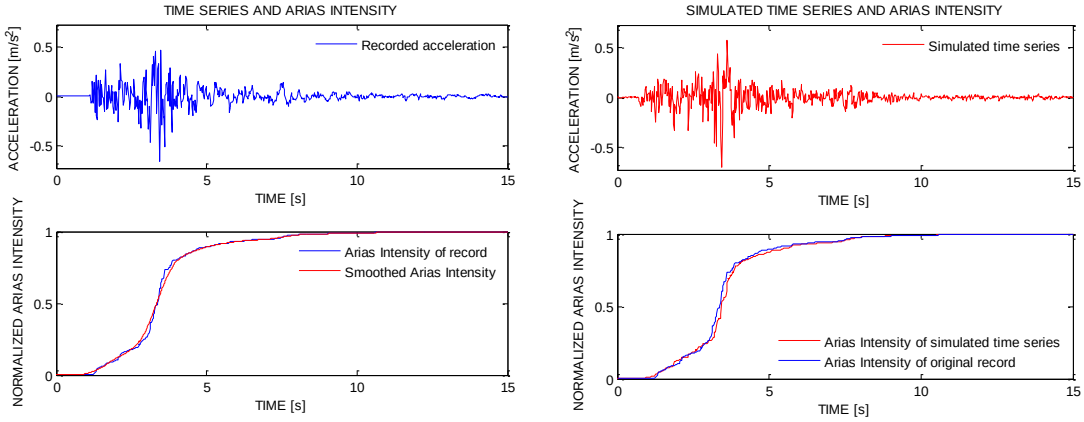

Figure J-7: Results from simulation of all three components, simulation 2 Friuli earthquake.

Simulation 3 – The Friuli earthquake

Friuli Earthquake, NS-component. PGA from simulation: 1.122 m/s²

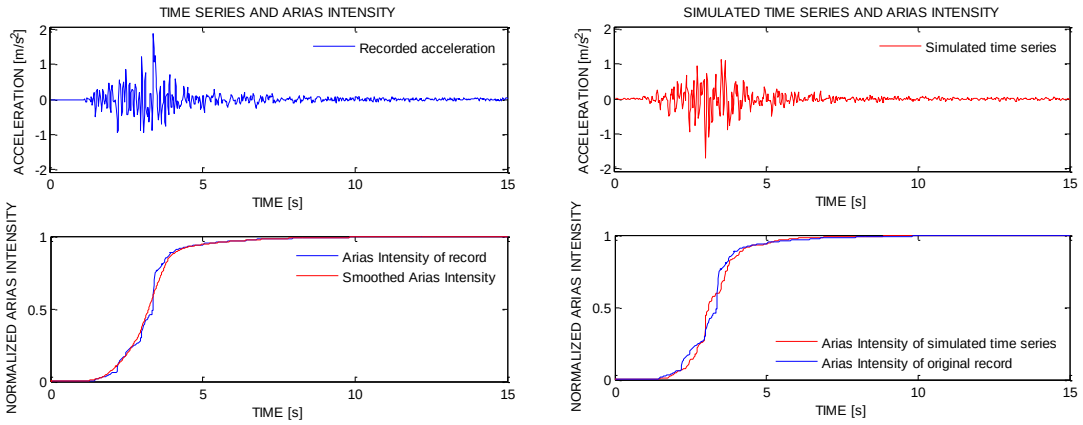

Friuli Earthquake, EW-component. PGA from simulation: 0.803 m/s2

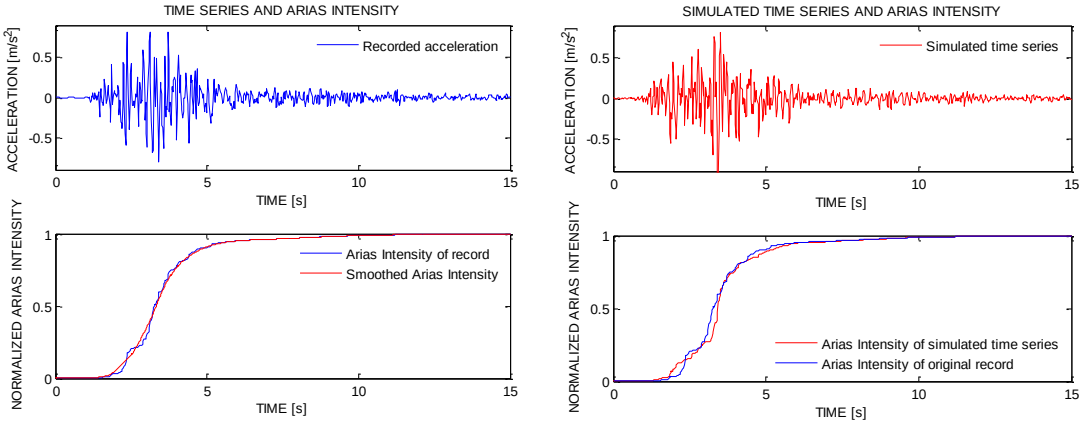

Friuli Earthquake, Vertical component. PGA from simulation: 0.632 m/s²

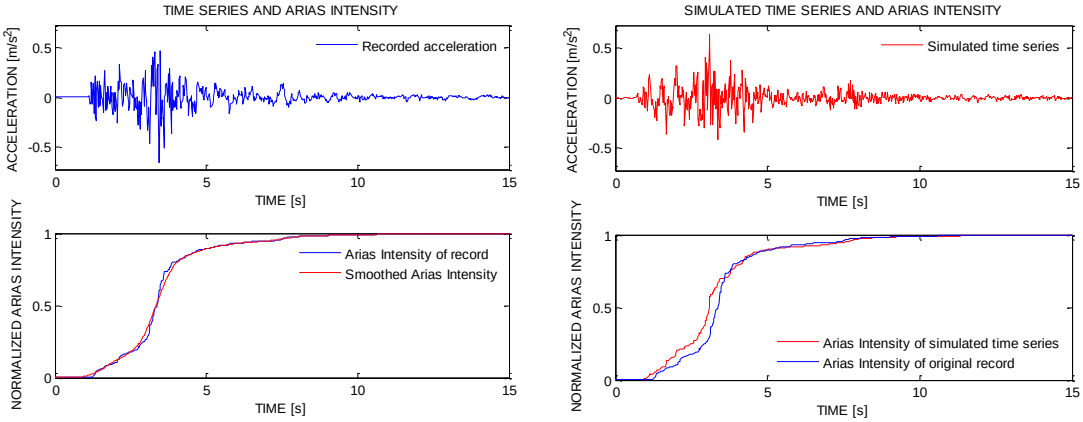

Figure J-8: Results from simulation of all three components, simulation 3 Friuli earthquake.

Simulation 4 – The Friuli earthquake

Friuli Earthquake, NS-component. PGA from simulation: 1.222 m/s²

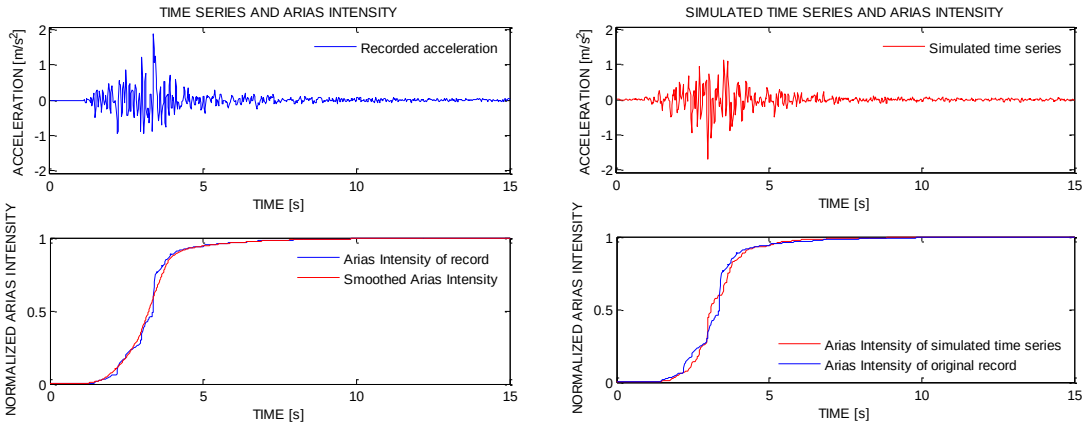

Friuli Earthquake, EW-component. PGA from simulation: 0.709 m/s2

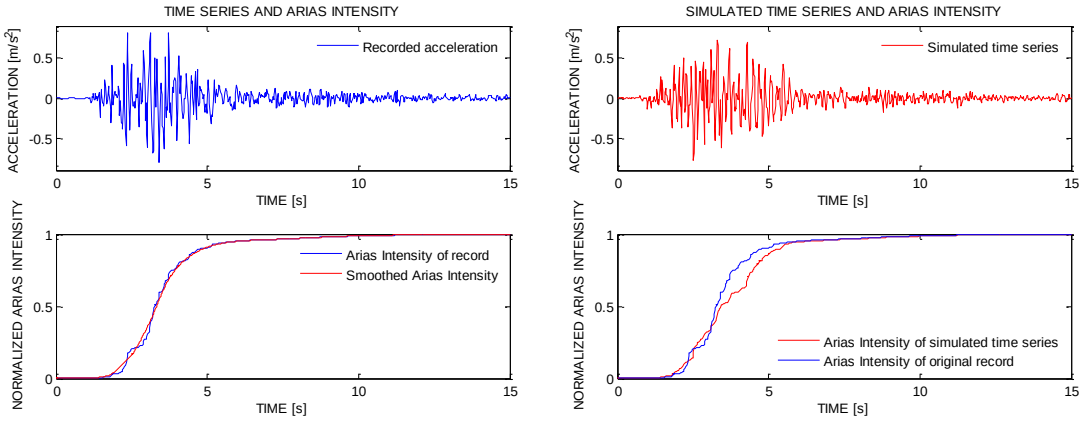

Friuli Earthquake, Vertical component. PGA from simulation: 0.725 m/s²

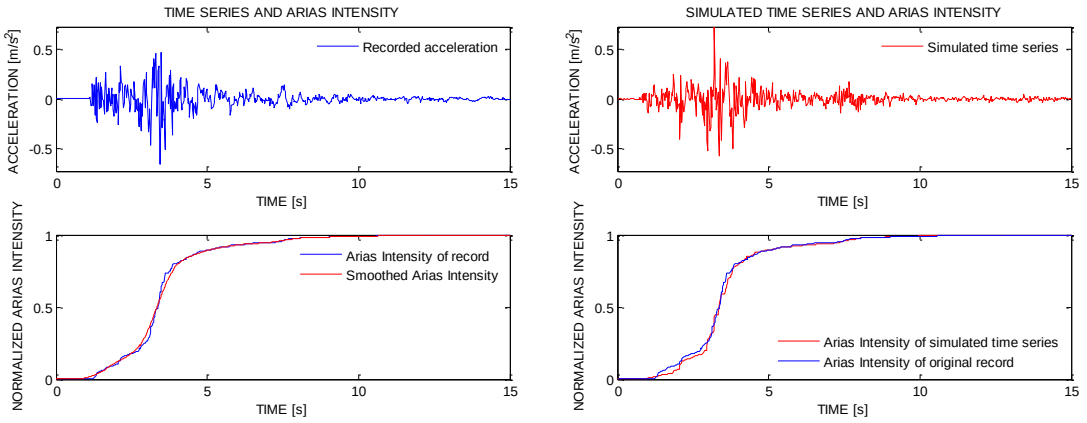

Figure J-9: Results from simulation of all three components, simulation 4 Friuli earthquake.

Simulation 5 – The Friuli earthquake

Friuli Earthquake, NS-component. PGA from simulation: 1.689 m/s²

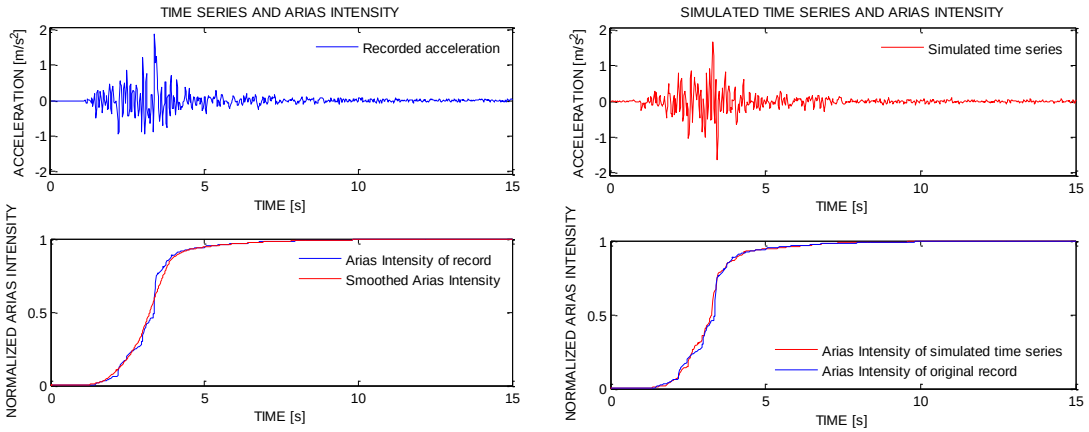

Friuli Earthquake, EW-component. PGA from simulation: 0.892 m/s2

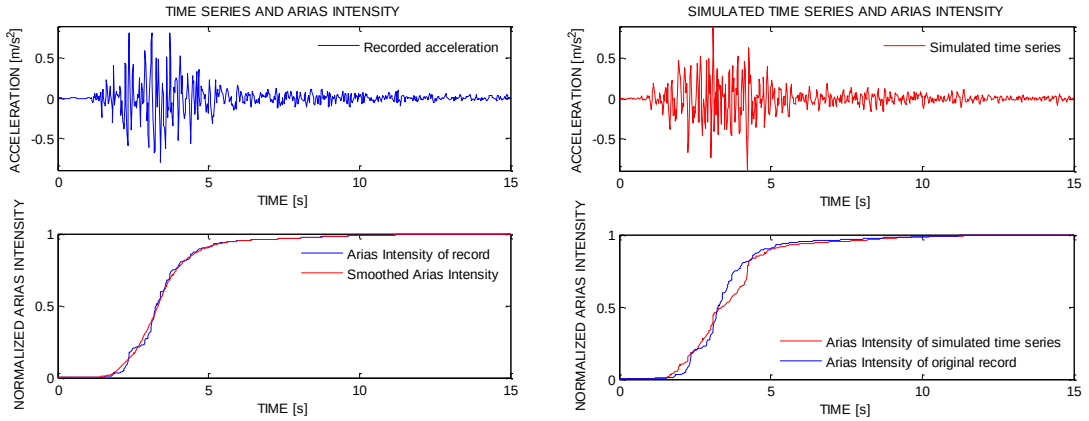

Friuli Earthquake, Vertical component. PGA from simulation: 0.478 m/s²

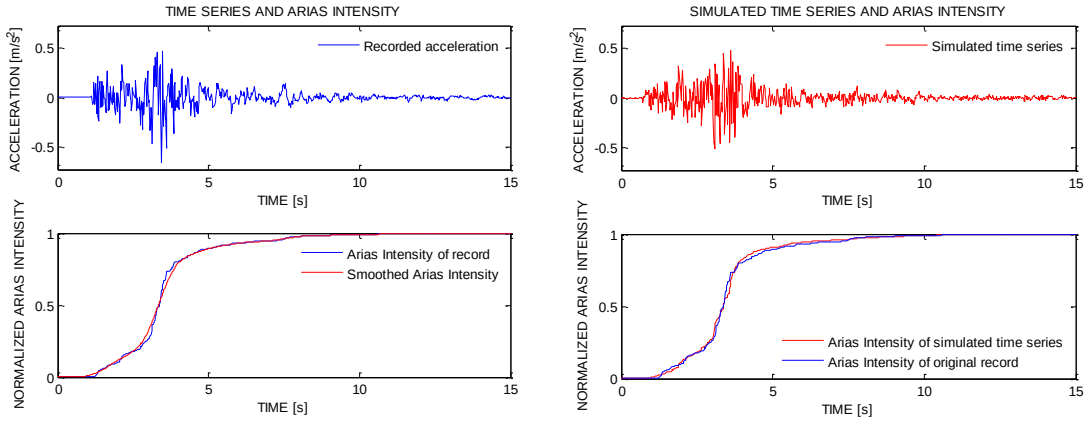

Figure J-10: Results from simulation of all three components, simulation 5 Friuli earthquake.

The Imperial Valley earthquake – Spectral density comparison of all three components obtained from the simulations

Simulation 1

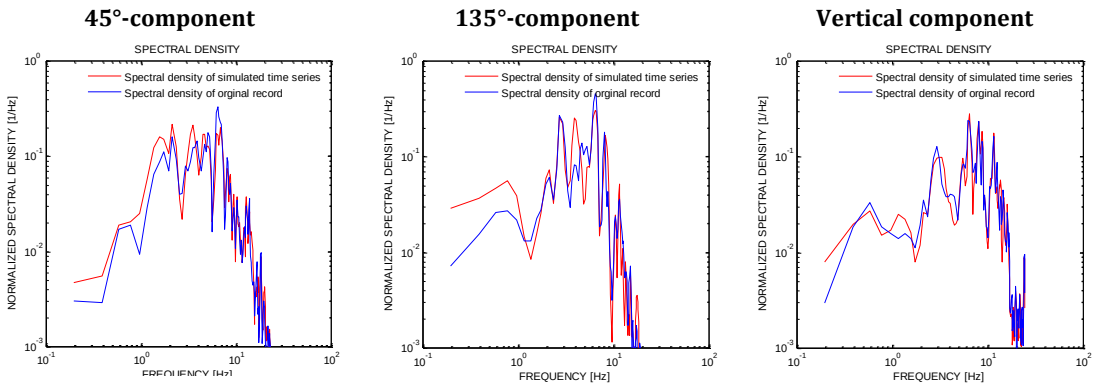

Figure J-11: Spectral density comparison of all three components, simulation 1 Imperial Valley earthquake.

Simulation 2

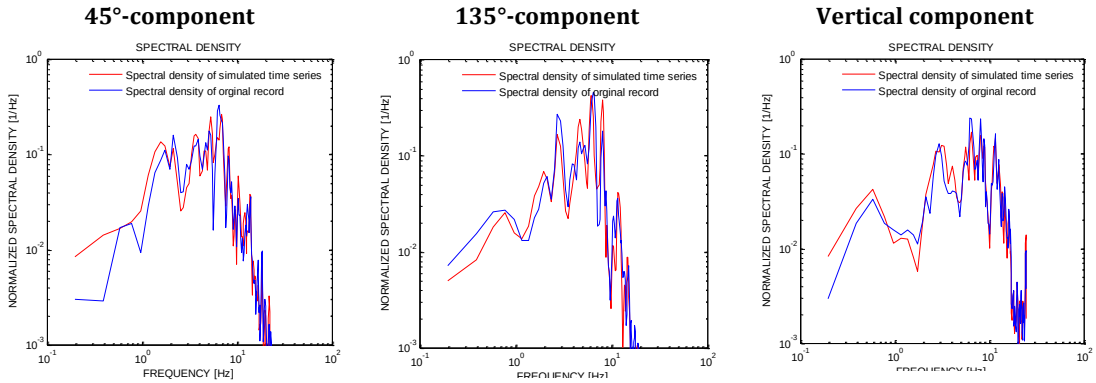

Figure J-12: Spectral density comparison of all three components, simulation 2 Imperial Valley earthquake.

Simulation 3

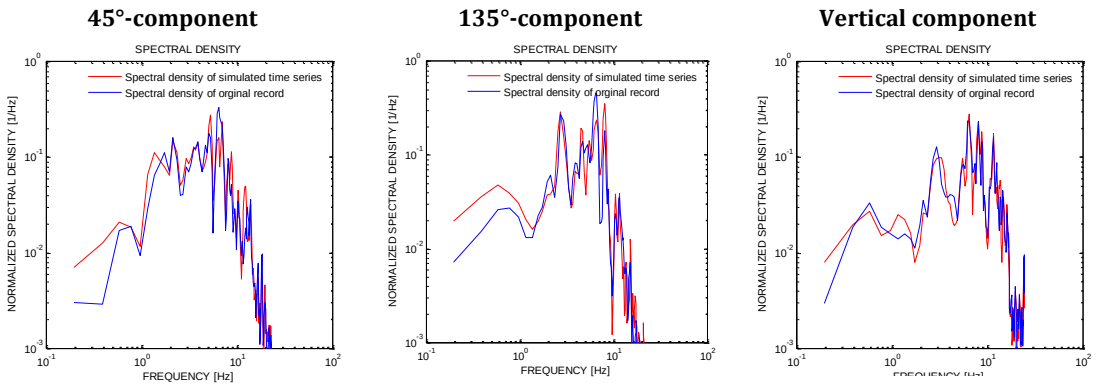

Figure J-13: Spectral density comparison of all three components, simulation 3 Imperial Valley earthquake.

Simulation 4

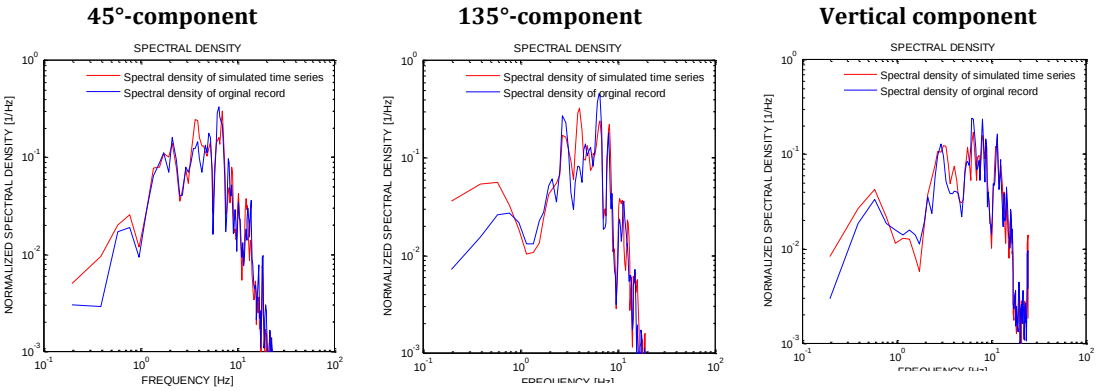

Figure J-14: Spectral density comparison of all three components, simulation 4 Imperial Valley earthquake.

Simulation 5

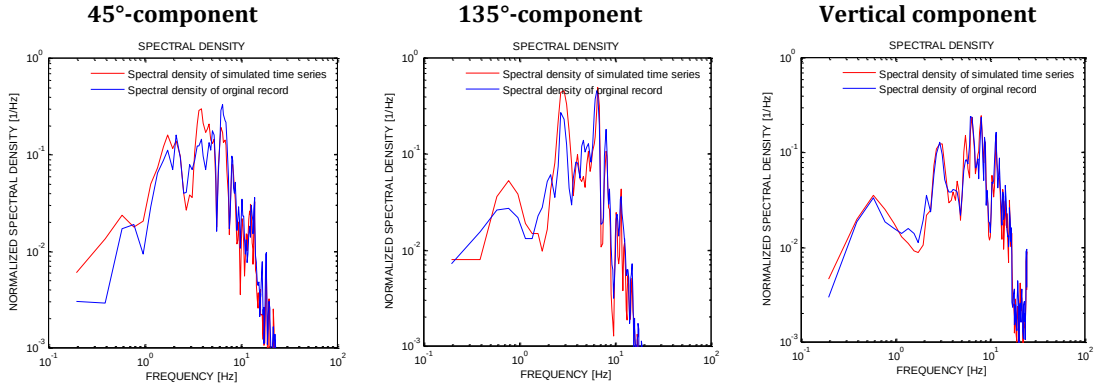

Figure J-15: Spectral density comparison of all three components, simulation 5 Imperial Valley earthquake.

Simulation 1 – The Imperial Valley earthquake

Imperial Valley Earthquake, 45°-component. PGA from simulation: 0.733 m/s²

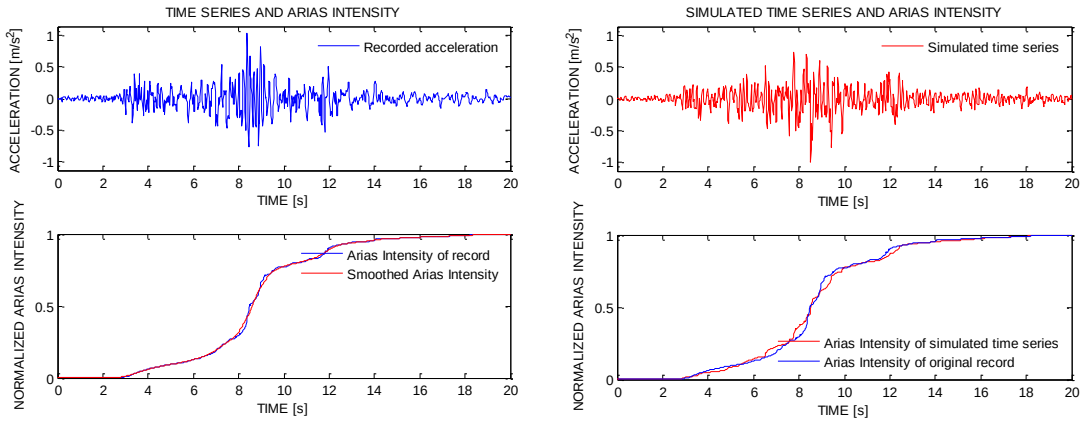

Imperial Valley Earthquake, 135°-component. PGA from simulation: 1.539 m/s2

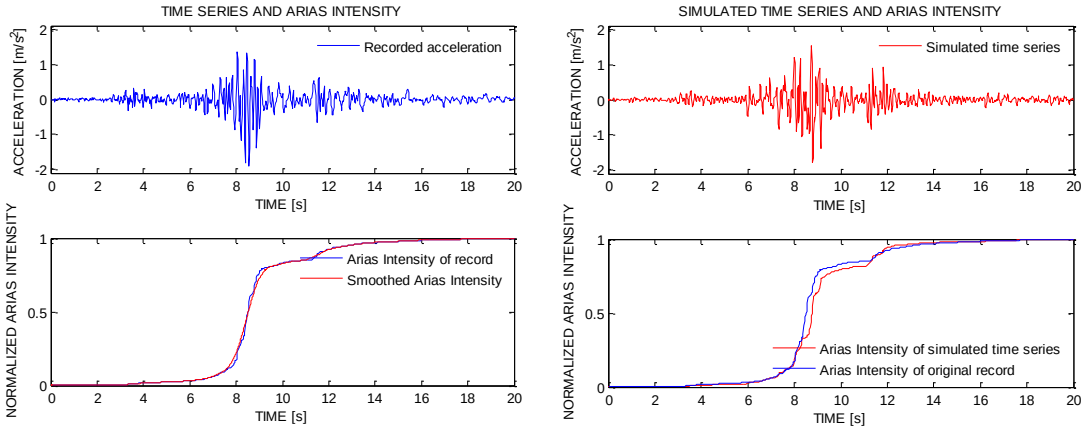

Imperial Valley Earthquake, vertical component. PGA from simulation: 0.529 m/s²

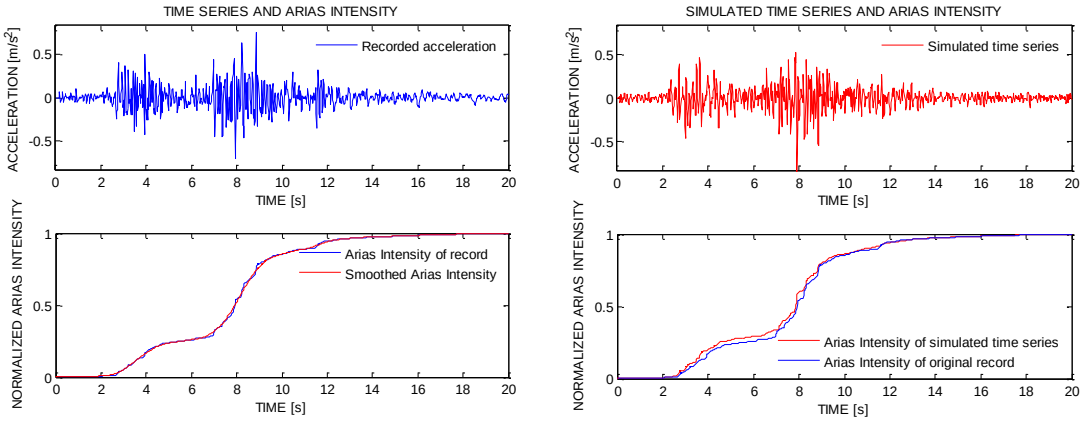

Figure J-16: Results from simulation of all three components, simulation 1 Imperial Valley earthquake.

Simulation 2 – The Imperial Valley earthquake

Imperial Valley Earthquake, 45°-component. PGA from simulation: 0.819 m/s²

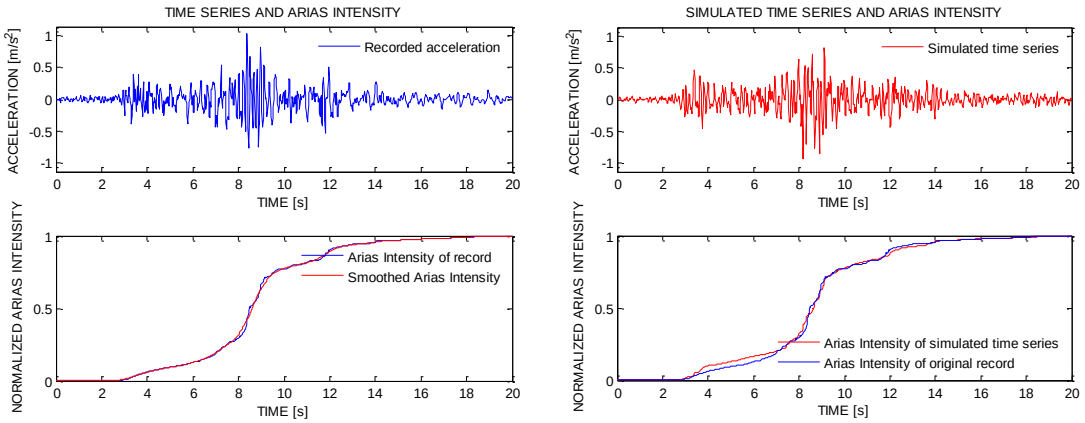

Imperial Valley Earthquake, 135°-component. PGA from simulation: 1.608 m/s2

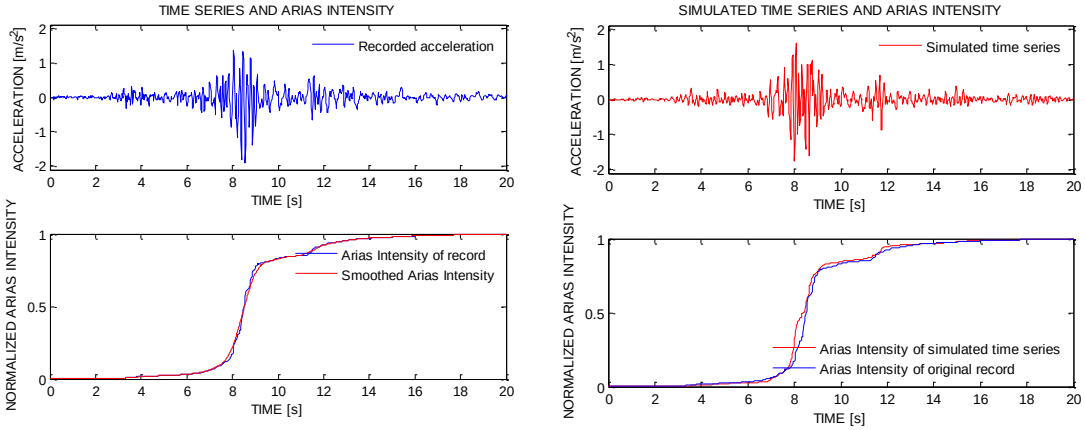

Imperial Valley Earthquake, vertical component. PGA from simulation: 0.576 m/s²

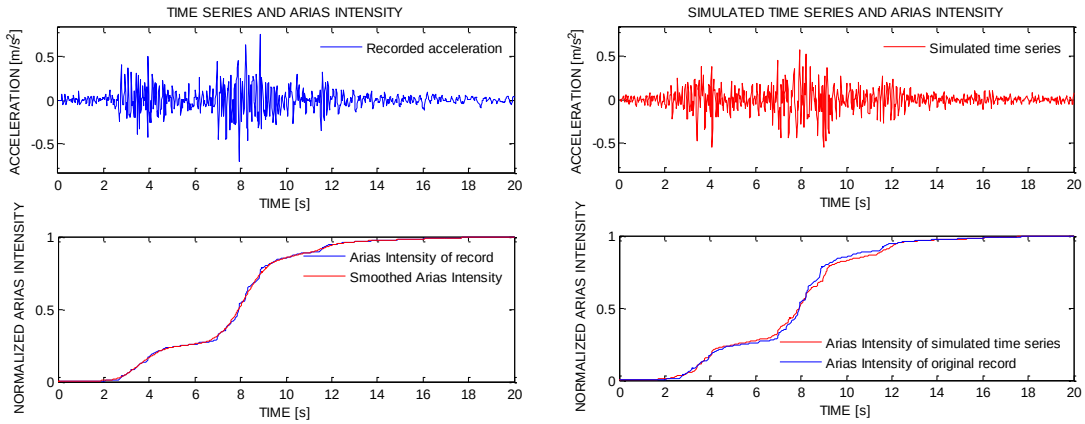

Figure J-17: Results from simulation of all three components, simulation 2 Imperial Valley earthquake.

Simulation 3 – The Imperial Valley earthquake

Imperial Valley Earthquake, 45°-component. PGA from simulation: 0.742 m/s²

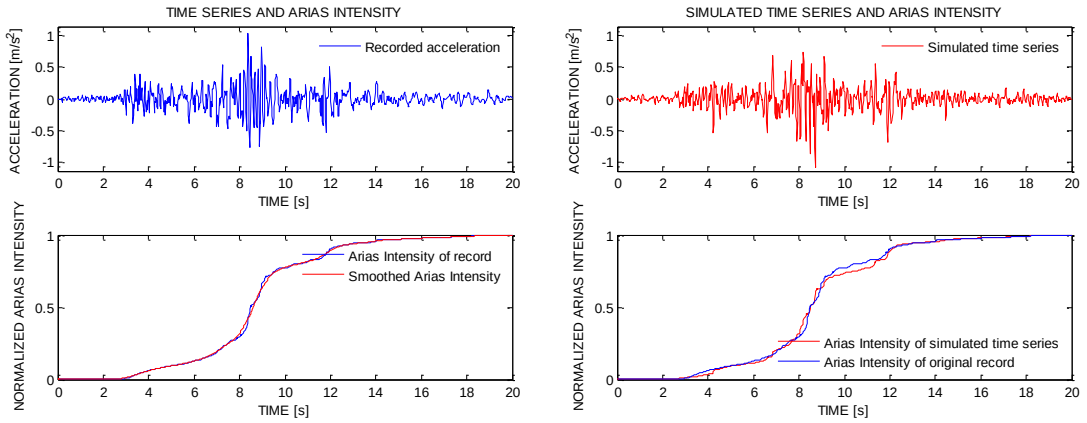

Imperial Valley Earthquake, 135°-component. PGA from simulation: 1.528 m/s2

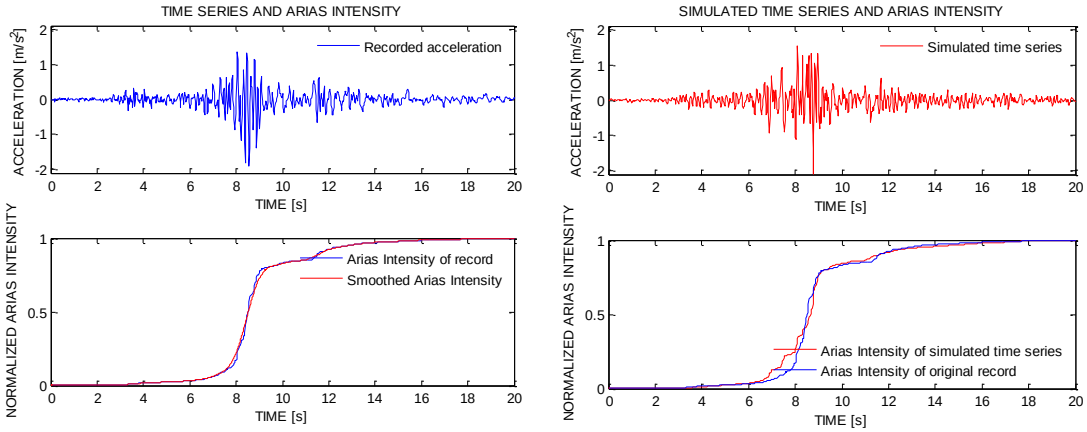

Imperial Valley Earthquake, vertical component. PGA from simulation: 0.529 m/s²

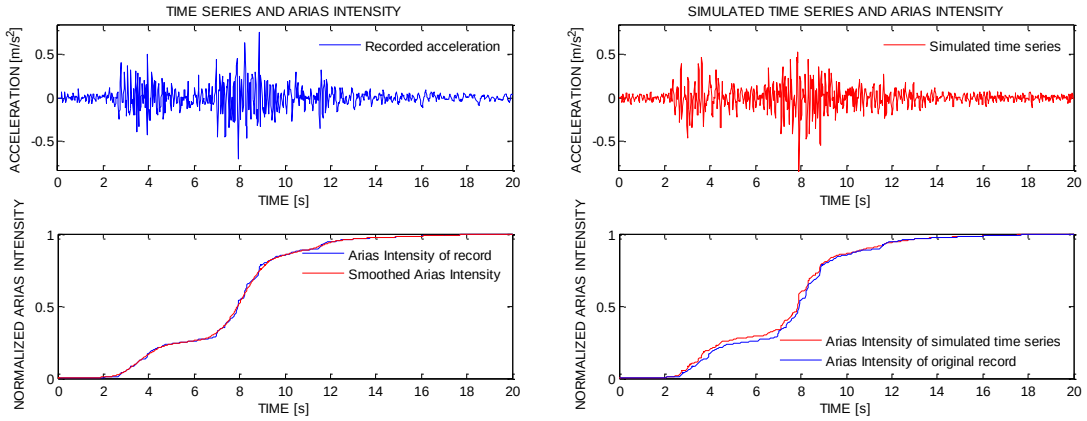

Figure J-18: Results from simulation of all three components, simulation 3 Imperial Valley earthquake.

Simulation 4 – The Imperial Valley earthquake

Imperial Valley Earthquake, 45°-component. PGA from simulation: 0.986 m/s²

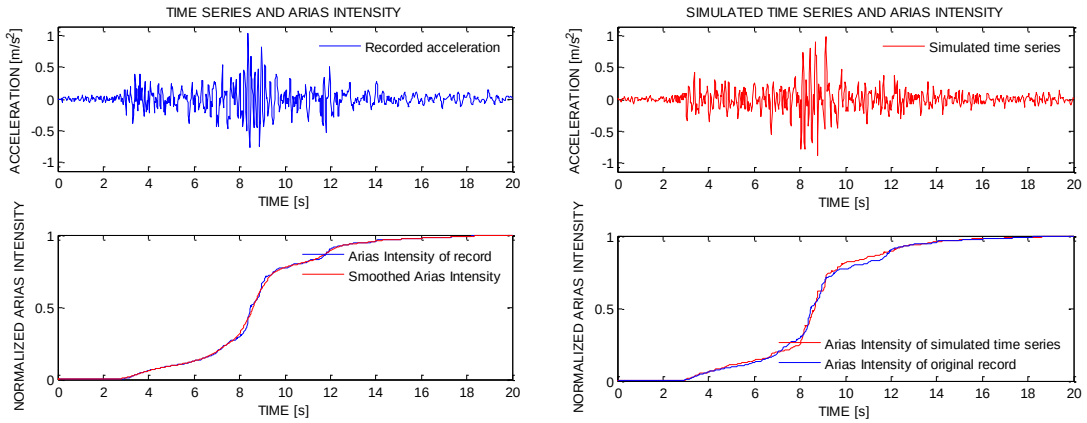

Imperial Valley Earthquake, 135°-component. PGA from simulation: 1.472 m/s2

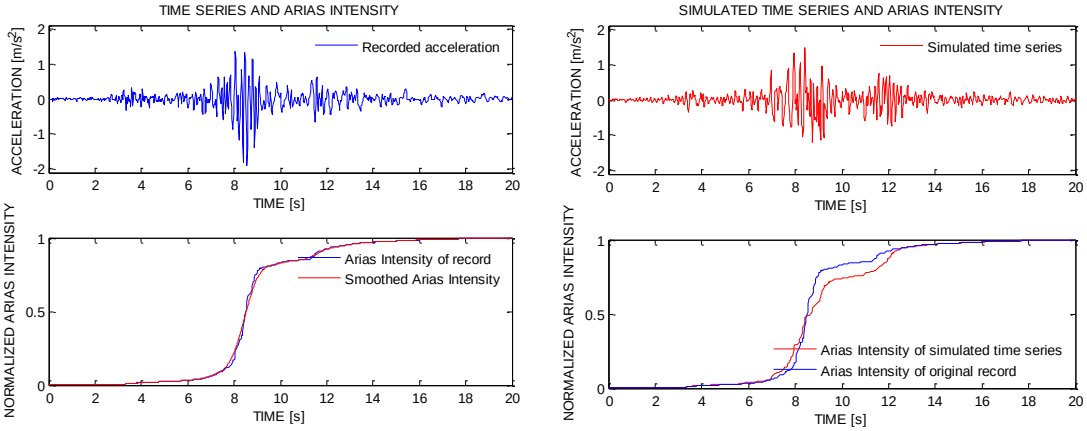

Imperial Valley Earthquake, vertical component. PGA from simulation: 0.576 m/s²

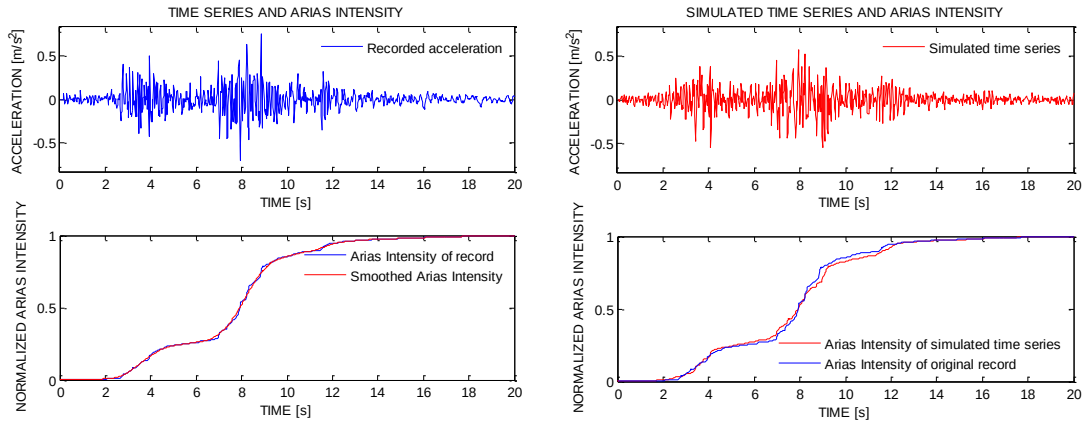

Figure J-19: Results from simulation of all three components, simulation 4 Imperial Valley earthquake.

Simulation 5 – The Imperial Valley earthquake

Imperial Valley Earthquake, 45°-component. PGA from simulation: 1.060 m/s²

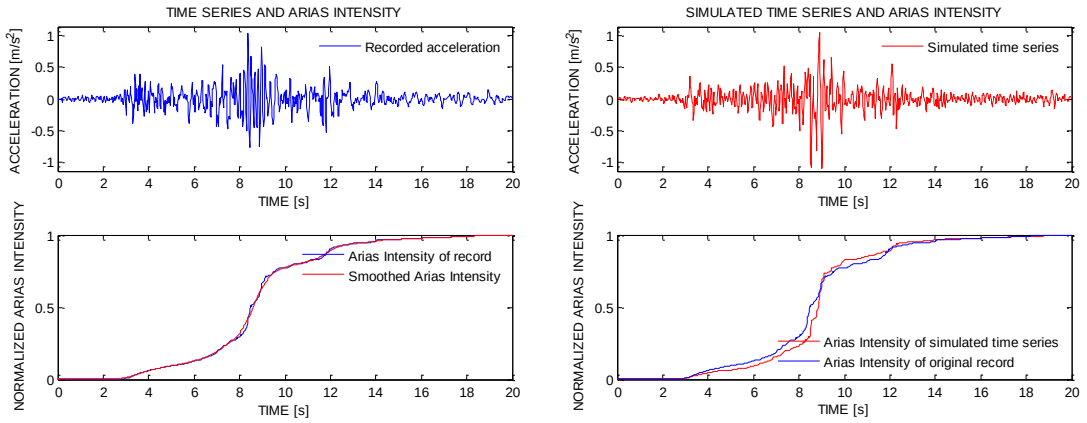

Imperial Valley Earthquake, 135°-component. PGA from simulation: 1.675 m/s2

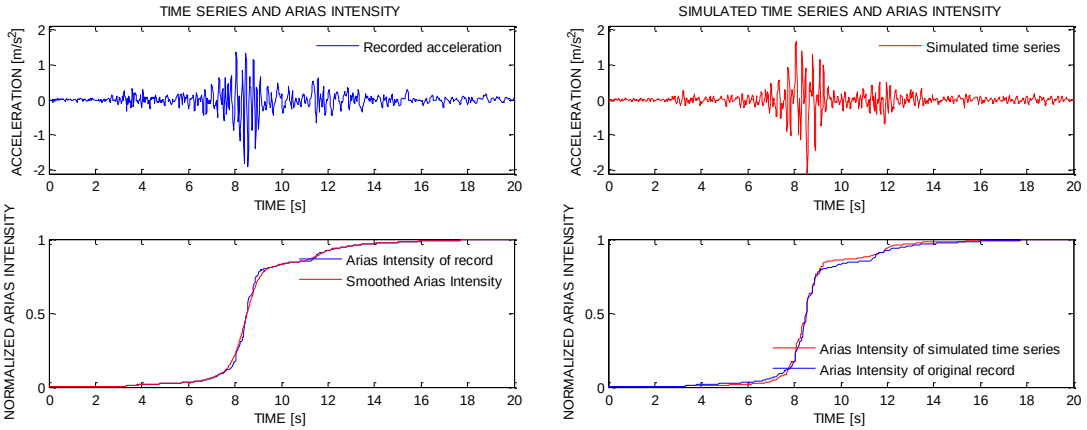

Imperial Valley Earthquake, vertical component. PGA from simulation: 0.739 m/s²

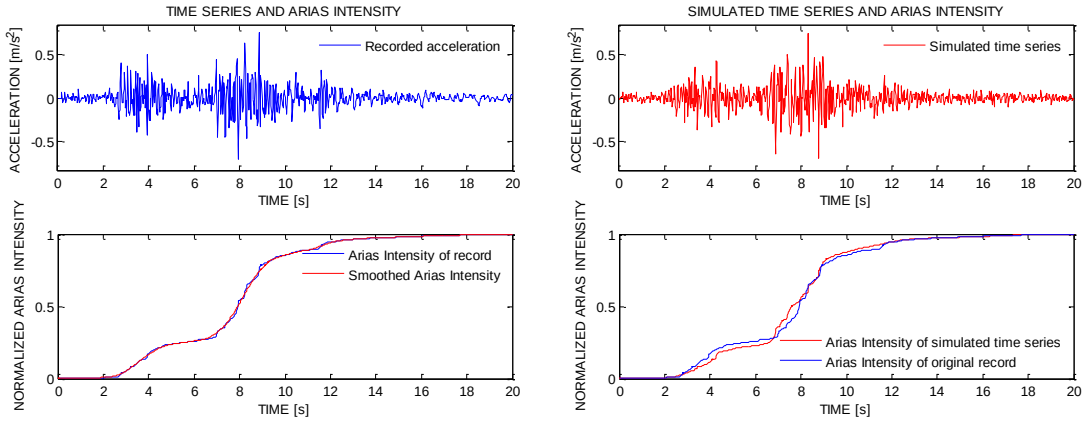

Figure J-20: Results from simulation of all three components, simulation 5 Imperial Valley earthquake.